(4)

Special Report 89-15

May 1989

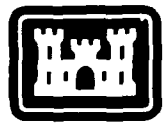

US Army Corps of Engineers

Cold Regions Research & Engineering Laboratory

Blasting and blast effects in cold regions

Part III: Explosions in ground materials

Malcolm Mellor

Prepared for
OFFICE OF THE CHIEF OF ENGINEERS

UNCLASSIFIED

SECURITY CLASSIFICATION OF THIS PAGE

REPORT DOCUMENTATION PAGE

Form Approved
OMB NO 0704-0188
Exp. Date: Jun 30, 1986

1a REPORT SECURITY CLASSIFICATION
Unclassified

1B RESTRICTIVE MARKINGS

2a SECURITY CLASSIFICATION AUTHORITY

3 DISTRIBUTION/AVAILABILITY OF REPORT
Approved for public release; distribution is unlimited.

2b DECLASSIFICATION/DOWNGRADING SCHEDULE

4 PERFORMING ORGANIZATION REPORT NUMBER(S)
Special Report 89-15

5 MONITORING ORGANIZATION REPORT NUMBER(S)

6a NAME OF PERFORMING ORGANIZATION
U.S. Army Cold Regions Research and Engineering Laboratory

6b OFFICE SYMBOL (If applicable)
CECRL

7a NAME OF MONITORING ORGANIZATION
Office of the Chief of Engineers

6c ADDRESS (City, State, and ZIP Code)
72 Lyme Road
Hanover, N.H. 03755-1290

7b ADDRESS (City, State, and ZIP Code)
Washington, D.C. 20314

8a NAME OF FUNDING/SPONSORING ORGANIZATION

8b OFFICE SYMBOL (If applicable)

9 PROCUREMENT INSTRUMENT IDENTIFICATION NUMBER

8c ADDRESS (City, State, and ZIP Code)

10 SOURCE OF FUNDING NUMBERS

PROGRAM ELEMENT NO	PROJECT NO	TASK NO	WORK UNIT ACCESSION NO
6.27.30A	4A76 2730AT42 ✓	CS	029

11 TITLE (Include Security Classification)
Blasting and Blast Effects in Cold Regions
Part III: Explosions in ground materials

12 PERSONAL AUTHOR(S)
Mellor, Malcolm

13a TYPE OF REPORT	13b TIME COVERED FROM ____ TO ____	14 DATE OF REPORT (Year, Month, Day)	15 PAGE COUNT
		May 1989	69

16 SUPPLEMENTARY NOTATION

17 COSATI CODES			18 SUBJECT TERMS (Continue on reverse if necessary and identify by block number)
FIELD	GROUP	SUB-GROUP	Cold regions; Explosions; Explosion effects; Underground explosions

19 ABSTRACT (Continue on reverse if necessary and identify by block number)

The effects of underground explosions are considered, first for deep explosions far from a free surface, then for shallow explosions which form craters and eject debris. The general pattern of behavior is established from compilations of test data for typical rocks and soils, and comparable compilations are made for the more limited test data relating to frozen soils, ice and snow.

20 DISTRIBUTION/AVAILABILITY OF ABSTRACT
☒ UNCLASSIFIED/UNLIMITED ☐ SAME AS RPT ☐ DTIC USERS

21 ABSTRACT SECURITY CLASSIFICATION
Unclassified

22a NAME OF RESPONSIBLE INDIVIDUAL	22b TELEPHONE (Include Area Code)	22c OFFICE SYMBOL
Malcolm Mellor	603-646-4100	CECRL-EE

DD FORM 1473, 84 MAR

83 APR edition may be used until exhausted
All other editions are obsolete

SECURITY CLASSIFICATION OF THIS PAGE

UNCLASSIFIED

PREFACE

This is one of a series of reports that summarize data relating to blasting procedures and blast effects in cold regions. They are organized to deal successively with 1) explosions in air, 2) explosions in water, 3) explosions in solid ground materials. For the most part, the blasting procedures used in cold regions are not much different from those that are in general use elsewhere. Similarly, the principles involved in assessing blast effects in cold regions are the same as those that apply to blast effects generally. The reports therefore summarize principles and data for general explosions technology, and then present the procedures and data for cold environments within this framework.

The purpose of the series is to provide a convenient reference source for engineers faced with problems of explosions or blasting in cold regions. Because not all engineers are well acquainted with explosions technology, relevant physical principles are explained or summarized, but there is no attempt to explore the underlying theory in depth, nor is there any treatment of the practical aspects of explosives use and safety practices. These topics are covered well in Army Technical Manuals and Army Materiel Command publications, as well as in commercial blasters' handbooks and in textbooks.

This report was prepared by Dr. Malcolm Mellor of the Experimental Engineering Division, U.S. Army Cold Regions Research and Engineering Laboratory. The work was done under DA Project 4A762730AT42, *Design, Construction, and Operations Technology for Cold Regions*; Task Area CS, *Combat Support*; Work Unit 029, *Explosives and Projectile Impact Under Winter Conditions.*

The author is grateful to Donald Albert and Paul Sellmann of CRREL for their careful reviews of the manuscript and suggestions for improvement.

CONTENTS

ILLUSTRATIONS

Figure Page

TABLES

Blasting and Blast Effects in Cold Regions
Part III: Explosions in Ground Materials

MALCOLM MELLOR

INTRODUCTION

Considerable attention has been given to explosive excavation in cold regions, and to the effects produced by explosions in frozen media such as snow, ice and permafrost. Many experiments, field tests and theoretical studies have been carried out, but the results that have been produced are insufficient to give a complete and coherent picture if frozen materials are treated in isolation. To gain a full understanding of the relevant behavior, the limited data for frozen materials have to be interpreted in the context of general explosion technology, as it applies to unfrozen rocks and soils. In this report, explosion effects in solid ground materials are summarized in general form, with frozen materials treated as special types of soils and rocks.

Ice is a characteristic constituent of frozen ground materials, and it has physical properties that differ considerably from those of typical rock-forming minerals and soil grains. For example, ice density is about one-third that of silicates, and the compressibility of ice under extreme pressure is much higher than the compressibility of typical rocks. However, in spite of the unusual properties of ice, frozen materials such as snow, ice and frozen soil behave much like other soils and rocks when they are subjected to blasting or to blast effects.

For most practical purposes, ice-bonded soils can be treated like rock or concrete when designing explosive excavation techniques or when assessing blast effects. For example, water-saturated frozen sand is like sandstone, frozen silt is like siltstone, and water-saturated frozen gravel is like concrete. Massive ice also behaves like rock under explosive attack. It attenuates a stress wave more strongly than do typical hard rocks, but its cratering characteristics are not much different from those of common sedimentary rocks like limestone; the idea that ice is a fragile material that shatters easily is quite unrealistic. Snow deposits have low bulk density and high porosity (commonly 40% to 80%), and it is no surprise to find that snow is highly effective in attenuating stress waves. However, the cratering characteristics of dense snow are not much different from those of common rocks and soils, since low strength and low density are to some extent offset by strong attenuation.

When the pore water freezes in common rocks and minerals, there is a significant increase in strength. This can affect the economics of a large-scale mining operation that is efficient and well-optimized, but it is not of major significance in ordinary blasting operations for excavation and construction.

This report is concerned mainly with explosions inside the ground material. The effects of explosions at or above the ground surface are considered in more detail in Part I.

DEEP UNDERGROUND EXPLOSIONS

When a concentrated explosive charge is set deep underground with the borehole stemmed, the initial effects of the explosion are spherically symmetrical as long as the surrounding material is not strongly anisotropic (Fig. 1). The ground is stressed by an initial shock wave and also by expanding gas. There is local heating by adiabatic compression of the ground material, and the surface of the blast cavity is exposed to the high temperature of the explosion. The effects on the surroundings vary to some extent with the properties of the ground material. For example, highly porous material with air-filled pores can compact locally to a high degree, whereas very dense material can suffer gross displacement only by distributing strains and displacements over a large surrounding volume.

When the shothole is completely filled by the charge, the ground material that is in direct contact with the charge experiences very high pres-

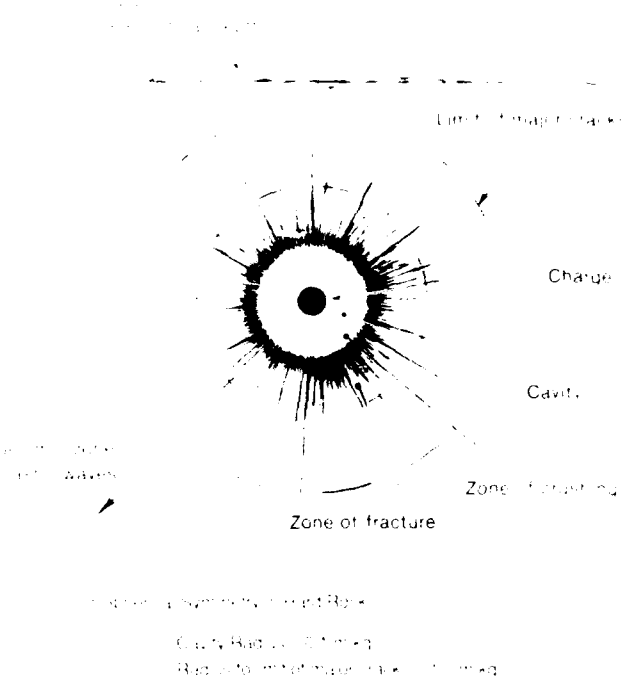

Figure 1. Effects of a fully contained explosion on the surrounding solid material. Spherical symmetry for a spherical charge; cylindrical symmetry for a long cylindrical charge.

sures (approaching detonation pressure). Since the initial amplitude of the shock wave from a typical high explosive far exceeds the deviatoric yield strength of any solid material, the ground material close to the charge undergoes intense compression that is essentially hydrodynamic and adiabatic. Brittle material such as rock is completely pulverized in this zone (Fig. 1). As distance from the charge increases, the shock wave amplitude decreases due to geometrical spreading of the wave front and also due to dissipation in the ground material. Inelastic (plastic) compression of the material becomes progressively less severe, and the shear resistance becomes increasingly important. At sufficient radius from the charge, the behavior of the material is that of an elastic solid rather than the hydrodynamic behavior of pulverized material. In the transition zone, the rock exhibits an elastic-brittle response, and radial cracks are formed by tensile hoop stresses, either from the radially propagating shock or from the pressure pulse produced by gas pressure in the explosion cavity. In principle, cracks can be pressurized and propagated by the expanding gases, provided that the gases are not "sealed in" by intense pulverization (and possibly fusion) of the cavity wall. However, crack propagation by gas intrusion probably does not occur in a fully contained explosion. Beyond the zone of cracking the stress wave propagates elastically at the acoustic velocity for the material, producing dilatation and shear.

SIZE OF THE CHAMBER AND THE CRUSHED ZONE (Spring Hole Blasting)

The cavity produced by a deeply buried explosion is termed variously a *chamber*, a *camouflet*, a *spring hole*, or simply a *cavity*. "Chamber" is a general term, "camouflet" is an old military term for an explosion smothered by burial, and "spring hole" usually means a cavity blasted at the base of a shothole to provide space for more explosive. The limit of the cavity is not always easy to define, since fragmented material can collapse back. Nor is the full extent of the crushed zone easy to measure, since it is extremely expensive to cut cross sections through hard rock at great depth.

Test data for rocks and soils

In various test programs carried out by the U.S. Bureau of Mines, spring holes were blasted by concentrated charges and loose fragments were then

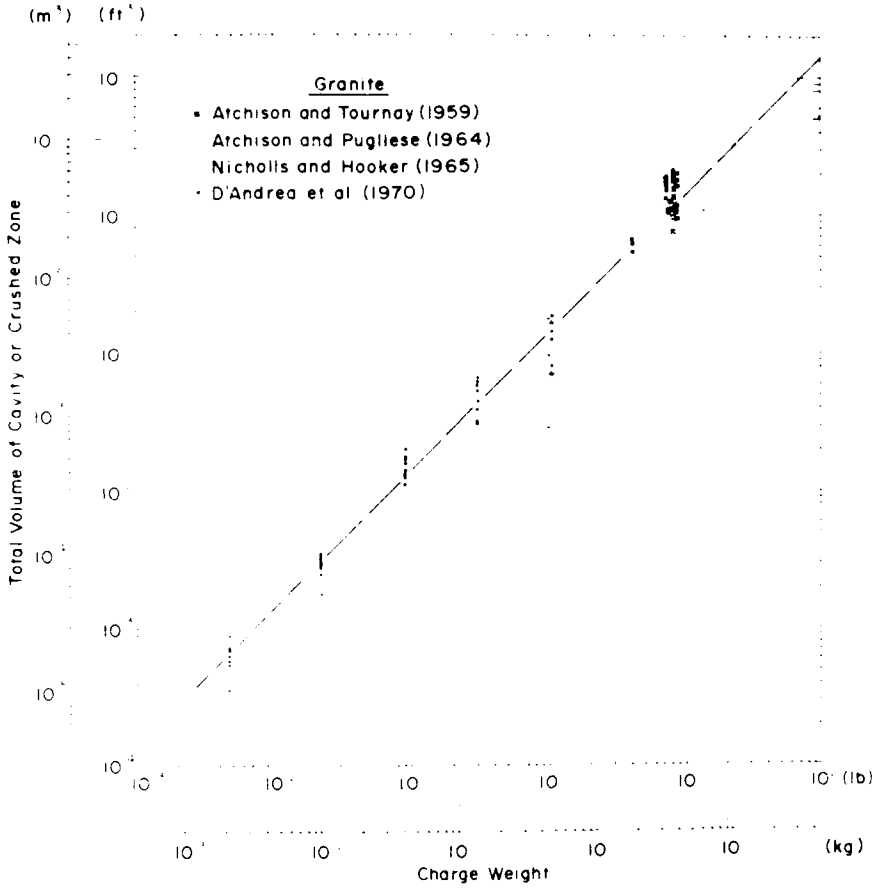

Figure 2. Summary of spring hole data from USBM tests in granite.

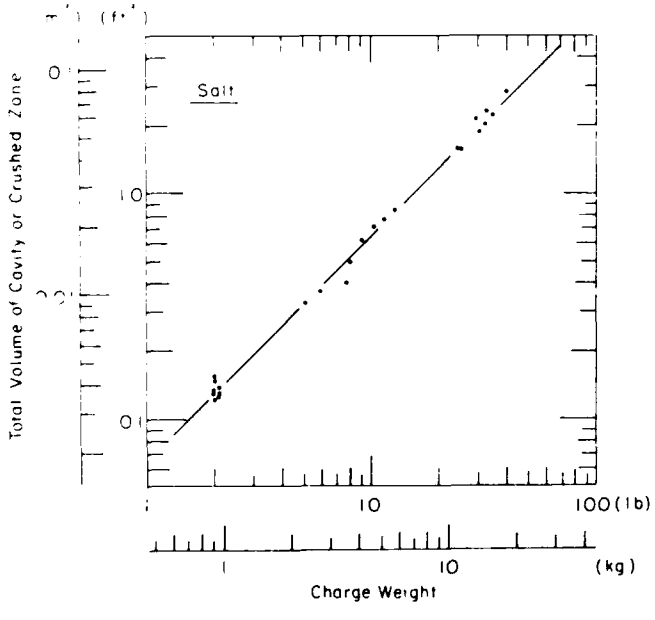

Figure 3. Results of USBM spring hole tests in salt. (After Nicholls and Hooker 1962a.)

blown out through the shothole by compressed air. These studies produced some of the best North American data for small explosions, but it has to be recognized that the volume of material excavated is somewhat arbitrary. The volume measured is certainly more than the volume of open cavity when no fragments are removed, but it is likely to be significantly less than the total volume of rock that is subject to severe cracking.

Figure 2 summarizes the results of four series of tests made in granite by the U.S. Bureau of Mines, using a variety of explosives. This plot of volume against charge weight displays considerable scatter, but there is a systematic linear trend over almost 5 orders of magnitude. The indication is that, for typical explosives well-coupled to granite, the volume of thoroughly crushed rock is about 0.14 ft^3/lb, or 8.7×10^{-3} m^3/kg. There is uncertainty by a factor of 2 on either side of this value (the volume could be twice as much, or half as much). The volumes plotted represent the total volume of the excavated cavity, with no deduction for the original volume of the charge.

Figure 3 gives the results of another series of

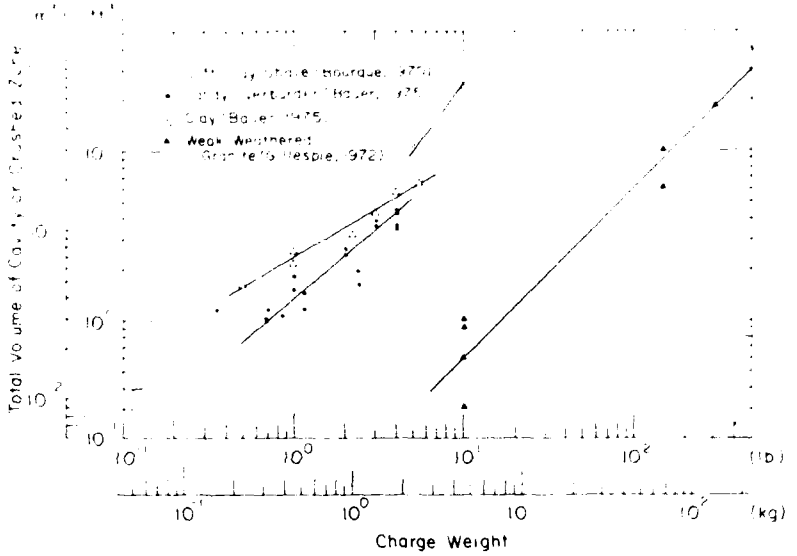

Figure 4. Summary of spring hole data from tests in weak, weathered granite, in clay, in sandy overburden, and in soft clay shale.

tests made in salt. Here the range of the data is smaller, but the data points lie very close to a straight line, with little scatter. The yield in salt was only half that in granite—about 0.064 ft^3/lb, or 4×10^{-3} m^3/kg.

One other study in rock produced a good linear correlation between chamber volume and charge size. In Project Buchanan (Gillespie 1972), spring charges were fired in a weak, weathered granite, giving the results shown in Figure 4. The data that have been plotted here are for spring charges in a fresh hole; during the project, second and third charges were loaded successively into spring holes produced by previous detonations. The data in Figure 4 give specific cavity volume as approximately 0.06 ft^3/lb, or 3.75×10^{-3} m^3/kg.

Other test programs in tonalite, weathered clay shale, sandy overburden, and clay have produced data that do not fit a linear relation between volume and charge weight. In general, these tests cover relatively small ranges of charge size, and they cannot be taken as strong evidence against the linear relation, especially as the log-log plots suggest power relations with exponents both above and below unity. Using mid-range values to establish representative yields for these tests, specific cavity volumes are about 0.06 ft^3/lb (3.9×10^{-3} m^3/kg) for tonalite, 2.2 ft^3/lb (0.14 m^3/kg) for weathered clay shale, 1.8 ft^3/lb (0.1 m^3/kg) for clay, and 1.2 ft^3/lb (0.07 m^3/kg) for sandy overburden.

Henrych (1979) accepts without question that chamber volume should be proportional to charge weight for concentrated explosions inside rocks and soils. For fully contained nuclear explosions in rock, Glasstone and Dolan (1977) also accept approximate proportionality between chamber volume and the energy yield of the explosion. From the evidence summarized above there seems to be no good reason to doubt this proportionality, so that chamber size can be expressed as a specific volume (Table 1a, 1b).

If it is assumed that the cavity produced by a compact charge is approximately spherical, the volume measurements give an effective radius for the cavity. The specific volume data for granite in Figure 2 imply a mean scaled radius of 0.32 $ft/lb^{1/3}$, or 0.13 $m/kg^{1/3}$. This is just over two charge radii—2.1, 2.2 and 2.3 charge radii for charge specific gravities of 1.0, 1.2 and 1.4, respectively. The results for salt imply a scaled radius of 0.25 $ft/lb^{1/3}$ or 0.10 $m/kg^{1/3}$. For charge specific gravity of 1.0, 1.2 and 1.4, the cavity radius is 1.6, 1.7 and 1.8 charge radii respectively. The data for weak, weathered granite suggest a cavity radius of 0.24 $ft/lb^{1/3}$ or 0.10 $m/kg^{1/3}$. This is equivalent to 1.6, 1.65 and 1.7 charge radii for charge specific gravities of 1.0, 1.2 and 1.4 respectively. In tonalite (Fig. 5), cavity radius is about 0.24 $ft/lb^{1/3}$ or 0.1 $m/kg^{1/3}$, i.e. the same as weathered granite. These results are summarized in Table 1a.

Henrych (1979) gives cavity radii for hard rocks in the range 1.1 to 2.5 charge radii, or 0.06 to 0.13 $m/kg^{1/3}$ (Table 1c). For weak and weathered rocks,

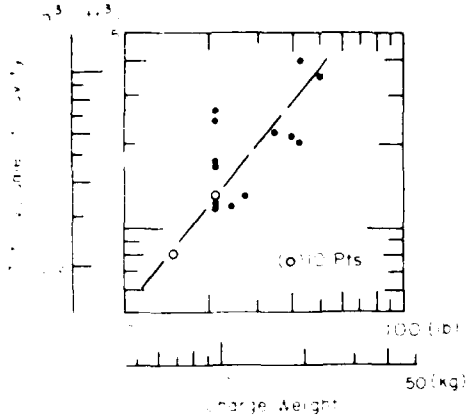

Figure 5. Results of spring hole tests in tonalite of medium-to-high strength. (After Gillespie 1972.)

values are in the range 1.7 to 4.0 charge radii, or 0.09 to 0.21 m/kg$^{1/3}$.

In *soils* and *very weak rocks*, the cavities are much bigger. In weathered clay shale the radius is about 0.81 ft/lb$^{1/3}$, or about 0.32 m/kg$^{1/3}$. For the slurry explosive that was used (DBA 22M), this is equivalent to 6 charge radii. In saturated clay, cavity radius is roughly the same, and in sandy overburden a little less (Table 1a). Henrych (1979) gives data for a variety of soils. The overall range of cavity radius is 3.8 to 13.1 charge radii, or 0.2 to 0.7 m/kg$^{1/3}$ (Table 1c).

Glasstone and Dolan (1977) give representative values of cavity radius for fully contained *nuclear* explosions deep inside rock (>2000 ft, or >600 m). For dense silicate rocks such as granite, the cavity radius is 35 ft/kt$^{1/3}$ (11 m/kt$^{1/3}$). For dense carbonate rocks (limestone, dolomite) the cavity radius is 25 ft/kt$^{1/3}$ (7.6 m/kt$^{1/3}$). If these values are converted directly into conventional HE units, assuming 1 kt fully equivalent to 1000 tons of TNT, the radii are approximately 0.27 ft/lb$^{1/3}$ (0.11 m/kg$^{1/3}$) and 0.2 ft/lb$^{1/3}$ (0.08 m/kg$^{1/3}$) for silicate and carbonate rocks respectively (Table 1b). If a cratering equivalency factor is used in the conversion, say 1 kt = 10^6 lb TNT, the cavity radii become 0.34 ft/lb$^{1/3}$ (0.14 m/kg$^{1/3}$) and 0.25 ft/lb$^{1/3}$ (0.098 m/kg$^{1/3}$) for silicate and carbonate rocks respectively. These values are in good agreement with the HE values in Table 1a.

In theoretical studies of rock blasting, Kutter and Fairhurst (1971) postulated an "equivalent cavity" of fractured material formed by the shock wave, and pressurized by the expanding gas. They deduced that this equivalent cavity should have a radius of 6 charge hole radii, or 6 charge radii, for spherical symmetry. For cylindrical charges, the corresponding figure was 9 charge hole radii, or 9 charge radii. The postulated equivalent cavity is therefore bigger than actual cavities formed in hard rock.

Test data for cylindrical cavities blasted by linear, or columnar, charges are not easy to come by. Table 1d gives a few reported values for cylindrical cavities in soils. There are also some reported values of about 3 to 4 charge radii for the "crushed zone" when cylindrical charges are fired in hard rock. These can probably be interpreted as cavity radii.

Experimental values for specific chamber volume can be interpreted as powder factors (i.e. reciprocal of specific hole volume, which is equal to specific charge). The values for chambering in rocks are more than two orders of magnitude higher than the powder factors that apply to typical blasting operations, but the values for chambering in soils and very weak rocks are quite low. For rocks, the effective powder factor is about 200–450 lb/yd^3 (115–270 kg/m^3) and for very weak rock, soils, and frozen soils the range is about 12–50 lb/yd^3 (7–30 kg/m^3).

Spring holes in frozen materials

Spring hole measurements have been made in frozen soils, usually without any attempt at excavation of loose debris. Benert (1961) fired 60% gelatin dynamite in a frozen till described as "gravelly silt." The results (Fig. 6) give a general idea of spring hole volume in frozen till, but they cannot be used to define a relation between volume and charge weight, since the length/diameter ratio of the charges increased with charge weight, reaching a value of 12 for the biggest charges.

Other tests were made in frozen silt, using sensitized nitromethane and composition C-4 (Mellor 1972, Sellmann, unpublished). These were not systematic studies, and the results (Fig. 6) are not suitable for defining general relations between chamber volume and charge weight. Bauer (1975) fired compact charges of ANFO (S.G. 0.85) in frozen clay. The results follow a linear trend, although Bauer himself did not accept a linear relation between cavity volume and charge weight.

Looking at the overall compilation of data in Figure 6, it appears that spring hole volumes for compact charges in frozen silt and frozen clay may be quite similar, with specific volume about 0.53 ft^3/lb (3.3×10^{-2} m^3/kg). The equivalent radius for a spherical chamber is about 0.5 ft/lb$^{1/3}$ (0.2 m/kg$^{1/3}$). This is 3.2 charge radii for a charge speci-

Table 1. Dimensions of blast cavities produced by underground explosions.

a. Cavity sizes for conventional underground explosions.
(See text and figures for data sources.)

Material	Specific volume ft³/lb	Specific volume m³/kg	Equivalent radius ft/lb^1/3	Equivalent radius m/kg^1/3	Charge radii (e.g. 1.4)
Granite (sound)	0.14	8.7 × 10⁻³	0.32	0.13	2.3
Granite (weathered)	0.06	3.75 × 10⁻³	0.24	0.10	1.7
Granite (?)	0.074	4.6 × 10⁻³	0.26	0.10	1.9
Salt	0.064	4 × 10⁻³	0.25	0.10	1.8
Tonalite	0.06	3.9 × 10⁻³	0.24	0.10	1.7
Clay shale (weathered)	2.2	0.14	0.81	0.32	5.8
Clay (saturated)	1.8	0.1	0.75	0.30	5.4
Sandy overburden	1.2	7 × 10⁻²	0.66	0.26	4.7
Frozen silt; frozen clay	0.53	3.3 × 10⁻²	0.5	0.2	3.6
Frozen till	≈ 0.2	≈ 1 × 10⁻²	≈ 0.35	≈ 0.14	≈ 2.5

b. Cavity sizes for nuclear underground explosions (based on full TNT equivalent).
(Data from Glasstone et al. 1977.)

Material	Specific volume ft³/lb	Specific volume m³/kg	Equivalent radius ft/lb^1/3	Equivalent radius m/kg^1/3
Granite (and other dense silicate rocks)	0.082	5.1 × 10⁻³	0.27	0.11
Limestone, dolomite (and other dense carbonate rocks)	0.034	2.1 × 10⁻³	0.2	0.08

c. Chamber dimensions for ammonite explosions in soils and rocks.
(After Henrych 1979.)

Soil or rock type	Chamber radius Charge radii	Chamber radius R/W (m/kg^1/3)
Plastic loam, moraine loam, water bearing sand, water bearing loam	11.3–13.1	0.6–0.7
Jurassic black loam	8.6–9.9	0.45–0.52
Moraine loam	7.0–9.5	0.37–0.5
Browny-yellow fireloam	7.0–7.6	0.37–0.4
Dark red fireloam	6.5–7.4	0.34–0.39
Soft, strongly cracked marl, loess	6.6–7.7	0.35–0.4
Soft, cracked marl, loess	5.4–6.5	0.29–0.34
Dark blue brittle loam	5.4–6.2	0.29–0.33
Heavy sandy loam, sandy loam	4.8–6.7	0.25–0.36
Soft chalk, shell limestone	3.8–4.7	0.20–0.25
Medium-strength marl, marl dolomite, soft limestone heavily permeated with cracks	2.4–4.0	0.13–0.21
Compact fine-grained gypsum, loamy shale, strongly cracked granite, medium-strength apatite, silicate, medium-cracked limestone	1.7–2.9	0.09–0.15
Medium-cracked granite, compact iron quartzite, compact gray quartzite, apatite-nepheline ore, compact limestone, snake-stone with asbestos, sandstone, dolomite	1.5–2.5	0.078–0.13
Hornstone, marble, granite, layered quartz, hard limestone, coarse- and fine-grained granite, hard phosphorite, hard dolomite, coarse-grained marble gypsum	1.1–2.0	0.058–0.11

d. Cylindrical blast cavities in soil. (Henrych 1979, quoting a 1969 Soviet document.)
Overall range for solids said to be 12–25 charge radii (upper limit contradicts tabulated values).

Soil or rock type	Cavity radius Charge radii (TNT equiv.)	Cavity radius W^1/3 scaled (m/kg^1/3)
Loam	≈ 28.3	≈ 0.4
Sandy soil	24.8	≈ 0.35
Soil (dry bulk density 1.57 Mg/m³, moisture content 30–33% by volume)	≈ 27	0.38
Soil (dry bulk density 1.4–1.6 Mg/m³, moisture content 4–5% by volume)	≈ 16.3	≈ 0.23

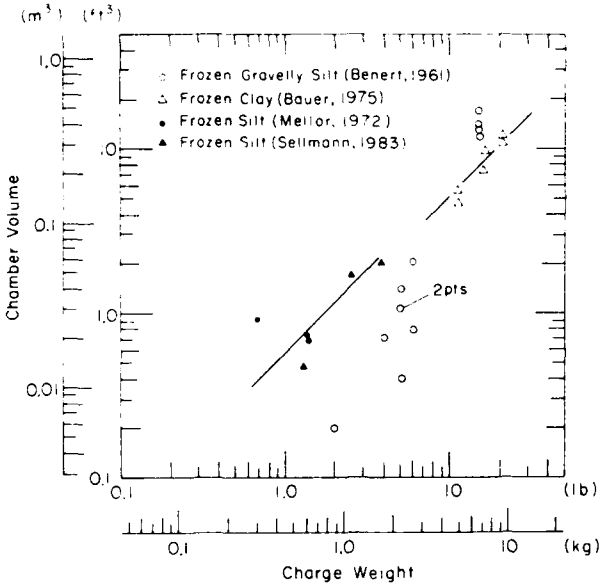

Figure 6. Summary of spring hole data for frozen soils.

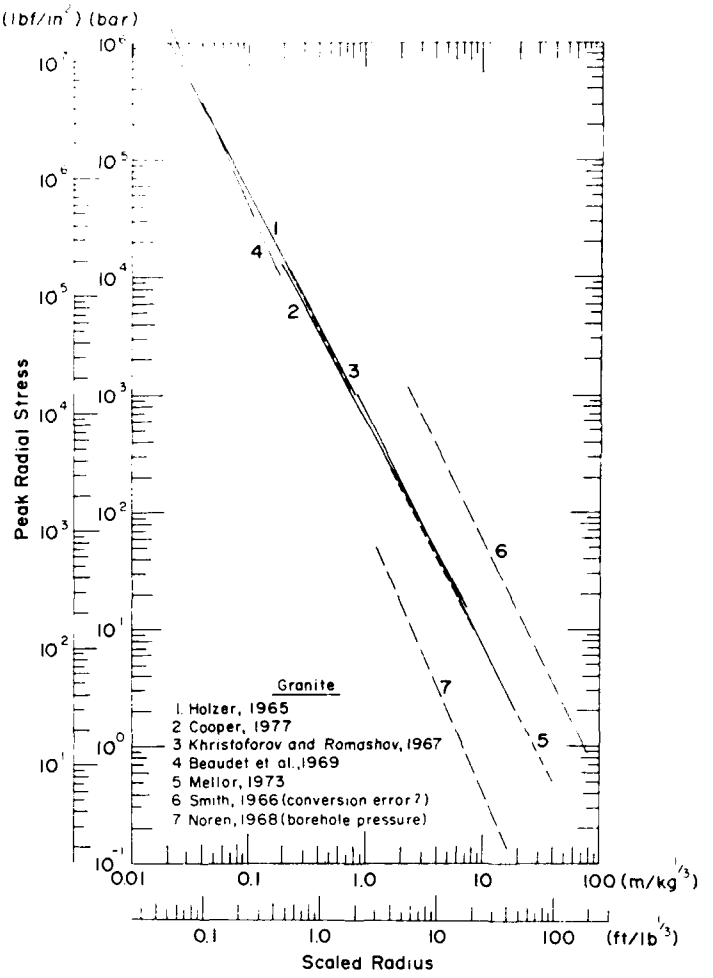

Figure 7. Summary of stress attenuation data for spherical propagation in granite.

fic gravity of 1.0, or 3.6 charge radii for a specific gravity of 1.4.

The data for frozen till are probably representative of the performance of a compact spring charge at the lower end of the data range, but at the upper end of the range they represent cylindrical rather than spherical geometry. In this material, specific volume is perhaps about three times smaller than in frozen silt and frozen clay.

SIZE OF THE CRACKED ZONE

It is not easy to determine the extent of radial cracking around a deeply buried explosion. To get a feel for the size of the cracked zone, results of the few direct observations have to be combined with deductions from indirect evidence.

Research studies (Olson et al. 1973) suggest that radial cracks from a *concentrated charge* in granite may extend about 18 to 20 charge radii (2.5–2.75 ft/lb$^{1/3}$, or 1.0–1.1 m/kg$^{1/3}$). Another estimate can be made by considering the empirical stress attenuation curve for granite in Figure 7. If the compressive radial stress of the graph is assumed equal to the tensile circumferential stress, and if the tensile strength of the granite is taken as 2000 lbf/in.^{2} (13.8 MPa), then radial cracks could perhaps extend out to a radius of 5.5 ft/lb$^{1/3}$ (2.2 m/kg$^{1/3}$), or about 39 charge radii. If the same type of argument is applied to the attenuation of peak radial strain (Fig. 12), and appropriate values are taken for the tensile failure strain of the rock, another estimate is obtained. Taking the tensile failure strains for granite and limestone as 4.5×10^{-4} and 3×10^{-4} respectively, the indicated values of maxi-

Table 2. Indications of crack extent for charges in an infinite rock mass.

a. Concentrated charges.

Indicator	*Maximum extent (charge radii)*	*ft/lb*	*m/kg*
Damage radius (determined by inspection)	18-20 (granite)	2.5-2.75	1.0-1.1
Stress attenuation	≈ 39 (granite)	≈ 5.3	≈ 2.1
Strain attenuation	≈ 29 (granite)	≈ 4	≈ 1.6
	≈ 40 (limestone)	≈ 5.5	≈ 2.2
Attenuation of particle velocity	≈ 94	≈ 13	≈ 5

b. Long cylindrical charges.

Indicator	*Maximum extent (charge radii)*
Damage radius (determined by inspection)	15-55
Shothole spacing in bench blasting	≈ 45 (extreme limits 20-80)
Shothole spacing in smooth blasting (limited burden)	45-56 (assuming decoupling ratio of 3.5)
Shothole spacing in presplitting (very large burden)	28-42 (assuming decoupling ratio of 3.5)
Elastic analysis (simple assumptions)	26-37 (probable range) 19-53 (extreme plausible range)
Elastic analysis (assuming cavity expansion)	21-33 (probable range) 15-46 (extreme plausible range)

mum crack radius are about 29 charge radii for granite (4 ft/lb$^{1/3}$, or 1.6 m/kg$^{1/3}$) and about 40 charge radii for limestone (5.5 ft/lb$^{1/3}$, or 2.2 m/kg$^{1/3}$). A very crude upper limit estimate can be made by drawing on attenuation curves for peak particle velocity, together with empirical damage criteria for near-surface waves. A safe limit of particle velocity for internal cracking of sound rock is about 25 in./s (635 mm/s); for a spherical wave in granite, this level is reached at a radius of about 13 ft/lb$^{1/3}$ (5.2 m/kg$^{1/3}$), or about 94 charge radii.

These rough estimates are summarized in Table 2a. It seems fairly clear that maximum cracking radius is in the range 10 to 100 charge radii. It is not unlikely that the actual range is about 20 to 40 charge radii for spherical symmetry.

For *long cylindrical charges*, there are more direct observations on the size of the cracking zone (Cattermole and Hansen 1962, Siskind et al. 1973, Siskind and Fumanti 1974). Maximum radius of the cracked zone seems to be in the range 15-55 charge radii. This fits quite well with empirically established values of hole spacing in practical bench blasting. A typical spacing/diameter ratio of 45 for bench blasting implies a crack extent of about 45 charge radii. The extreme limits in bench blasting are 20 to 80. Looking at established practice for smooth blasting and presplit blasting, and assuming a decoupling ratio of 3.5, the ranges of hole spacing in *charge* diameters are 45 to 56 for smooth blasting and 28 to 42 for presplitting. This can perhaps be interpreted as an expectation that crack extension from a single charge will be in the range of 45-56 and 28-42 for smooth blasting and presplitting respectively.

Another estimate can be based on the static plane strain elastic analysis for a hole in a thick plate. Consider a hole of radius a in a plate that has in-plane principal stresses $\sigma_1 = \sigma_2 = P$. If the hole has internal pressure p, the radial and circumferential stresses at radius r from the center of the hole are, respectively:

$$\sigma_r = P + (p - P)(a/r)^2 \quad (1)$$

$$\sigma_\theta = P - (p - P)(a/r)^2. \quad (2)$$

If $p >> P$,

$$\sigma_\theta = -\sigma_r = -p(a/r)^2. \quad (3)$$

When a borehole is pressurized abruptly, an elastic stress field can establish itself in the surrounding medium at the acoustic velocity for the medium. For that part of the material that does not fracture during passage of the shock, the limiting radius for crack formation is the value of r where σ_θ equals the tensile strength of the rock σ_T. This is assuming that the borehole pressure can be sustained for longer than it takes to establish the elastic stress field.

A first inclination is to identify hole radius a with the drill hole radius $d/2$, d being the drill hole (and charge) diameter. Corespondingly, the hole pressure p might be identified with the detonation pressure of the explosive p_D, or with some fraction of p_D. However, it may be more reasonable to take a as half the diameter of the blast cavity, or half the diameter of the crushing zone, either of which can be denoted Kd, where $K > 1$. The corresponding hole pressure p would then be the pressure p_H which is reached after adiabatic expansion of the explosion products from the detonation pressure p_D at diameter d to p_H at diameter Kd.

For the first set of assumptions, the potential limit for crack extent is given by

$$r = a(p_D/\sigma_T)^{1/2} = (d/2)(p_D/\sigma_T)^{1/2}. \quad (4)$$

For the second set of assumptions, the limiting radius for crack extent is given by

$$r = (Kd/2)(p_H/\sigma_T)^{1/2} \quad (5)$$

where, for a long cylindrical charge, adiabatic expansion gives

$$p_H = p_D K^{-2\gamma} \quad (6)$$

in which $\gamma \approx 1.2$ for expanding explosion products. Thus

$$r = (Kd/2)(p_D/K^{2\gamma}\sigma_T)^{1/2}$$

$$= K^{1-\gamma}(d/2)(p_D/\sigma_T)^{1/2}. \quad (7)$$

With $K = 2$ to 3, $K^{1-\gamma}$ is in the range 0.8 to 0.87, so the choice of assumptions does not have a strong effect on the final result.

For exploratory estimates, take the tensile strength of fairly strong rocks as 1000 to 2000 lbf/in.^{2} (6.9 to 14 MPa). Take $K = 2$ to 3, and p_D in the range 0.7×10^6 to 2.8×10^6 lbf/in.^{2} (5 to 19 GPa). The factor $(p_D/\sigma_T)^{1/2}$ controls the result; pairing high and low limits for p_D and σ_T gives a range from 19 to 53, while the pairing of low and high limits for both reduces the range to 26 to 37. These are maximum crack lengths in charge radii for the first and simplest set of assumptions. For the second set of assumptions, maximum crack lengths are 80% to 87% of these values.

Table 2b summarizes the deduced limits for maximum crack length around a long cylindrical charge in rock. Again it seems safe to conclude that maximum crack length will be in the range 10–100 charge radii. The actual range is probably narrower, say 20 to 55 charge radii.

ATTENUATION RELATIONS FOR SHOCK PROPAGATION

Spherical symmetry

In reviewing the available data for spherical propagation of blast effects in ground materials, the standard forms of presentation used in the literature will be followed (next section). In the standard presentations, data are plotted on logarithmic scales for good reason, since the values can span many decades. There is also a common practice of representing the data by straight lines on log-log plots, and hence by simple inverse power relations, i.e. $I = I_0 r^{-n}$, where I is the magnitude of the effect, r is the radius from the source, and I_0 and n are empirical constants. This is convenient, but it is not necessarily good science; n has to vary for different ranges of r, I must tend to infinity as r tends to zero, and there is no separation of geometrical effects and dissipation effects.

As a stress wave propagates spherically, it attenuates because the wave spreads over an ever-increasing surface area, and also because energy is dissipated in displacing and straining the medium through which the wave passes. The effect of geometrical spreading is the same for any material and at any distance from the source; the area of a spherical wave front is proportional to r^2. By contrast, the effects of dissipation tend to decrease with distance; close to the source, much energy is expended in pulverizing and fracturing rock, but at distant range the wave is elastic and not subject to much loss.

For a simple wave. the energy is proportional to the square of the amplitude. The area traversed by the wave front is a spherical surface, and thus the energy is spread over an area that increases with r^2. The *energy per unit area* is then inversely proportional to r^2. The *amplitude* is thus inversely proportional to r. If the wave propagation were

perfectly lossless, with no dissipation of energy in the medium and no change of wavelength, the amplitude I would attenuate as

$$I = I_*(r/r_*)^{-1} \tag{8}$$

where I_* and r_* are reference values of amplitude and radius respectively, and a finite lower limit is set for r. In air, pressure wave attenuation far from the source is not much more rapid than $1/r$, and in water the attenuation follows an approximate $1/r$ trend even at fairly close range.

In general, it is to be expected that energy will be absorbed, or dissipated, as a wave travels through any real material. Whatever the term used for the dissipation (internal friction, absorption, etc.), the expectation is that the amplitude of a plane wave (no spreading) will attenuate exponentially, i.e.

$$I = I_0 e^{-\alpha r} \tag{9}$$

where I_0 is the amplitude at $r = 0$ and α is an attenuation constant with the dimension of (length)$^{-1}$.

Combining the effects of geometrical spreading and internal dissipation, a rational form for the attenuation relation of a non-dispersive wave in isotropic material is

$$I = I_0(r/r_0)^{-1} e^{-\alpha r} \tag{10}$$

where r_0 is a lower limit of r, approximately equal to the charge radius, and I_0 is the value of I at $r = r_0$.

Equations similar to eq 10 are used in geophysics to express the attenuation of seismic waves, and applicability to explosive stress waves in rock has been demonstrated by Duvall and Petkof (1959) and by Atchison and Roth (1961). Equation 10 can be written in logarithmic form as

$$\ln\left[\frac{I}{I_0}\left(\frac{r}{r_0}\right)\right] = -\alpha r \tag{11}$$

and therefore a semi-log plot of the product Ir (log scale) against r (linear scale) should be a straight line, with the slope giving α. Duvall and Petkof (1959) plotted data for the peak amplitude of strain waves, and obtained linear trends for many different explosives, four different rock types, and various charge sizes. Fogelson et al. (1959) did similar work with six different explosives in granite. Atchison and Roth (1961) obtained similar results for strain waves in marble. Values of the attenuation constant α were found from the slope of the regression line. All data were for the elastic region, starting just outside the limit of major cracking. Scaled values of α by Duvall and Petkof varied slightly with the explosive type, but mean values were:

Granite	0.034 (ft/lb$^{1/3}$)$^{-1}$
Sandstone	0.048 (ft/lb$^{1/3}$)$^{-1}$
Chalk	0.027 (ft/lb$^{1/3}$)$^{-1}$
Shale	0.026 (ft/lb$^{1/3}$)$^{-1}$

A value of 0.085 (ft/lb$^{1/3}$)$^{-1}$ was accepted for marlstone, but the data show a distinct break in slope on the semi-log plot. Fogelson et al. (1959) found a mean value of 0.031 (ft/lb$^{1/3}$)$^{-1}$ for granite. The scaled values listed above are applicable when r is used in corresponding scaled form. If r is expressed in feet, then the values of α given above are numerically equal to values of α in ft^{-1}. Atchison and Roth (1961) give a mean value for marble of $\alpha = 0.011$ ft^{-1}. Taking α with dimensions (length)$^{-1}$, the SI equivalents of these values are:

Granite	0.110 m^{-1} (0.103 m^{-1})
Sandstone	0.158 m^{-1}
Chalk	0.088 m^{-1}
Shale	0.086 m^{-1}
Marble	0.037 m^{-1}

While eq 10 has some attractive features, its applicability is likely to be restricted to a certain range of radius, in the same way as the power relation is restricted, since the dissipation mechanisms are very different at different ranges (e.g. crushing, fracture, anelastic vibration). Attenuation by internal dissipation is also dependent on frequency; in general, attenuation rate increases with increase of frequency. High frequency components of a complex wave tend to be filtered out first, and the frequency characteristics are thus changed at long range. This effect may be fairly insignificant in some materials, but not in others. Finally, the geometric attenuation is only a $1/r$ function for a non-dispersive wave, or a pulse with constant phase duration.

Taking a purely empirical approach, measured relations between I and r can be described very well by a polynomial, e.g.

$$I = a_1 r^{-1} + a_2 r^{-2} + a_3 r^{-3} \tag{12}$$

in which the coefficients a_n are curve-fitting parameters and the radius r can be expressed in any convenient scaled form. However, there is little point in fitting a polynomial to badly scattered

data over a small range of r while ignoring boundary conditions. Some empirical attenuations obtained in this way give ridiculous values of I when the charge radius is substituted for r (e.g. Henrych 1979).

Whatever the relative merits of different attenuation relations for wave amplitude, the simple inverse power relation is still the most favored form in explosion technology. It embraces all types of attenuation arising from geometry, absorption, dispersion and frequency filtering. It is simple, convenient and, when appropriately restricted, quite acceptable. To avoid problems with dimensions and boundary conditions, the power relation can be written as

$$I = I_0(r/r_0)^{-n} \qquad (13)$$

where I_0 is the amplitude at the lower limit of applicability for distance, r_0. For lossless propagation, such as might occur with an acoustic wave in an ideal elastic medium, $n = 1$. Where there is dissipation, $n > 1$; in rocks, $n \approx 2$ is common and in soils n can be as much as 3 to 4 at close range.

Cylindrical symmetry

With ideal cylindrical propagation, the energy per unit area of wave front is proportional to the radius r and therefore the wave amplitude is inversely proportional to $r^{1/2}$. This is the same as the stress/distance relation for a static elastic stress field (eq 3). If attenuation is expressed in the form of eq 13, perfectly lossless propagation is represented by $n = 1/2$. When there is dissipation, $n > 1/2$ but it should be a bit less than the corresponding value for spherical propagation. Henrych (1979) gives a value of $n = 1.44$ for sandy loam at fairly long range ($r/r_0 > 30$).

ATTENUATION OF STRESS, STRAIN AND GROUND MOTION

Just as in water and air, the amplitude of the spherically propagating shock front decreases with increasing radius from the charge. However, the stress field created in a solid by a shock wave or an elastic wave is not isotropic, as it is in water and air; the radial and circumferential stress components are not necessarily equal outside the close range "hydrodynamic" zone. In a fluid there is only a compression wave, whereas in a solid there is, in the elastic response range, a compression wave (P-wave) oscillating in the radial direction, plus a shear wave (S-wave) oscillating transversely to the radial direction. The front of a shock wave can be characterized by the peak radial stress, and this can be plotted against scaled radius to give attenuation curves for various types of ground materials. Measurements of shock pressure in solid materials are more difficult and uncertain than corresponding measurements in water and air. In addition to the usual problems of frequency response and calibration for the gauges, there are problems of coupling, impedance matching, and directional resolution. Furthermore, measurements may be affected by proximity to the surface, and also by anisotropy and inhomogeneity in the ground material.

Attenuation data for peak radial stress

Figure 7 gives a compilation of results for the attenuation of peak radial stress in *granite* when the test conditions are such as to approximate spherical symmetry. Data for extremely high stress levels refer to nuclear explosions, which can induce close-range pressures greater than the detonation pressure of high explosives. The nuclear data are from tests designated Hardhat (5 kilotons, 290 m depth), Shoal (12.5 kilotons, 366 m depth), and Piledriver (50 kilotons, 460 m depth). Different authors interpret the same measurements in slightly different ways. One of the low stress curves seems erroneous, perhaps because of incorrect conversion of units. The high explosive data by Noren (DuPont) are for water pressure in boreholes, which is not necessarily the same thing as rock stress. However, if the analysis of Khristoforov and Romashov (1967) is applied to Noren's data, the agreement with the other results is excellent. Taking a representative line through all of the credible data, the decay of stress with distance is very close to an inverse square relation (actual exponent -1.92) for distances out to about 25 ft/lb$^{1/3}$ (10 m/kg$^{1/3}$).

Figure 8 gives some attenuation data for spherical propagation in *volcanic tuff*. In this material, stress levels are somewhat lower than they would be in granite at the same range. Overall, the decay of peak stress with distance is very close to an inverse square relation for distances out to about 25 ft/lb$^{1/3}$ (10 m/kg$^{1/3}$). Comparable data for *alluvium* are shown in Figure 9.

Smith (1966) gave decay exponents for a variety of materials. Not all of the values given are accepted by this writer, but results for dry sand, clay, silt and loess indicate close-range attenuation with an exponent of -4 (Fig. 11).

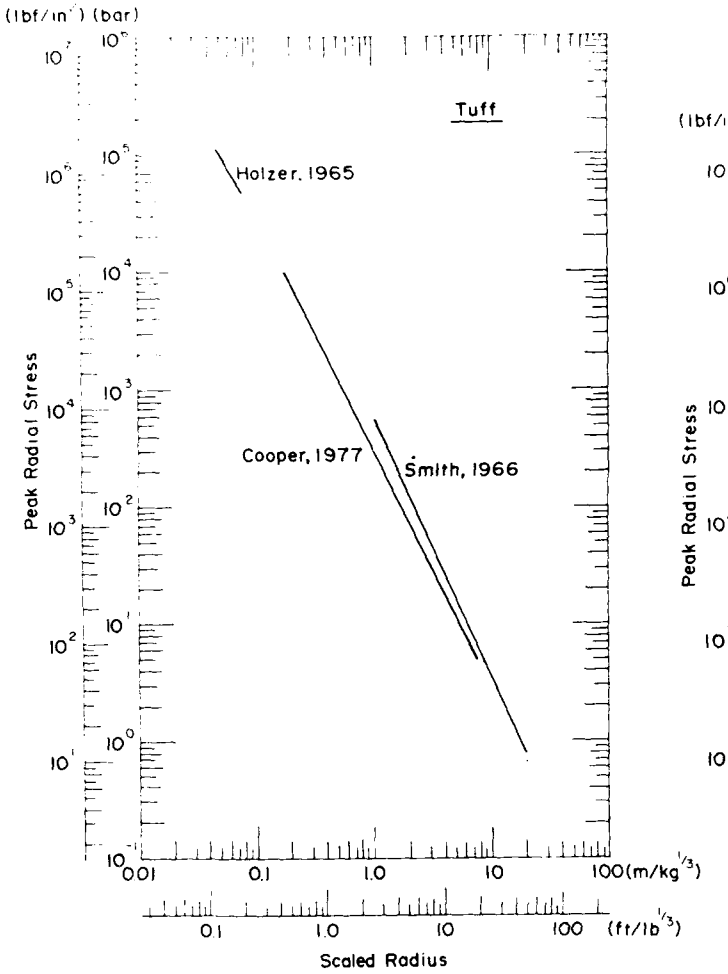

Figure 8. Stress attenuation data for spherical propagation in volcanic tuff.

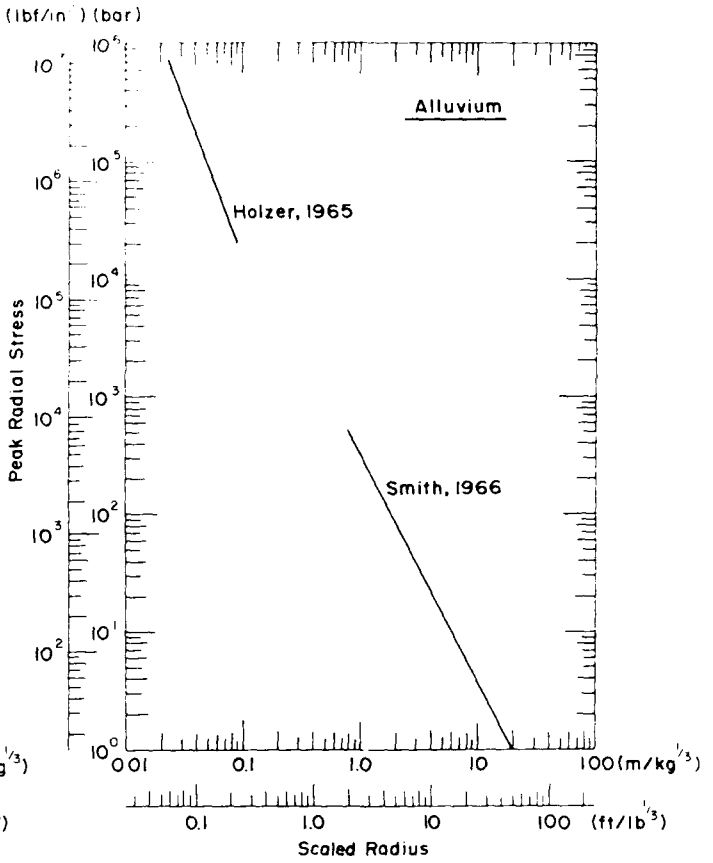

Figure 9. Stress attenuation data for spherical propagation in alluvium.

Henrych (1979) shows how the stress attenuation in sand varies with the water content and the air content (or dry bulk density). For saturated sand, the attenuation exponent is -1.05 with zero air content, -1.5 with 5×10^{-4} air content, -2.0 with 10^{-2} air content, and -2.5 with 4×10^{-2} air content. In other words, saturated sand with no air gives attenuation like water, while saturated sand with plenty of air bubbles gives attenuation like rock. For unsaturated sand of dry bulk density ϱ, the attenuation exponent was -2.8 for ϱ = 1.6-1.7 Mg/m³, -3.0 for ϱ = 1.52-1.6 Mg/m³, and -3.5 for ϱ = 1.45-1.5 Mg/m³.

The attenuation of stress in *glacier ice* and in *deposited snow* is illustrated in Figure 10. In *ice*, stress appears to decrease with distance raised to the power -2.3, a decay rate that is a bit more rapid than rates found in typical rocks, and much faster than the decay rate for liquid water (see Part II, Fig. 1). Within the range of available data, overpressures in ice are well below the values for corresponding distances in water. By comparison with granite (Fig. 11), overpressures in ice are lower than the values in granite at close range (< 1 m/kg$^{1/3}$), but comparable at longer distances (e.g. 10 m/kg$^{1/3}$). Attenuation in *dense snow* appears to be strong in the near field; the decay exponent is -3.75, or close to the approximate value of -4 that was given above for near-range attenuation in soils. Within the range of existing data, the peak stresses in snow are lower than corresponding values in air, water, ice, rocks and typical soils (Fig. 11).

Attenuation data for peak strain

In some attenuation studies the emphasis has been on strain rather than stress. Figure 12 represents a compilation of data for the attenuation of peak radial strain with distance for various types

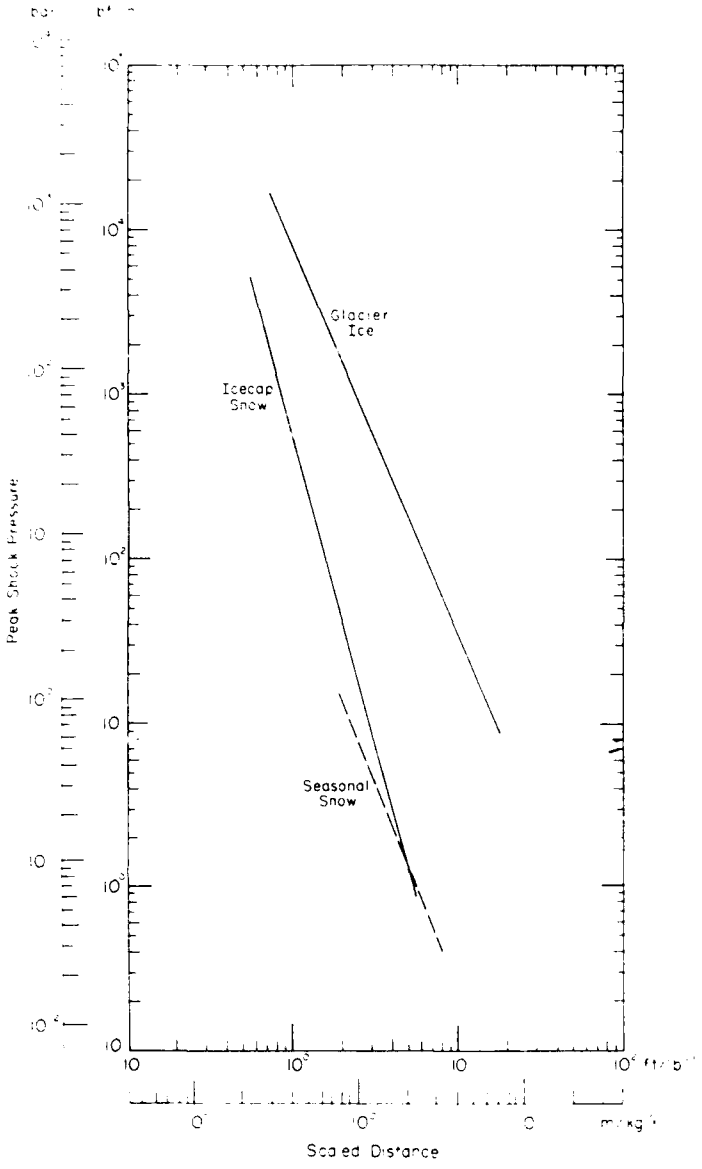

Figure 10. Stress attenuation for spherical propagation in glacier ice and deposited snow. (Ice data from Ingram and Halper 1960, Livingston 1960, Joachim 1967. Snow data from Ingram and Strange 1958, Ingram and Halper 1960, Joachim 1967, Livingston 1968.)

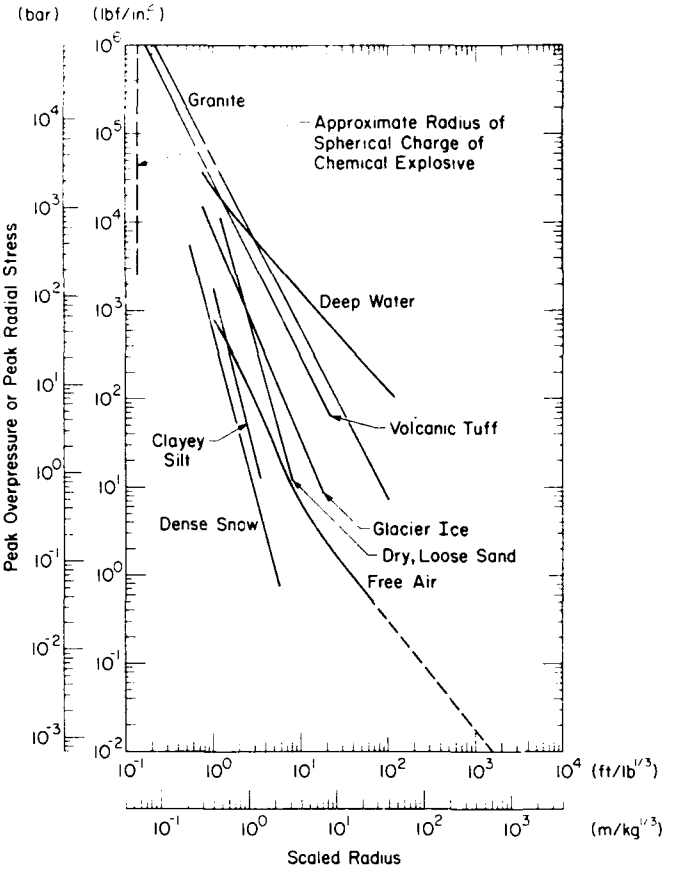

Figure 11. Comparison of stress attenuation for spherical propagation in water, air, rocks, soils, snow and ice.

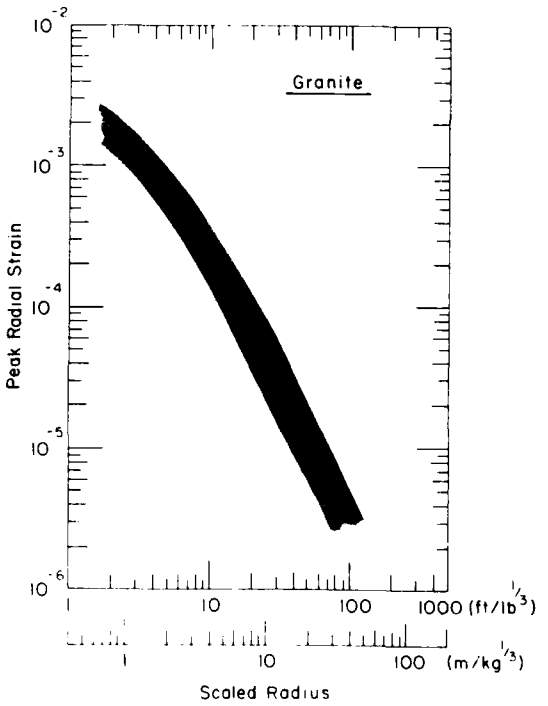

Figure 12. Attenuation of peak radial strain for spherical propagation in granite. (Data from Duvall and Atchison 1957, Atchison and Tournay 1959, Duvall and Petkof 1959, Atchison and Pugliese 1964, Nicholls and Hooker 1965.)

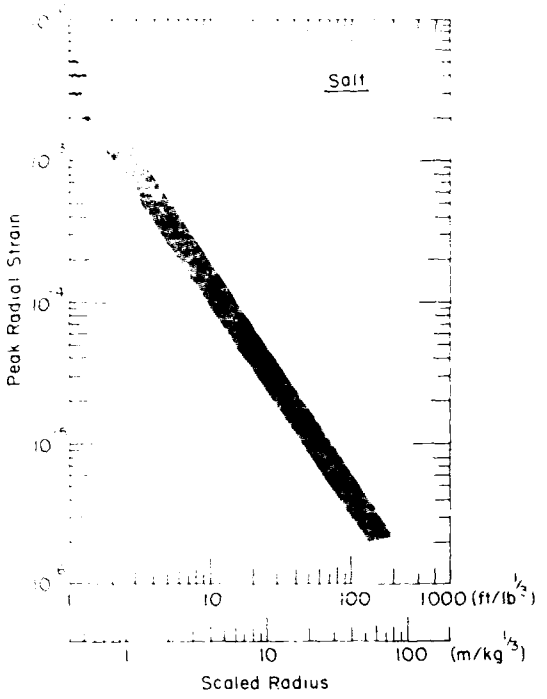

Figure 13. Attenuation of peak radial strain for spherical propagation in salt. (Data from Nicholls 1962, Nicholls and Hooker 1962a.)

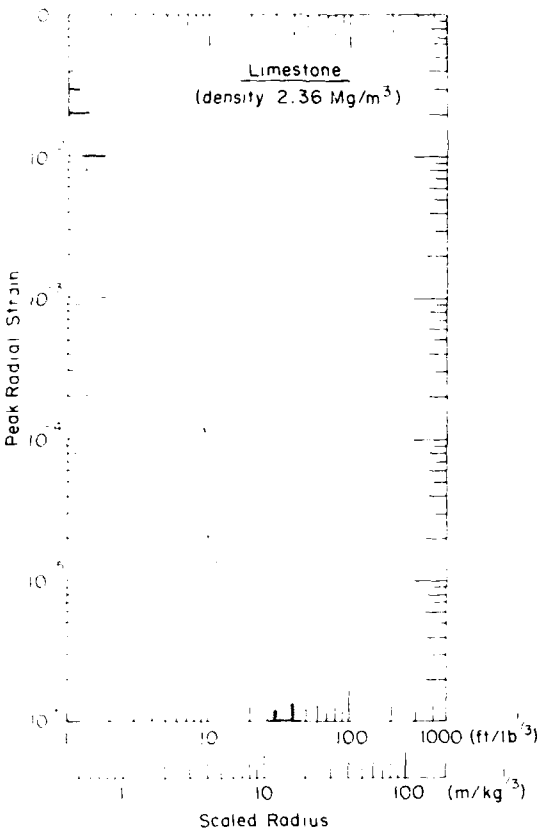

Figure 14. Attenuation of peak radial strain for spherical propagation in limestone. (Data from Atchison and Pugliese 1964b.)

of high explosive in *granite*.* Beyond the range where the peak compressive strain is comparable to the failure strain of the rock, the response should be approximately elastic, and related to the peak stress components through the elastic moduli. In this elastic range, peak strain appears to be inversely proportional to the square of distance from the charge, which is in agreement with the stress attenuation. The test results may be influenced by proximity of the wave to the surface.

Figure 13 gives an impression of the attenuation of peak radial strain in *salt*. The original reports have the detailed data points fitted by a line that changes slope on the log-log plot, with slightly steeper slope at the shortest distances. Overall, the combined results follow a trend in which peak strain is approximately proportional to radius raised to the power $-3/2$.

Figure 14 gives strain attenuation data for a variety of explosives detonated in a *limestone* (density 2.36 Mg/m^3). The original authors (Atchison and

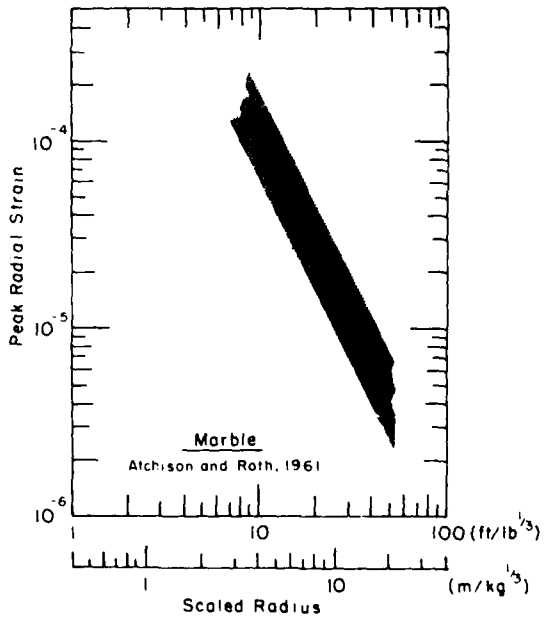

Figure 15. Attenuation of peak radial strain for spherical propagation in marble. (Data from Atchison and Roth 1961.)

* Data from Nicholls and Hooker (1962b) have been omitted. They do not fit the general trend, and the same test results seem to have been used to give different values of strain in a later report (Nicholls and Hooker 1965).

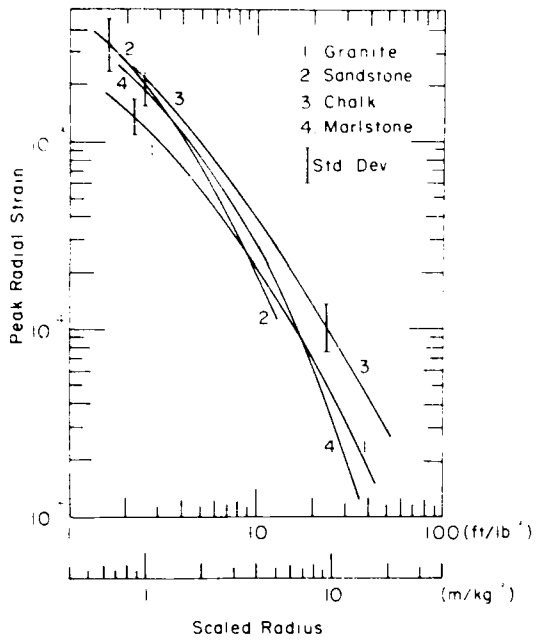

Figure 16. Comparison of attenuation curves for peak radial strain in four different rocks. (Data from Duvall and Atchison 1957.)

Pugliese 1964b) fitted power relations to their data so as to give an exponent of -2.64 for all explosive types, but the inverse cube trend shown in Figure 14 is an adequate approximation for the overall data band.

Figure 15 indicates the strain levels recorded in *marble* for a variety of explosives. The data band has been drawn here to represent inverse square decay.

In Figures 12–15, the range of variation for the strain at a given scaled distance probably represents variation of explosive type. The differences in detonation velocity (or pressure) produce differences in impedance matching between different explosives and the rock. In the original studies by the U.S. Bureau of Mines, the charges filled the diameter of the shothole at the required depth, but the explosives were chosen so as to cover a wide range of detonation velocity, and hence a wide range of characteristic impedance (product of density and velocity).

Figure 16 compares average attenuation curves for four different rock types. Each curve represents an average for several types of explosives, with detonation velocities ranging from 6500 to 21,000 ft/s (2000 to 6400 m/s). The left side of the plot represents the response of the rock where strains are greater than, or comparable to, the failure strains for uniaxial stress. The trend to a low attenuation rate near the source, seen also in Figure 12, could be interpreted as an indication of a limiting compressive strain at close range.

Attenuation of displacement, velocity and acceleration

For some purposes, the internal stresses and strains of the ground material are of less interest than the displacement and its time derivatives, i.e. velocity and acceleration. This is particularly true in the outer zone of elastic disturbance, where the effects are of a seismic nature.

If a wave travels through a medium, passage of the disturbance causes each particle of the medium to be displaced a distance x in time t, where t is the time for first arrival of the wave at that particle. The instantaneous particle velocity is $\Delta x/\Delta t$, or dx/dt; the instantaneous acceleration is d^2x/dt^2. The particle actually oscillates about its original position, and if the disturbance is idealized as a simple sine wave, the displacement x can be expressed as a function of time:

$$x = A \sin \omega t = A \sin(2\pi f t) \tag{14}$$

where A is the amplitude of the sinusoidal displacement, ω the angular frequency and f the frequency in cycles per unit time. The particle velocity v is thus

$$v = \frac{dx}{dt} = A\omega \cos \omega t$$
$$= A 2\pi f \cos(2\pi f t) \tag{15}$$

and the acceleration a is

$$a = \frac{d^2x}{dt^2} = -A\omega^2 \sin \omega t$$
$$= -A(2\pi f)^2 \sin(2\pi f t). \tag{16}$$

The peak values of displacement, velocity and acceleration are

$$x_{max} = A \tag{17}$$

$$v_{max} = 2\pi f A \tag{18}$$

$$a_{max} = (2\pi f)^2 A \tag{19}$$

and the maximum value of velocity is $\pi/2$ out of phase with the maximum values of displacement and acceleration.

Recalling the shock equations, outlined previ-

ously in connection with air blast (Part I), it can be seen that there is a relation between particle velocity and overpressure. Thus, in principle, measurements of peak velocity can give corresponding values of peak pressure. However, to make this conversion, the relation between pressure and density for the ground material must be known. This relation is the Rankine-Hugoniot characteristic.

Close to the source of an explosion, the radiating stress wave is certainly not sinusoidal—for the positive phase, the rise of pressure with time is very abrupt, while the decay with time is quite gradual and approximately exponential. As the wave propagates outward, the front becomes less steep, the positive phase duration may increase, and a plot of displacement against time for the positive phase may take on the approximate shape of half a sine wave. Thus the sinusoidal approximation is not too bad for the elastic range of behavior beyond the hydrodynamic zone.

Ground motion from deep explosions is scaled on the assumption of spherical symmetry, which is fully justified for uniform isotropic material. As usual, radius r is scaled with respect to the charge radius R_c, or to the cube root of charge weight $W^{1/3}$. Particle velocity v is not scaled, just as peak overpressure is not scaled in attenuation relations. Because time intervals for explosion effects scale in proportion to charge radius or the cube root of charge weight (see Part I), the accelerations and displacements, being time derivatives and integrals of velocity respectively, have to be scaled with respect to R_c or $W^{1/3}$. Anticipating a linear trend of data on log-log plots, the general form of the attenuation relations for spherically symmetric ground motion would be

$$v_{max} = K_1 \left(\frac{r}{R_c}\right)^{-n_1} = K_1' \left(\frac{r}{W^{1/3}}\right)^{-n_1} \quad (20)$$

$$\frac{x_{max}}{R_c} = K_2 \frac{x_{max}}{W^{1/3}} = K_2' \left(\frac{r}{R_c}\right)^{-n_2}$$

$$= K_2'' \left(\frac{r}{W^{1/3}}\right)^{-n_2} \quad (21)$$

$$a_{max} R_c = K_3 a_{max} W^{1/3} = K_3' \left(\frac{r}{R_c}\right)^{-n_3}$$

$$= K_3'' \left(\frac{r}{W^{1/3}}\right)^{-n_3} \quad (22)$$

where K is a coefficient and n is an exponent in each relation.

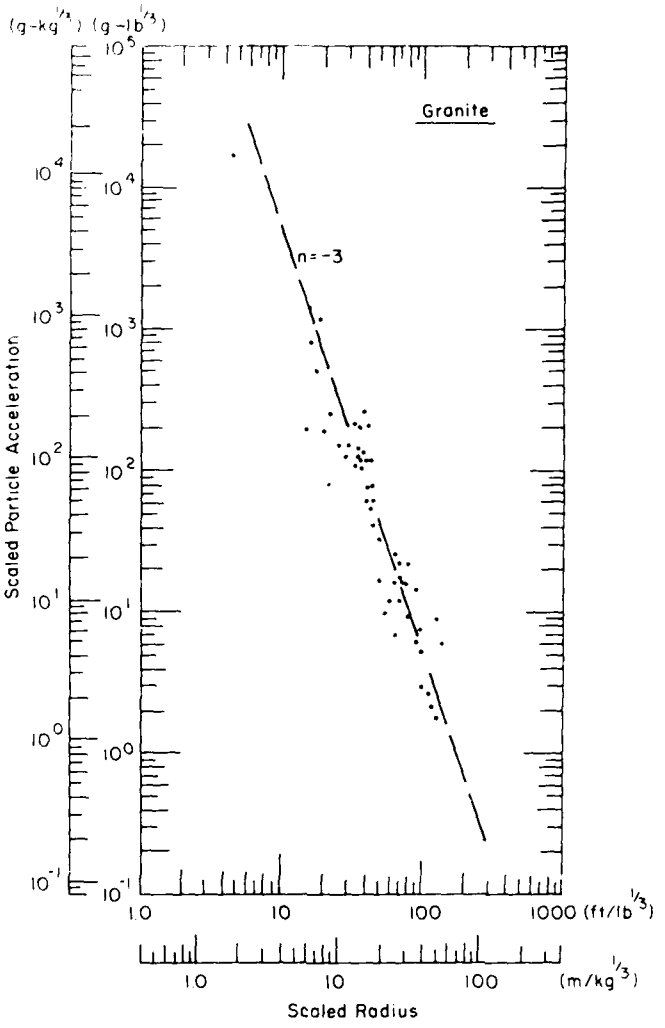

Figure 17. Attenuation of particle acceleration for spherical propagation in granite. (Data from Nicholls and Hooker 1965.)

Data for approximate spherical propagation have been published by Nicholls and Hooker (1965), who fired high explosives in granite. The original data have been re-scaled with respect to charge weight and plotted in Figures 17–19. These results refer to a range of scaled distance that is further from the source than the range for the stress and strain plots. Plots by the original authors omitted some data points and fitted trend lines of shallower slope. The acceleration data (Fig. 17) show a trend that is close to inverse cube decay, i.e. n_3 in eq 22 is approximately 3. The data for velocity and displacement (Fig. 18 and 19) appear to attenuate less rapidly, with n_1 and n_2 in eq 20 and 21 approximately 2.5.

Henrych (1979) considers that internal dissipation in soils is negligible, so that velocity attenu-

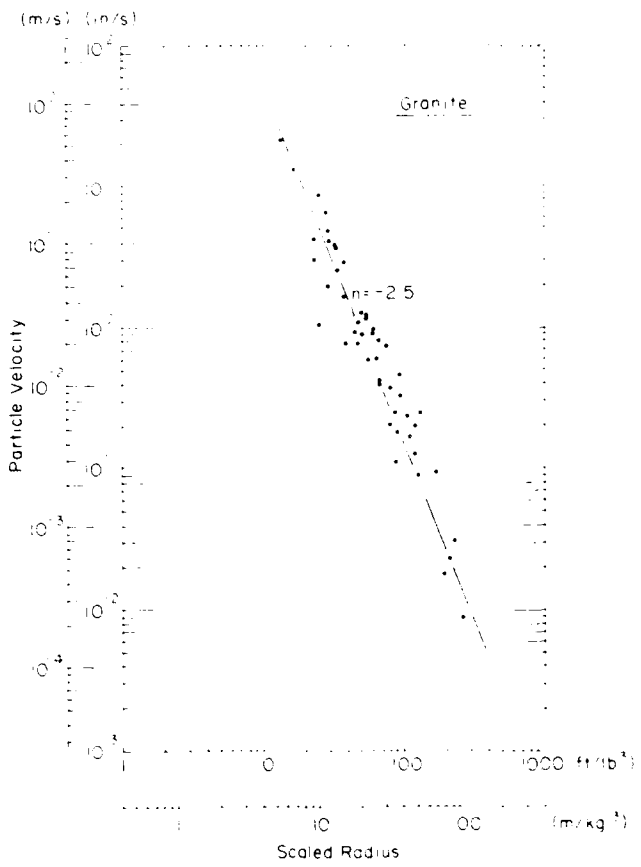

Figure 18. Attenuation of particle velocity for spherical propagation in granite. (Data from Nicholls and Hooker 1965.)

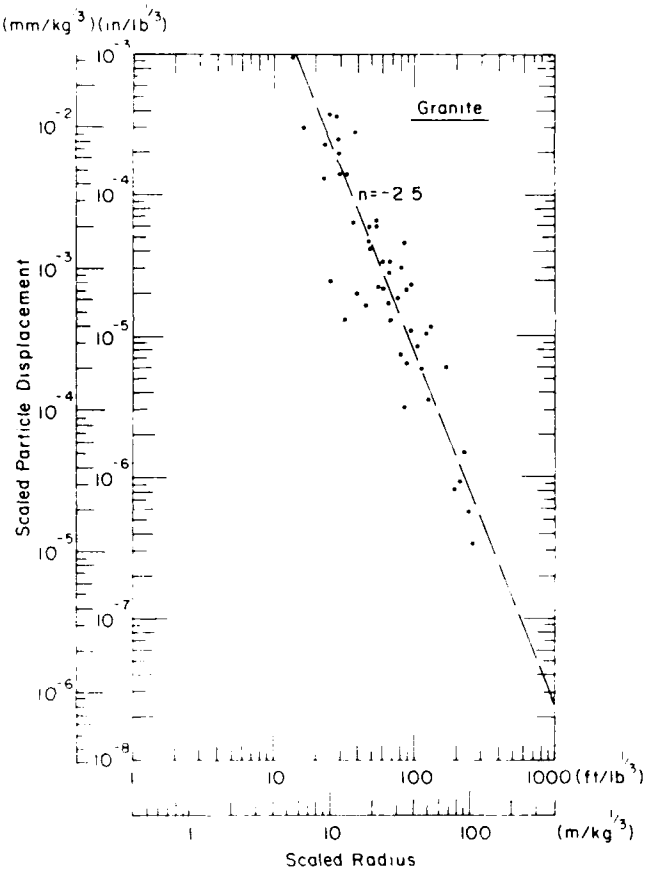

Figure 19. Attenuation of particle displacement for spherical propagation in granite. (Data from Nicholls and Hooker 1965.)

ates with $n_1 = 2$. He illustrates test data that show $n_1 = 2$ for both soils and hard rocks, which is rather surprising (range was 1.5 to 150 m/kg$^{1/3}$).

Attenuation of ground motion is dealt with again in a later section, where the concern is the more common one of ground motion near the surface.

STEMMING OF SHOTHOLES

Traditional stemming materials include sand, fine gravel, crushed stone, or mixtures of fine-grained soil (silt, clay) with coarse granular material (sand, gravel). The particle size should not exceed 10% of the hole diameter. Layers of different material are sometimes placed in the column, e.g. clay above the charge, followed by sandy gravel, followed in turn by coarse gravel. Special stemming material packaged in bags or cartridges can be purchased, and special bags are available for packaging standard material on site. Drill cuttings are also used to backfill shotholes, especially when the holes are of relatively large diameter and the cuttings are coarse. In underground mining, cartridges of non-combustible foams, pastes or gels are sometimes used. In recent years, it has been accepted that water alone is often as good as, or better than, traditional solid stemming in both vertical and horizontal shotholes (Anon. 1970, Gillespie 1972, Knudson et al. 1972, Rooke et al. 1974). Water has appreciable practical advantages over solid materials, which have to be procured, delivered to the job site, and loaded into the hole relatively slowly. Provided the hole is reasonably watertight and has a downward inclination, then direct filling with water is cheap and easy. Apart from the fact that some holes are not watertight, the only major disadvantage with this procedure is incompatibility with explosives that have poor water resistance (e.g. unpackaged ANFO). These objections to water stemming can be overcome by

packaging the water in special self-sealing plastic tubes, ampoules or bags, which can also be placed in horizontal holes. Water stemming has become important, or dominant, for shot-firing in West European coal mines in recent decades (Anon. 1970). Special water-filled ampoules are packed tightly in the shothole with positive restraint; the advantages include suppression of dust, fumes, ignition and ejected fragments. In frozen ground or massive ice where the temperature is well below 0 °C, a solid plug of stemming can be formed by freezing water, water ice slurry, or wet soils.

The length of stemming needed to contain a cratering explosion does not seem to have been investigated systematically. Practical guidelines for crater blasting may recommend backfilling to one-third or to one-half of the hole depth, which is not completely rational. A more reasonable expectation for this situation is that the required length would be a function of the hole diameter, the properties of the stemming material, and the charge depth. For well-placed granular material that tends to lock under pressure, an absolute lower limit for the required length of stemming might be about 10 hole diameters, but it is probably prudent to fill to at least 20 hole diameters. In bench blasting, where stemming extends from the top of the charge to the surface, the required length of stemming ("collar distance") is typically taken as proportional to the burden, which itself is a multiple of the hole diameter. These recommendations translate to 14 to 28 times the hole diameter. Fourney et al. (1985) found that a ratio of at least 26 was needed for complete "bridging" and sealing. When using water for stemming, the best practical guidance is to fill the hole completely.

Small "blocking charges" are sometimes placed between sections of inert stemming. These fire at the same time as the main charge, pressurizing the column of stemming so as to resist blowout.

SHALLOW SUBSURFACE EXPLOSIONS

The foregoing is concerned mainly with deep explosions, where the effects are fully contained and the disturbance spreads in a symmetrical pattern that is either spherical or cylindrical, depending on the charge geometry. A different situation prevails when the charge is at shallow depth; the ground surface then breaks out and releases detonation products, forming a crater (Fig. 20), a trench, or a planar surface, depending on the geometry and layout of the charge or charges. Even when the charge is below the *critical depth*, where breakout ceases, the ground disturbance (stress, strain, displacement, acceleration) is affected by proximity to the surface and by the lack of three-dimensional symmetry in the field of propagation.

CRATER FORMATION

For purposes of discussion and analysis, a cratering charge is assumed to be a concentrated charge of high explosive, ideally spherical but usually cylindrical. A cylindrical charge with length/diameter ratio less than four produces results that are indistinguishable from those of a spherical charge, and length/diameter ratios up to six are usually considered to give a "concentrated" charge. When cratering data are given, it is also assumed that the charge lies at the base of a narrow drill hole, with 100% geometric coupling, and the hole is assumed to be adequately stemmed. The ground surface is assumed to be horizontal, so that gravity body forces in the ground and gravity forces on displaced fragments act in a radially symmetric pattern.

Crater geometry varies considerably, depending mainly on the scaled charge depth and the properties of the ground material. However, Figure 20

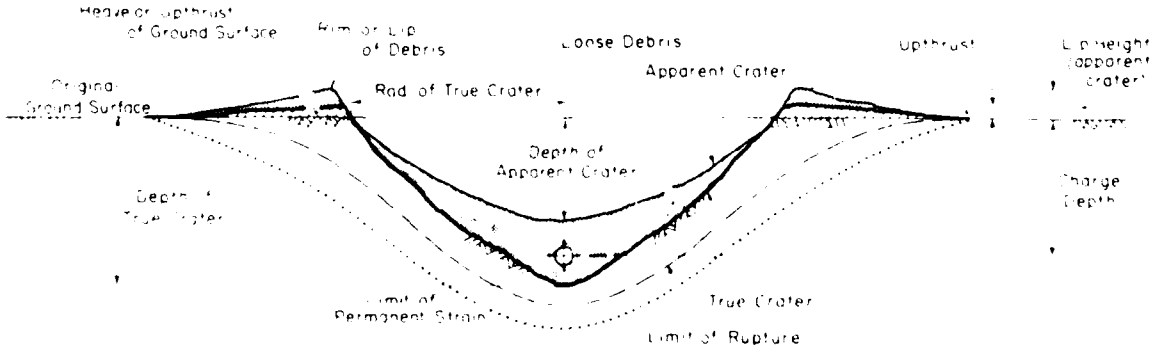

Figure 20. Crater terminology.

serves to illustrate the general features of a typical crater. Charge depth is measured from the original surface to the center of gravity of the charge. After detonation, some material, mainly in a conical zone above the charge, is completely fractured and subjected to large displacements. Fragments are thrown upward and outward; in general, some of this material is ejected and some falls back into the crater. The ground slightly more distant from the charge is fractured or otherwise strongly disturbed, but it is not detached from the parent mass. At still greater distance the explosion may produce permanent strain in the ground material, but there is no obvious damage. Beyond this zone, the ground experiences transient stress, strain and displacement, but there are no permanent changes.

A typical crater in rock (Fig. 20) is seen as a bowl-shaped depression with a rim of debris. This open hole is called the *apparent crater*, and its sides and base are formed mainly by shattered debris. If all the loose debris is dug out and cleared away, the *true crater* appears. It is bounded by material that has been damaged, but not grossly displaced. The true crater has a slightly raised rim where the original ground surface has been heaved or peeled back. Further excavation or core drilling reveals a transition zone in which the damage or permanent strain becomes progressively less severe with increasing distance from the surface of the true crater. Some military texts use very elaborate schemes for defining zones of disturbance beyond the boundary of the true crater, and they also employ a highly detailed set of characteristic crater dimensions. For most practical purposes other than research, these intricacies can be ignored; there are no sharply defined boundaries between zones that experience different degrees of strain. Figure 20 gives a representation that is adequate for most purposes.

The process of crater formation starts with transmission of a shock wave from the charge to the surrounding material, as in a deep underground explosion. The efficiency of shock transmission from the charge to the ground depends on the geometric coupling and the impedance match, as described earlier for deep explosions. With efficient shock transmission, the ground material immediately adjacent to the charge undergoes intense compression and it is completely pulverized. This material is also displaced radially, forming a cavity that is considerably bigger than the original charge. This cavity is pressurized by expanding gas from the explosion. Around the crushed zone, cracks radiate outward, some of them reaching the ground surface, or coming close to it. As the shock radiates outward it reaches the surface and reflects.

The shock is the first disturbance to reach and displace the ground surface. The reflection of the shock as a tensile pulse causes small particles and larger spall fragments to break loose and jump into the air. The vertical ejection velocity decreases with the horizontal radius from surface zero, as described previously for the surface effects of underwater explosions (Part II). If the explosion is fairly deep (by cratering standards), this surface spalling only affects a relatively thin surface layer.

Radial cracks probably reach the vicinity of the ground surface later than the shock; if they form by extension from the pressurized blast cavity, their propagation speed is much lower than the shock velocity (about 20% of the acoustic *P*-wave velocity). These cracks, and their radial limits relative to the ground surface, help to define the limits for the final conical breakout of fragmented material.

While the shock produces only transient stress waves of limited thickness, the pressurized blast cavity establishes behind the intial shock an overall stress field that is more akin to a static elastic stress field. This stress field is influenced by proximity to the surface; there is yielding towards the surface, and the blast cavity expands preferentially in the direction of the surface.

Growth of the gas bubble displaces and separates the cracked material; the surface rises in a mound and accelerates, with velocities greatest near the center, thus producing progressive steepening of the mound. As the ground domes upward, the large tensile strains in the convex area tend to form two orthogonal crack systems, one in the radial (meridional) direction and the other in the circumferential (latitudinal) direction. These cracks increase in width progressively as the surface layer pushes up and stretches. The gas then vents through the fissures of the rising mound, typically forming a fountain of faster ejection plumes that shoot out of the top of the dome. Small fragments carried in these plumes may be fired to great height or over long horizontal distance. The bulk of the material usually drops back into the crater and onto the area immediately surrounding the crater.

A charge lying on the ground surface does not make a big crater, but it can fire debris a long way. Burial of the charge at shallow depth produces a large increase in crater size. By increasing the charge depth, the surface radius of the crater even-

tually reaches a maximum. This is a type of crater likely to be advantageous in military engineering. At somewhat greater charge depth, the volume of the true crater reaches a maximum, without much reduction of the surface radius. This gives maximum efficiency when broken material is excavated by a secondary mechanical process. Still further increase of charge depth subdues the eruption to the point where fragmented material heaves up into the air and then flops back into the crater, leaving a mound of bulked material on top. This type of crater is likely to be advantageous in civil construction, since it is deep and steep, and there is very little flyrock. At slightly greater charge depth, crater formation ceases. This is termed *critical charge depth*. The charge forms a subsurface cavity, as described earlier, and in competent material there may be slight heave and cracking at the surface. In some materials (e.g. soils or weak rocks), the cavity can collapse and cause minor subsidence at the ground surface, even when the absolute values of charge depth and charge size are small. Most rocks collapse to form these vertical "chimneys" when nuclear explosions occur at great depth.

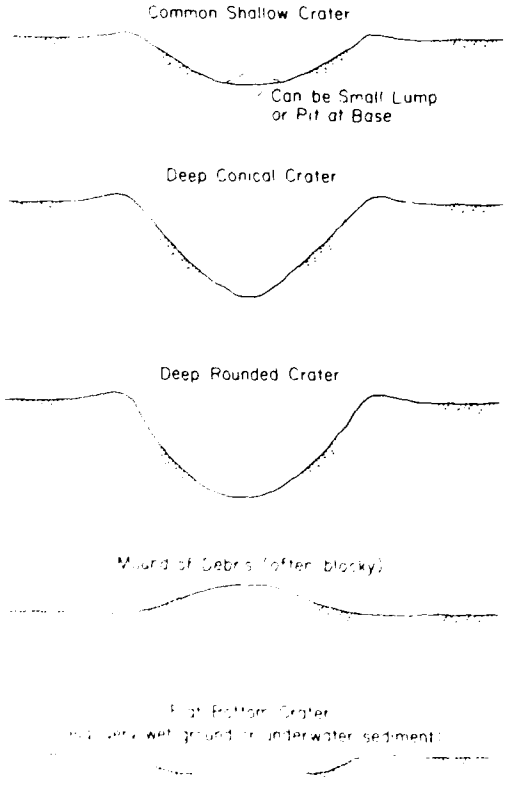

Figure 21. Cross sections of apparent craters.

Craters are usually thought of as conical or bowl-shaped, and as a general idea this is not far from the truth, for the true crater and often for the apparent crater. However, apparent craters can vary greatly, from pits to surface mounds, depending on charge depth, variations in ground material, and differences in the behavior of the fallback debris. Figure 21 gives some examples of cross-section shapes for apparent craters.

Soviet writers use a "crater shape characteristic" n that is the ratio of crater radius, r, to charge depth, d_c; i.e. $n = r/d_c$ (see Henrych 1979). The value $n = 1$ (i.e. $r = d_c$) gives the so-called "standard crater." As can be seen from the data compilations that are given later in this section, $n = 1$ is hardly "standard" in rocks and other competent materials. If this value is reached at all, it occurs with charges that are just a bit shallower than critical depth.

CRATER SCALING

Crater dimensions, and also the trajectories of flyrock, are scaled in order to remove the effect of charge size, thereby facilitating comparisons of test data. As for other explosion phenomena that involve concentrated charges and three-dimensional effects, an obvious first approximation for adjusting crater dimensions is cube root scaling, which implies geometric similarity. In other words, linear dimensions are scaled with respect to charge radius (giving a dimensionless variable), or with respect to the cube root of charge weight or energy (giving physical dimensions that are ugly but convenient). However, both theoretical reasoning and experimental results suggest that there are other possibilities for scaling relations.

To simplify the considerations, we first assume that the ground material is isotropic, and that there is no overall variation of bulk properties (such as density, strength, and modulus) with depth or with radius from the shot point. We also ignore variation of explosive type, assuming that the mass and energy of the charge are proportional with a constant ratio.

If crater size is controlled by the inherent strength and density of the material, the effects of constant gravity can be neglected. Dimensional analysis then shows crater volume to be proportional to either charge mass or charge energy (see, for example, Holsapple and Schmidt 1980). For geometrically similar craters, corresponding linear dimensions are proportional to the cube root of charge

mass, or the cube root of charge energy. Use of cube root scaling in rock blasting goes back to the nineteenth century, when presumably it was deduced empirically.

By contrast, if gravitational effects are considered significant, the component of material strength that derives from gravity body forces increases with depth, and a significant amount of energy is needed to lift debris from the crater against gravity. If gravitational forces become dominant in controlling the crater formation, and if the gravitational acceleration remains constant, dimensional analysis shows crater volume to be proportional to charge energy raised to the power ¾. Thus, for geometrically similar craters, corresponding linear dimensions would be proportional to energy, or charge mass, raised to the power ¼. This is called fourth root scaling, or gravity scaling (White 1973, Holsapple and Schmidt 1980). Fourth root scaling also applies to underwater explosions when gravitational effects dominate over hydrodynamic effects (see Part II). Referring to Part II, this can be appreciated from eq 8, eq 18 and Figure 20 when conditions are such that the charge depth is proportional to the maximum bubble radius and is also much greater than the atmospheric head. Comparison with underwater explosions brings out the point that, for cratering in impermeable solids, the effective static pressure is the overburden pressure *plus* the atmospheric pressure.

In general, it would be reasonable to expect cube root scaling to apply where: 1) the scale of the problem is small, so that depths in the ground (or gravity body forces) are also small; and 2) the ground material has high inherent cohesive strength (not depending much on the overburden pressure). Fourth-root, or gravity, scaling might look like a better bet where: 1) very big charges are being used, so that depths and overburden pressures are relatively large; and 2) the ground material has little inherent cohesion, deriving its strength mainly from overburden pressure (like dry sand).

Most materials have finite shear strength, even under zero gravity, and in all terrestrial situations there are finite gravity body forces. Thus, in the real world, it might be expected that the scaling exponent for linear dimensions would vary between ⅓ and ¼. However, there are other complications, both theoretical and practical. Among the latter are: 1) variation of effective rock strength with the stressed volume (flaw probability), 2) variation of rock strength with strain rate (see Gaffney 1984a,b), and 3) the inevitability of rock variation with depth.

Direct experimental determination of crater scaling is quite difficult. Charge weight, or energy, has to vary by several orders of magnitude to get reliable results. At the same time, scaled charge depth has to be maintained constant, even though the scaling relation for charge depth is not known with certainty. Ideally, the ground material should be completely uniform, so that all tests are made in the same material. Finally, the same explosive should be used for all tests (equal energy for HE and nuclear explosions does not necessarily produce the same mechanical effects). The experimental scatter in field data is considerable, and replicate tests are needed to establish representative values for the crater dimensions. However, it is simply not feasible to have replications of very large experimental cratering explosions, especially nuclear ones.

Because of these complications, test results do not always define clear relations when crater dimensions are plotted against charge weight on logarithmic scales. Some specialists take limited available data for particular ground materials and particular moisture conditions and then derive scaling exponents by power law regression. This procedure results in exponents between, or even outside, the limits of ⅓ and ¼, and exponents are often given to three significant figures. Such a procedure does not commend itself to this writer; there is no strong reason to doubt that cube root scaling is applicable to most small explosions,

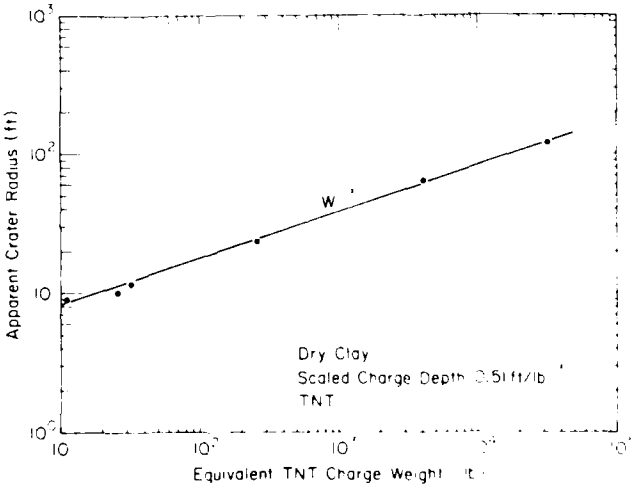

Figure 22. Radius of the apparent crater plotted against charge weight. Data are for TNT explosions in dry clay at a scaled depth of 0.51 ft lb^-1/3 (0.2 m kg^-1/3). (From data compiled by Rooke et al. 1974.)

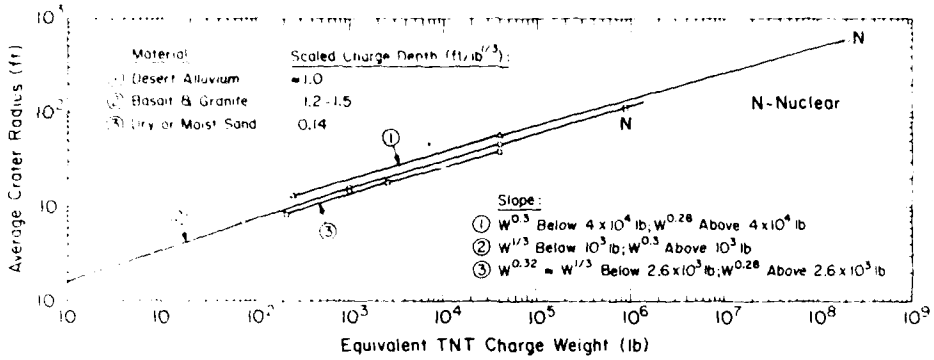

Figure 23. Radius of the apparent crater plotted against charge weight for chemical and nuclear explosions in various ground materials. (From data compiled by Rooke et al. 1974.)

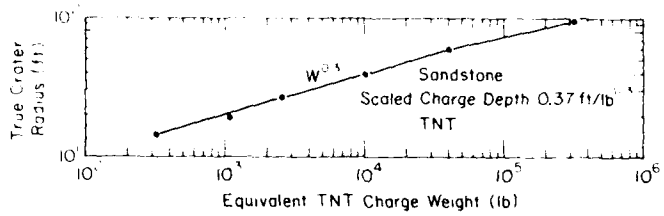

Figure 24. Radius of true crater plotted against charge weight for TNT explosions in sandstone at a scaled charge depth of 0.37 ft/lb$^{1/3}$ (0.15 m kg$^{-1/3}$). (From data compiled by Rooke et al. 1974.)

where gravity body forces are small, while a slow transition to fourth root scaling is to be expected as explosion size increases. Figures 22-24 demonstrate the applicability of cube root scaling in dry clay and hard rock for the apparent crater radius from large chemical explosions. However, for charges in the range 1 to 100 tons, a scaling exponent of 0.3 seems to give better representation of the data (Fig. 24).

CRATER DIMENSIONS

Crater dimensions for a given material are usually presented as plots of radius, depth and volume against charge depth. Linear dimensions may be scaled with respect to the cube root of charge weight, or with respect to equivalent charge radius. Volume is usually scaled with respect to charge weight, or energy yield. Because of the limitations of cube root scaling that were discussed above, the scaling factor may be charge weight raised to an arbitrary power (approximately 0.3). Most of the available data are for the apparent crater, which is easy to measure, although for some engineering purposes the dimensions of the true crater are more informative and useful. When the results of many cratering shots with widely varying charge weights and charge depths are compiled for a single ground material, there is usually wide scatter. The scatter tends to be greatest for charges that are close to optimum depth, probably because of the abrupt transition from optimum depth to critical depth. In this section, some test results are shown as data bands which represent the scatter that can be expected due to variations in ground conditions and explosive type. Other tests results are necessarily shown as simple curves, since that form of presentation was used by the original investigators. However, in reality test results do not define clean curves unless: 1) the test site has highly uniform ground material (no variation of properties, horizontally or vertically), 2) a single explosive type is used, and 3) the geometry of charge and shothole is similar for all shots.

For HE charges somewhere around 1 ton, Johnson (1971) suggested scaling with respect to charge weight raised to the power 0.3. Figure 25 gives scaled dimensions for the *apparent crater* based on a 1-ton charge of TNT and a scaling exponent of 0.3.

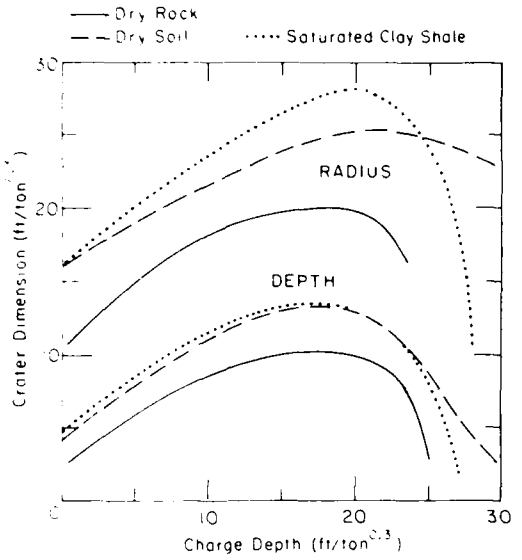

Figure 25. Scaled dimensions of apparent craters in three kinds of ground materials. Scaling exponent taken as 0.3. (After Johnson 1971.)

Rooke et al. (1974) used test data and empirical scaling to derive representative crater dimensions for a 1-ton sphere of TNT in a wide variety of materials. The results for *apparent craters* are summarized in Figure 26. To use these curves for prediction or for blast design, it would seem reasonable to use cube root scaling when scaling *down* from 1 ton to significantly smaller charge sizes, and perhaps something closer to fourth root scaling when scaling *up* to significantly bigger HE charges.

In Figure 27, dimensions of *apparent craters* made by 256-lb (116-kg) charges of TNT in dry alluvium are shown in unscaled form. The data bands give some indication of the uncertainty that exists for a single material with identical charges of the same explosive. Cube root scaling should give an acceptable approximation if these results are used to predict for charges in the range 50 to 1200 lb (25 to 550 kg).

A set of data for *apparent craters* in "sandy overburden" blasted by ANFO or sensitized slurry is shown in Figure 28. The charge weights were 25 lb and 125 lb.

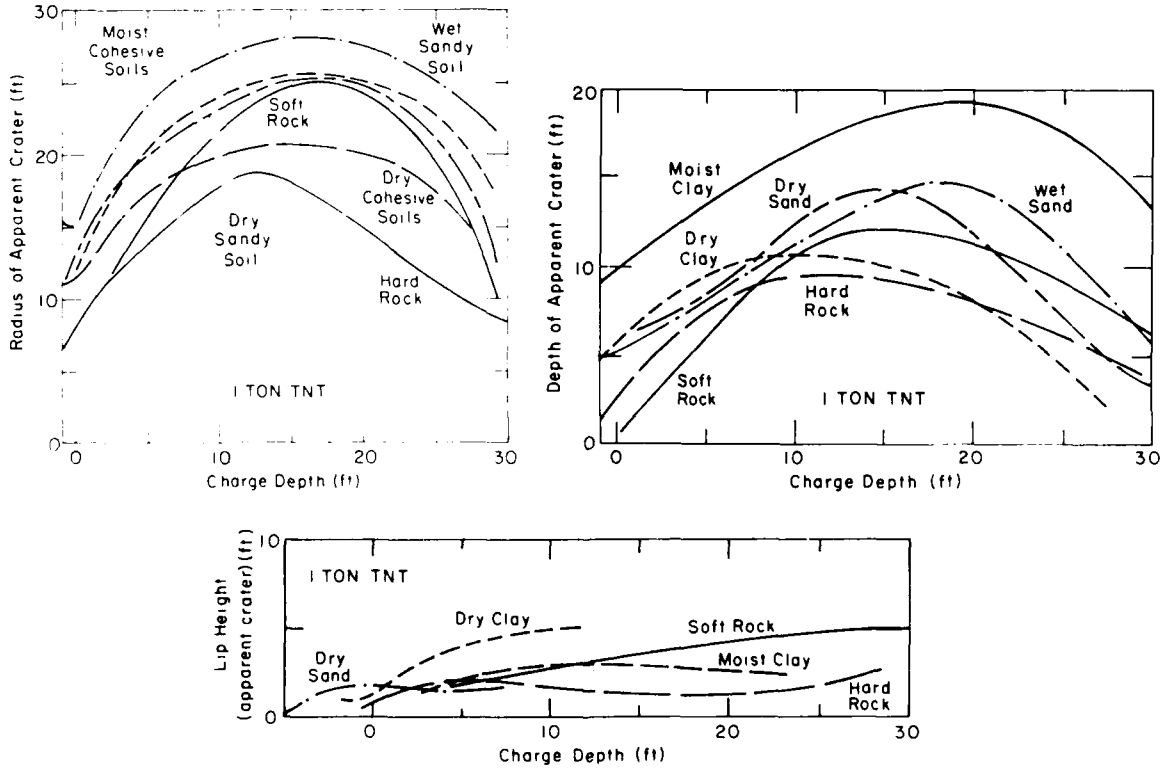

Figure 26. Dimensions of apparent craters formed in a range of ground materials by the explosion of a 1-ton charge of TNT. (After Rooke et al. 1974.)

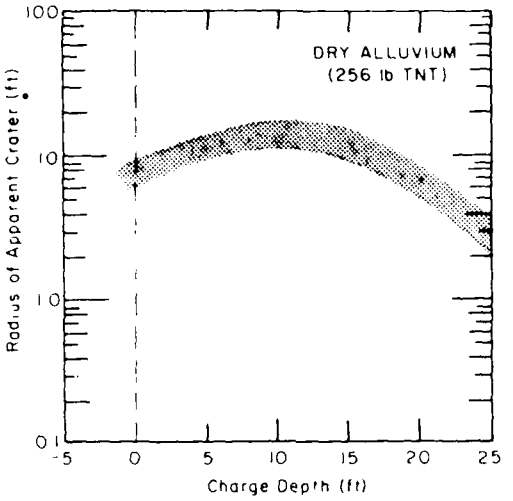

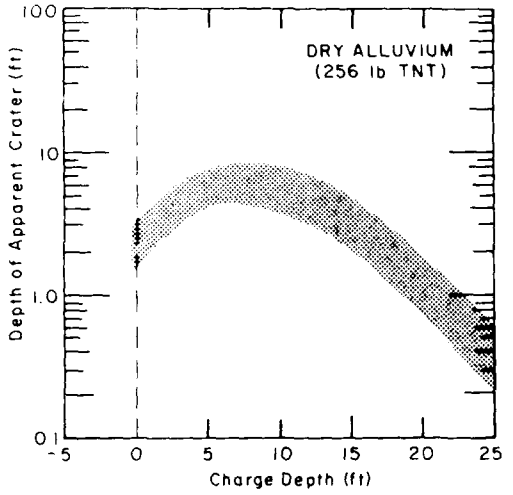

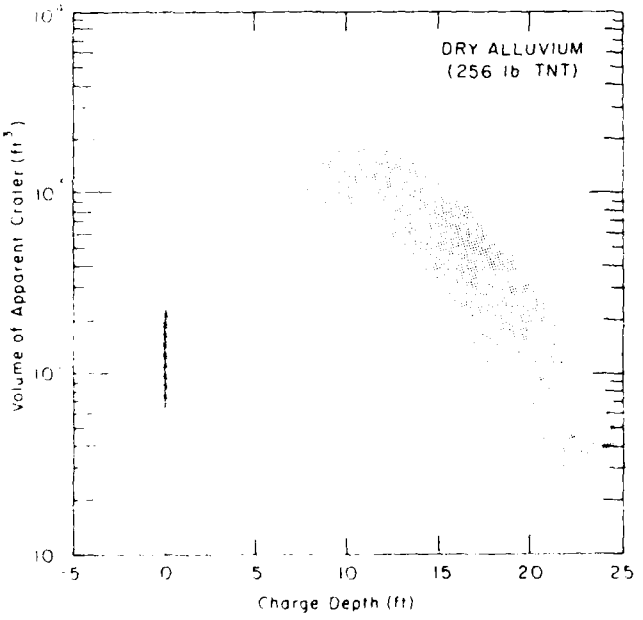

Figure 27. Dimensions of the apparent crater in dry alluvium after explosion of a 256-lb (116-kg) charge of TNT. (After Cooper 1976.)

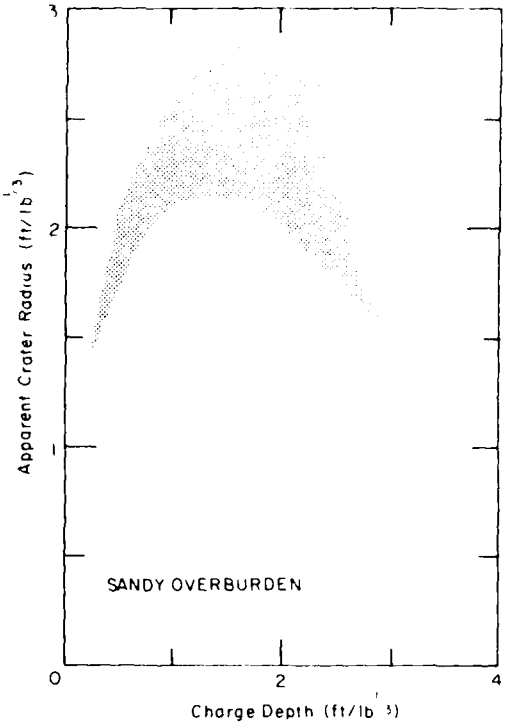

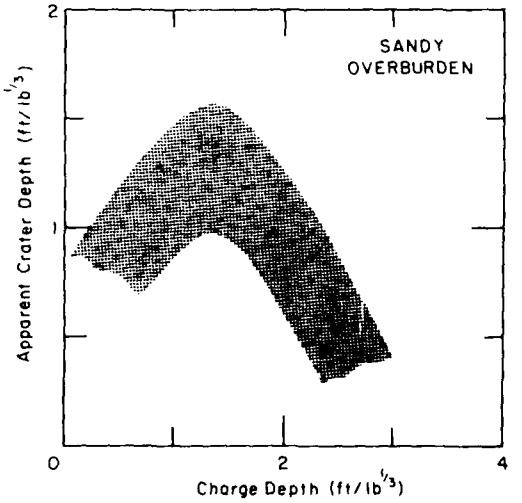

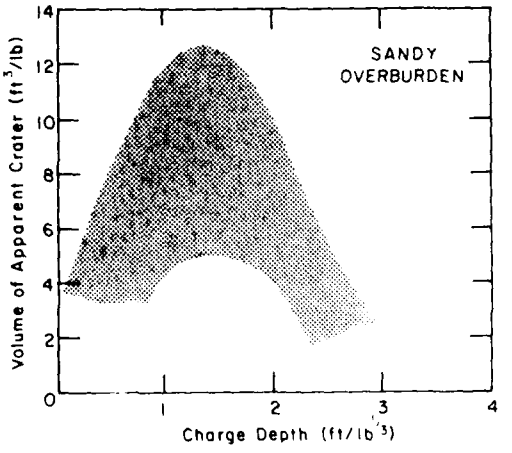

Figure 28. Scaled dimensions of apparent craters in sandy overburden. (After Bauer et al. 1972.)

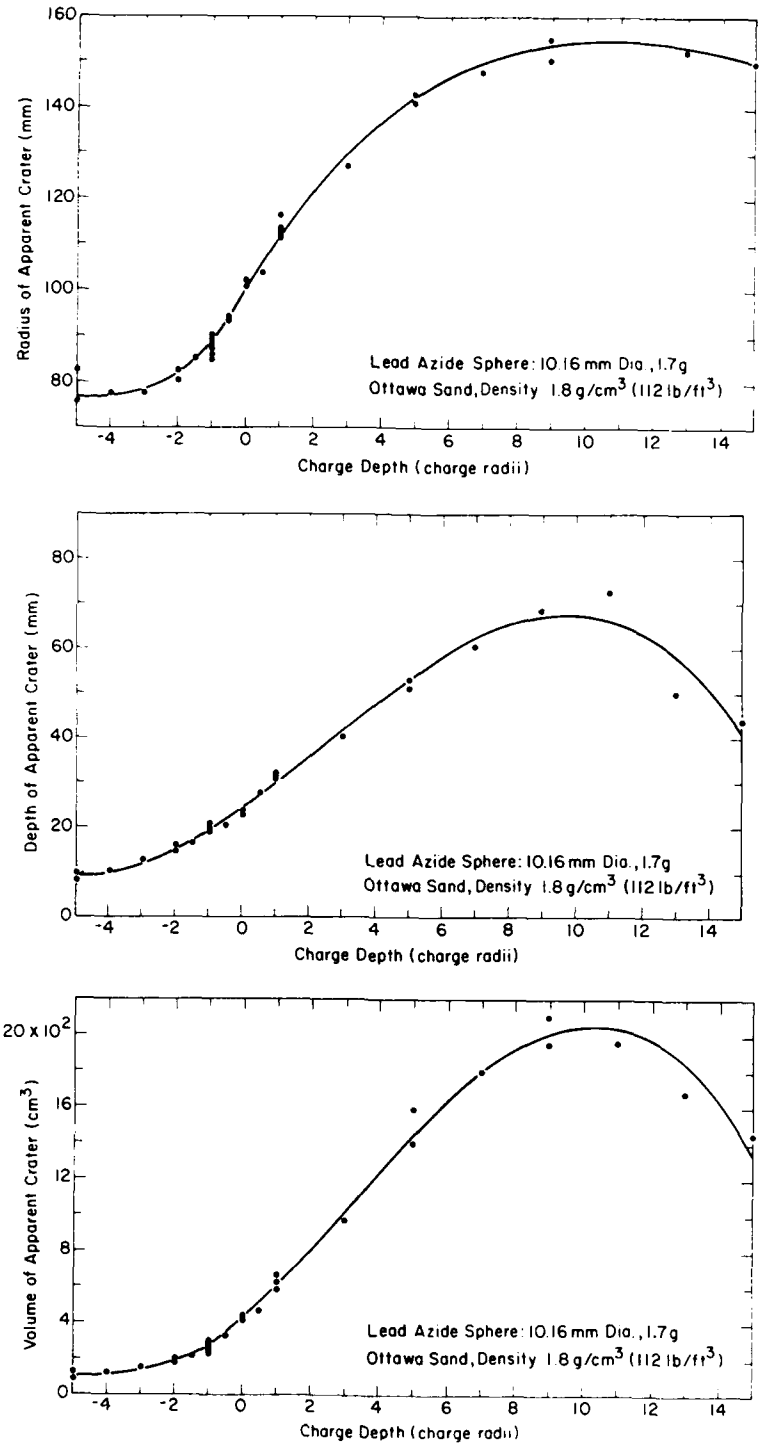

Figure 29. Dimensions of apparent craters formed by extremely small charges in Ottawa sand. (After Piekutowski 1974.)

Figure 29 gives cratering curves for blasts in dry Ottawa sand by tiny, pea-size charges of lead azide. A remarkable thing about these results is that they scale so as to give credible values for much bigger charges (Table 3).

Some data on *true crater* dimensions for small charges in a variety of rocks are given in Figures 30-33. The results for granite do not conform to typical crater characteristics, as can be seen from the plot of crater depth. The charges in granite did not break out the rock immediately surrounding the charge itself; see Duvall and Atchison (1957)

Table 3. Approximate dimensions of apparent craters in rocks and soils (conventional explosives).

Material	Crater radius, ft·lb$^{-1/3}$ (m·kg$^{-1/3}$)		Crater depth, ft·lb$^{-1/3}$ (m·kg$^{-1/3}$)		Crater volume, ft^3·lb^{-1} (m^3·kg^{-1})		Critical charge depth for zero crater depth, ft·lb$^{-1/3}$ (m·kg$^{-1/3}$)
	Maximum crater radius	Optimum charge depth	Maximum crater depth	Optimum charge depth	Maximum crater volume	Optimum charge depth	
Sandy overburden	2.2-2.9 (0.9-1.1)	1.5-1.6 (0.6-0.63)	1.0-1.6 (0.4-0.63)	1.35 (0.54)	5-13 (0.3-0.8)	1.4 (0.55)	2.8 (1.1)
Dry sandy soil	2.0 (0.8)	1.35 (0.54)	1.1 (0.44)	1.15 (0.46)			2.6 (1.0)
Sand	2.5 (1.0)	1.2 (0.5)	1.8 (0.7)	1.3 (0.5)			
Wet sandy soil	2.2 (0.9)	1.3 (0.5)	1.15 (0.46)	1.4 (0.56)			
Dry alluvium	1.9-2.7 (0.75-1.1)	1.7 (0.67)	0.7-1.3 (0.28-0.52)	1.1-1.3 (0.44-0.52)	3.2-8.3 (0.2-0.5)	1.3-1.6 (0.52-0.63)	3.9 (1.5
Alluvium	2.4 (1.0)	1.8 (0.7)	1.1 (0.45)	1.4 (0.6)			
Dry clayey soil	1.7 (0.67)	1.1 (0.44)	0.85 (0.34)	0.75 (0.3)			2.4 (0.95)
Moist clayey soil	2.2 (0.9)	1.3 (0.5)	1.5 (0.6)	1.5 (0.6)			2.8 (1.1)
Dry soil	2.0 (0.8)	1.7 (0.67)	1.0 (0.4)	1.4 (0.55)	3-20 (0.2-1.2)	1.2-1.6 (0.48-0.63)	
Wet soil					9-43 (0.6-2.7)	1.7-2.2 (0.67-0.87)	
Soft rock	2.0 (0.8)	1.35 (0.54)	0.95 (0.4)	1.2 (0.48)			
Hard rock	1.5 (0.6)	1.0 (0.4)	0.75 (0.3)	0.9 (0.36)			
Basalt	1.9 (0.8)	1.3 (0.5)	1.0 (0.4)	1.2 (0.5)			
Dry rock	1.6 (0.6)	1.4 (0.55)	0.8 (0.32)	1.4 (0.55)			
Dry clay shale	2.3 (0.9)	1.9 (0.8)	1.1 (0.4)	0.8 (0.3)			
Saturated clay shale	2.2 (0.9)	1.55 (0.6)	1.1 (0.44)	1.35 (0.54)			
Playa	1.9 (0.8)	1.0 (0.4)	1.0 (0.4)	0.8 (0.3)			
Dry Ottawa sand (extremely small charges)	3.3 (1.3)	1.15 (0.46)	1.4 (0.57)	1.0 (0.4)	19 (1.2)	1.1 (0.44)	

for details. The same type of behavior was found for very small charges in granite (D'Andrea et al. 1970), but the crater depth data did not scale well. Figure 34 gives a general idea of crater radius and crater volume for very small charges ($\leq$ 1 lb) in granite. On a larger scale, dimensions of true craters produced by 1-ton charges in sandstone are indicated in Figure 35.

Nuclear explosions differ from chemical ones—energy density, temperature and pressure at the source are all higher, and gas expansion is produced indirectly from the surrounding material by vaporization. This suggests that dimensions for nuclear craters might be different than those for HE craters, but some of the test data show close similarity between the two types when an appro-

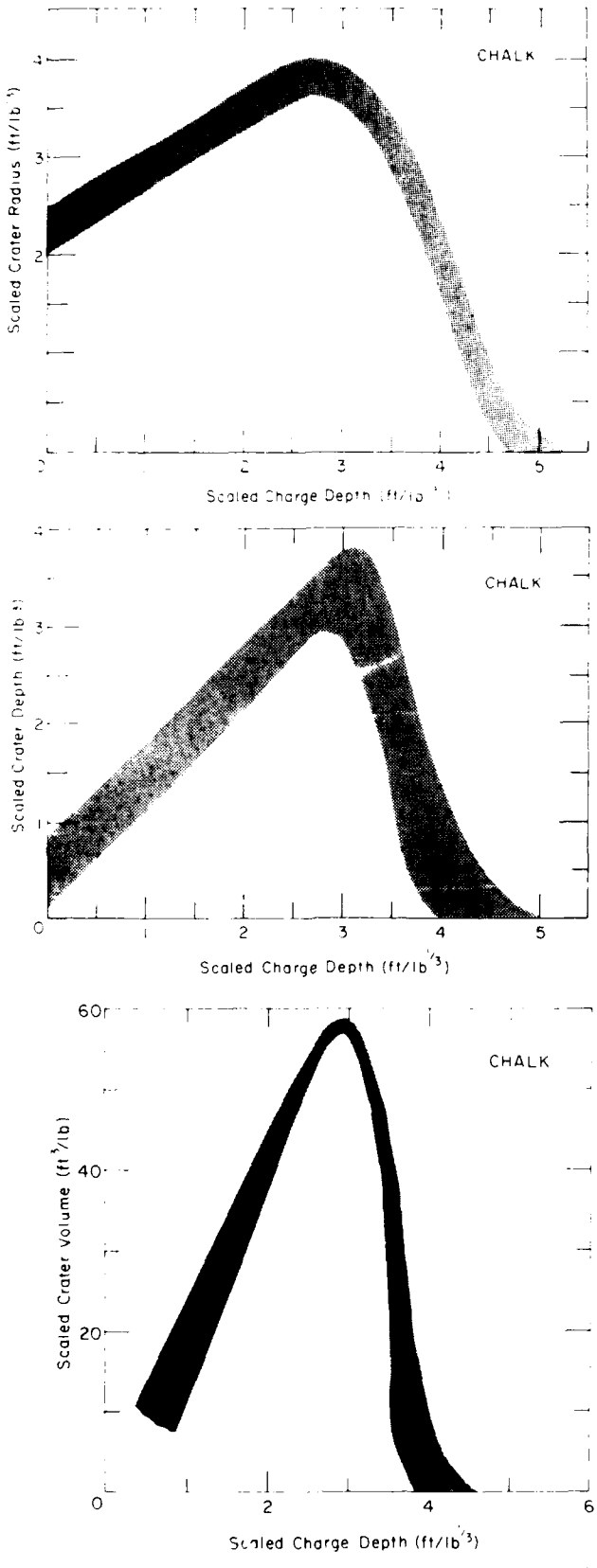

Figure 30. Scaled dimensions of true craters in chalk. (After Duvall and Atchison 1957.)

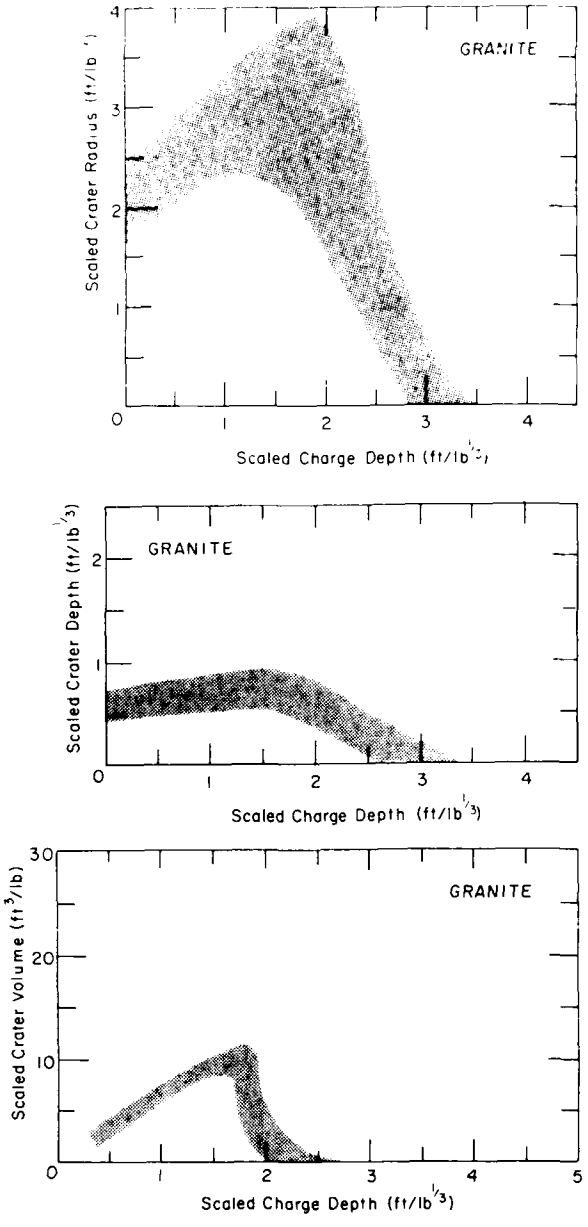

Figure 31. Scaled dimensions of true craters in granite. (After Duvall and Atchison 1957.)

priate energy factor is applied. From consideration of theoretical simulations and empirical comparisons, it has been accepted by some authorities that 1 kiloton of nuclear energy gives about the same cratering performance as 10^6 lb of TNT, i.e. for crater comparisons the "weight" of a nuclear device is multiplied by 0.5. However, it is not clear to this writer whether the factor is based on direct comparisons for equal energy, or whether the factor simply produces compatibility according to some preconceived scaling rule.

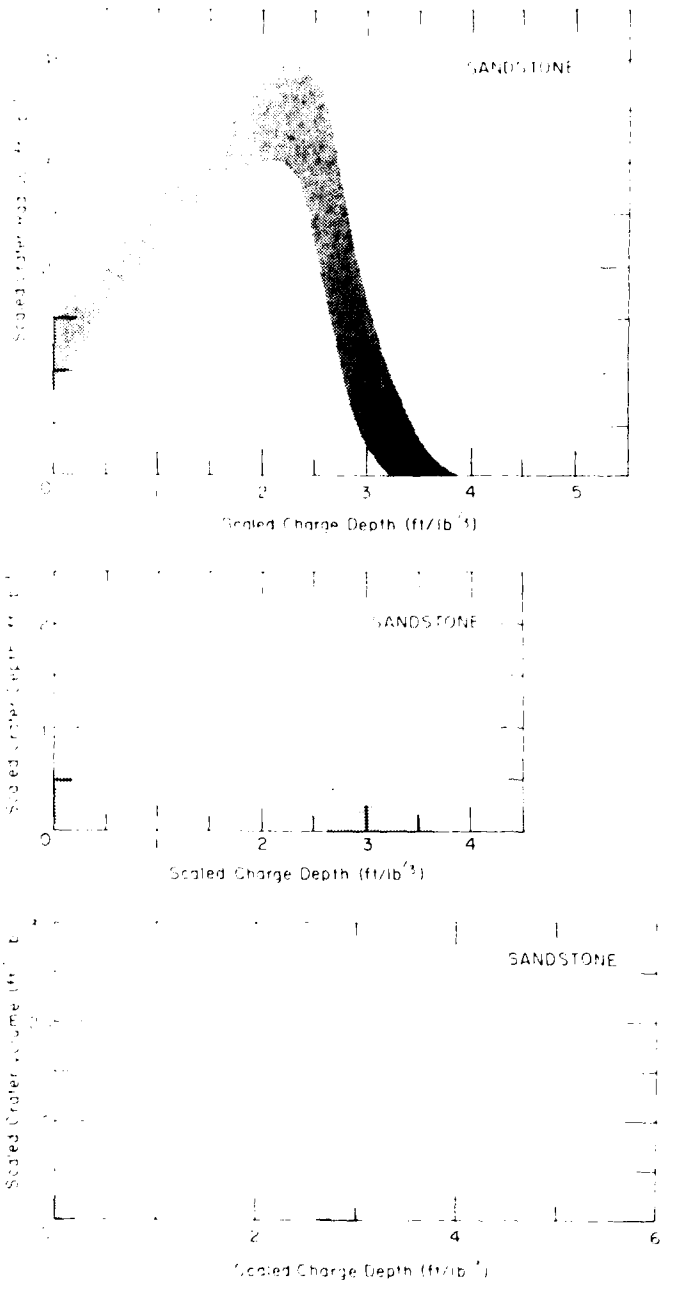

Figure 32. Scaled dimensions of true craters in sandstone. (After Duvall and Atchison 1957.)

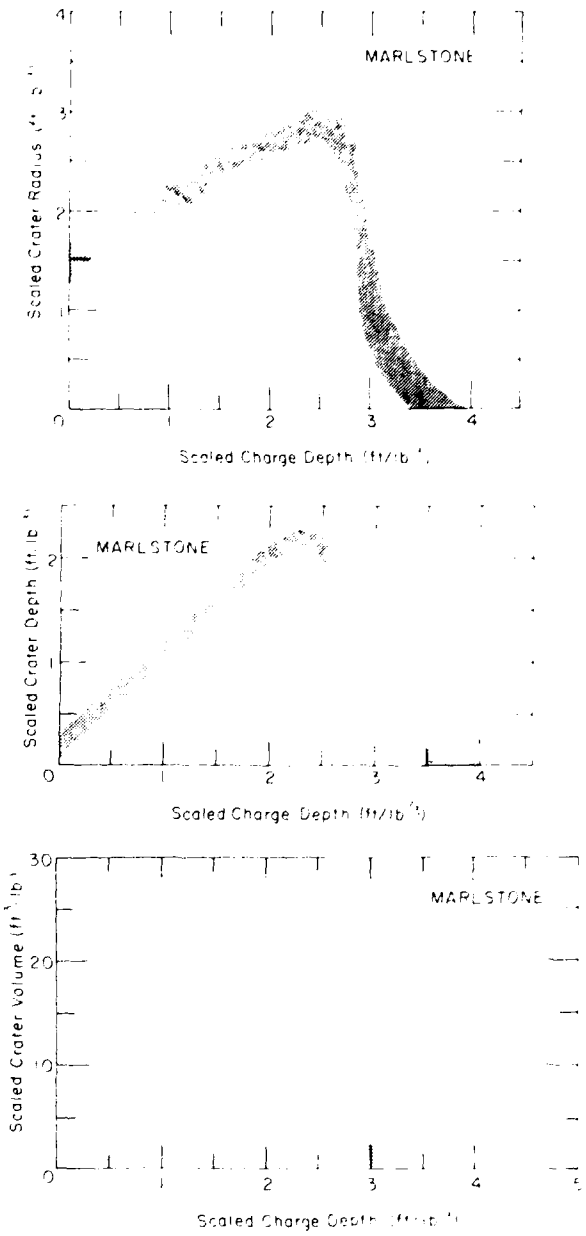

Figure 33. Scaled dimensions of true craters in marlstone. (After Duvall and Atchison 1957.)

A set of curves for *nuclear apparent craters* in soil and rock is given in Figure 36. The depth scales on these curves imply applicability of cube root scaling. Representative dimensions for nuclear apparent craters in soils and rocks are given in scaled form in Figure 37.

Figure 38 gives dimensions of *true craters* from 1-kt *nuclear* bursts in rock and desert alluvium. For rock, cube root scaling is apparently a good approximation. For alluvium, cube root scaling applies for crater depth and charge depth, but the empirical scaling for radius is apparently closer to fourth root. Figure 39 gives another curve for the true crater radius in hard, dry rock. The dashed line shows the relation for true crater depth suggested by the original author (Hughes 1968); this type of relation can apply only if crater depth is redefined as the depth below surface of the base of

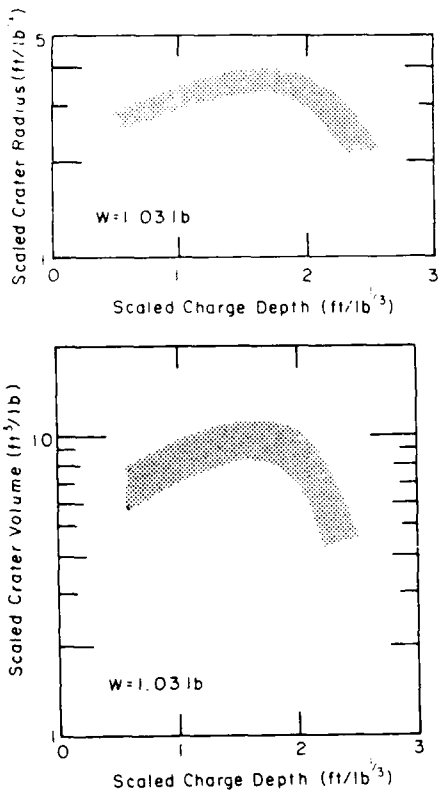

Figure 34. Scaled dimensions of crater formed by small charges in granite. (After D'Andrea et al. 1970.)

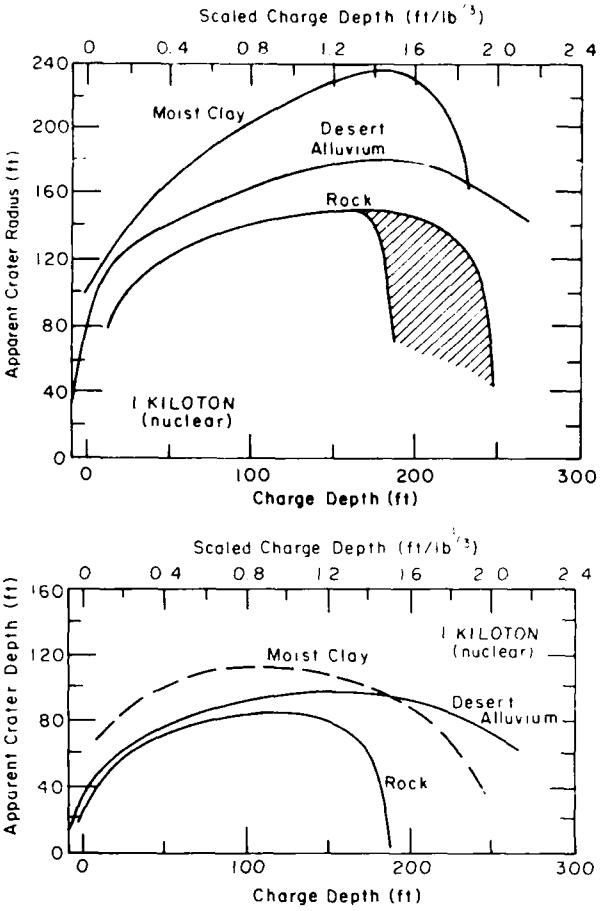

Figure 36. Dimensions of apparent craters formed in soils and rock by 1-kiloton nuclear explosions. The same data are given in scaled form by Hughes (1968), using a scaling exponent of 1/3.4, i.e. 0.294. (After Rooke et al. 1974.)

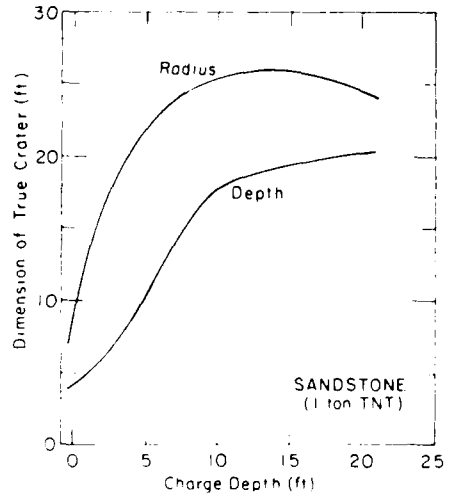

Figure 35. Dimensions of true craters produced in sandstone by 1-ton charges of TNT. (After Rooke et al. 1974.)

the explosion cavity, irrespective of whether it is a crater or a camouflet chamber.

The cratering curves given in this section and the next one represent test results from large numbers of explosions in a wide range of ground materials. At first sight the curves may appear confusing or even contradictory, but when the data are compared in scaled form they are very consistent. Tables 3 and 4 give some characteristic dimensions for apparent craters and true craters in soils and rocks when the charge size is up to 1 ton or so. Tables 5 and 6 give comparable data for craters formed by nuclear explosions. It turns out that there is surprisingly little difference in the crater dimensions for materials that have widely different properties. For example, the maximum scaled radius of the crater varies only by a factor of 2 over the whole range of soils and rocks, including frozen soils and ice (see Tables 10 and 11).

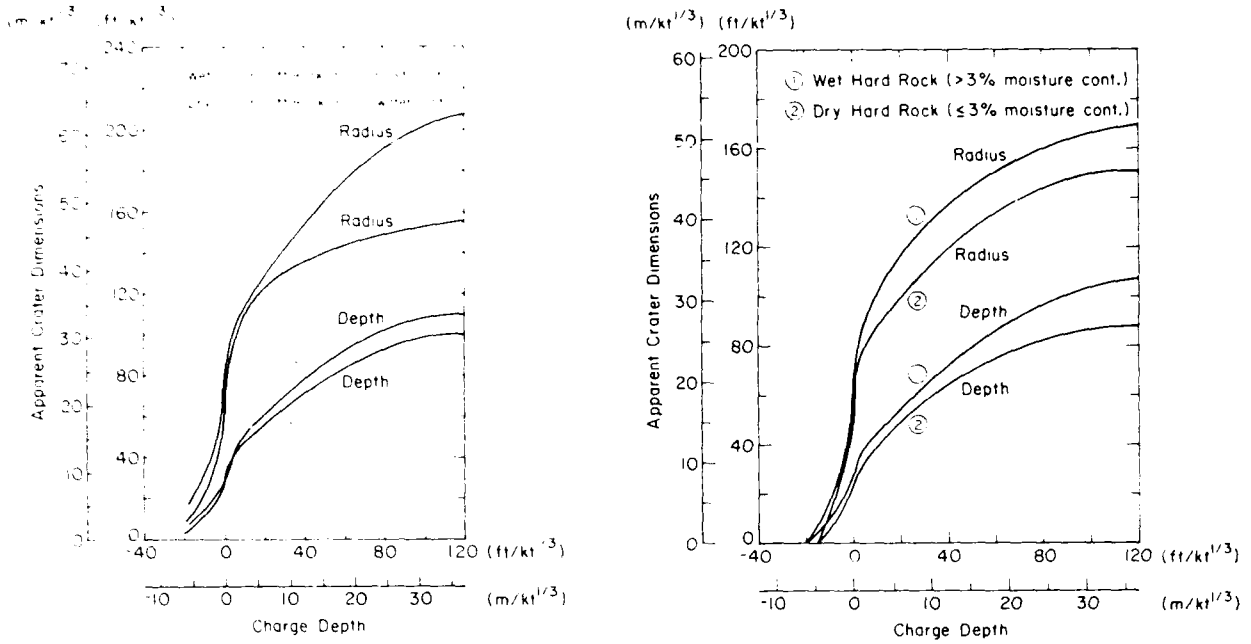

Figure 37. Scaled dimensions of apparent craters formed in soils and rocks by nuclear explosions. (After U.S. Army 1984.)

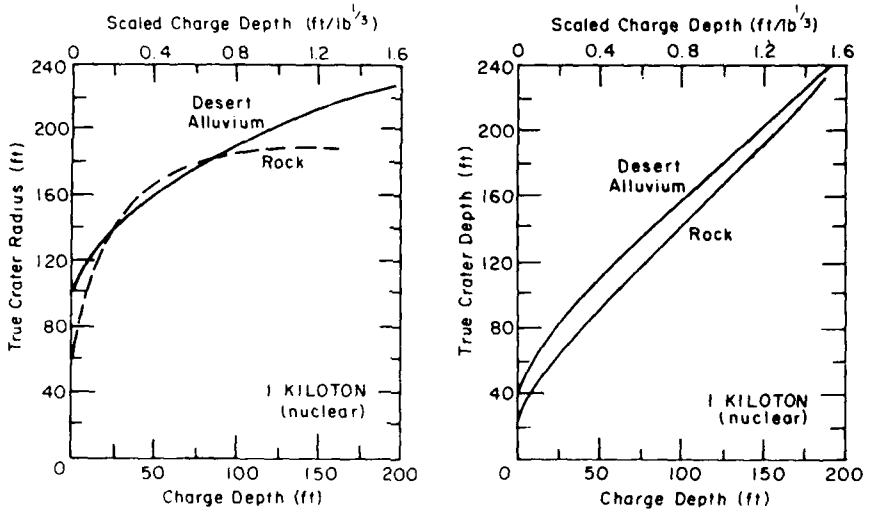

Figure 38. Dimensions of true craters formed in rock and alluvium by 1-kiloton nuclear explosions. (After Rooke et al. 1974.)

In order to develop a practical feel for cratering, it is useful to have some easily appreciated numbers for describing crater proportions. In Tables 7 and 8, the ratio of crater depth to crater radius is listed for apparent craters and true craters, and an equivalent sideslope angle is given. The numbers are derived from cratering curves given in Figures 22-24, and from other sources.

For *apparent craters*, the equivalent sideslope for most materials tends to be around 20° when the charge depth is zero. When the charge is deep enough to produce maximum crater radius, the equivalent sideslope is around 26° to 30°. When the charge depth is such that it gives maximum crater depth, the equivalent sideslope is just a bit steeper, say about 28° to 32°.

There is very little systematic information on *true craters* in rock. For zero charge depth, the first three entries in Table 8 suggest 20° to 26° for the equivalent sideslope, while the last four entries

Table 4. Approximate dimensions of true craters in rocks (conventional explosives).

Material	Crater radius, ft lb$^{-1/3}$ (m kg$^{-1/3}$)		Crater depth, ft lb$^{-1/3}$ (m kg$^{-1/3}$)		Crater volume, ft^3 lb^{-1} (m^3/kg)		Critical charge depth for zero crater depth, ft lb$^{-1/3}$ (m kg$^{-1/3}$)
	Maximum crater radius	Optimum charge depth	Maximum crater depth	Optimum charge depth	Maximum crater volume	Optimum charge depth	
Marlstone	2.7–3.1	2.55	2.1–2.3	2.3	23–24.5	2.4	3.5
	(1.1–1.2)	(1.0)	(0.83–0.91)	(0.9)	(1.4–1.5)	(0.95)	(1.4)
Chalk	3.6–4.0	2.7	2.9–3.8	2.9–3.1	57–59	2.9	4–5
	(1.4–1.6)	(1.1)	(1.2–1.5)	(1.2)	(3.6–3.7)	(1.2)	(1.6–2.0)
Sandstone	3–4	2.2–2.3	1.4–1.9	1.5	18–21	1.85	3
	(1.2–1.6)	(0.87–0.91)	(0.56–0.75)	(0.6)	(1.1–1.3)	(0.73)	(1.2)
Sandstone	2.1	1.1	1.6	1.7			
	(0.83)	(0.44)	(0.63)	(0.67)			
Granite	2.3–3.9	1.2–1.8	0.6–0.9	1.6	8–11.5	1.6–1.8	2.5
	(0.91–1.5)	(0.48–0.71)	(0.24–0.36)	(0.63)	(0.5–0.7)	(0.63–0.71)	(1.0)
Granite	3.3–4.0	1.7			8.2–10.3	1.7	
	(1.3–1.6)	(0.67)			(0.5–0.6)	(0.67)	

Table 5. Approximate dimensions of nuclear apparent craters in soil and rock.

Material	Maximum crater radius, ft/kt$^{1/3}$ (m/kt$^{1/3}$)		Maximum crater depth, ft/kt$^{1/3}$ (m/kt$^{1/3}$)	
	Maximum radius	Optimum charge depth	Maximum depth	Optimum charge depth
Soil or soft rock (dry)	≥157	≥120	100	110
	(≥48)	(≥37)	(30)	(34)
Soil or soft rock (wet)	≥208	≥120	110	110
	(≥63)	(≥37)	(34)	(34)
Hard rock (dry)	152	110	88	110
	(46)	(34)	(27)	(34)
Hard rock (wet)	≥170	≥120	106	120
	(≥52)	(≥37)	(32)	(37)
Rock	150	170	85	120
	(46)	(52)	(26)	(37)
Desert alluvium	180	180	≥5	150
	(55)	(55)	(29)	(46)
Moist clay	235	180	110	105
	(72)	(55)	(34)	(32)

Table 6. Approximate dimensions of nuclear true craters in soil and rock.

Material	Maximum crater radius, ft/kt$^{1/3}$ (m/kt$^{1/3}$)		Maximum crater depth, ft/kt$^{1/3}$ (m/kt$^{1/3}$)	
	Maximum radius	Optimum charge depth	Maximum depth	Optimum charge depth
Desert alluvium	~230	~200	~240	~190
	(~70)	(~61)	(~73)	(~58)
Rock	185	140	230	~190
	(56)	(43)	(~70)	(~58)
Hard, dry rock	240	190		
	(73)	(58)		

Table 7. Proportions of apparent craters.

Material	Explosive	Charge depth: Zero — Crater depth / Crater radius	Zero — Equivalent sideslope* (°)	For maximum crater radius — Crater depth / Crater radius	For maximum crater radius — Equivalent sideslope* (°)	For maximum crater depth — Crater depth / Crater radius	For maximum crater depth — Equivalent sideslope* (°)
Moist clay	TNT	0.802	38.7	0.755	37.1	0.766	37.5
Moist clay	Nuclear			0.419	25.3	0.538	28.3
Dry desert alluvium	TNT	0.352	19.4	0.542	28.4	0.610	31.4
Dry desert alluvium	TNT	0.286	16.0	0.357	19.7	0.444	24.0
Dry desert alluvium	Nuclear	0.364	20.0	0.527	27.8	0.544	28.6
Basalt and granite	TNT	0.376	20.6	0.510	27.0	0.549	28.8
"Rock"	Nuclear	0.352	19.4			0.581	30.2
"Dry hard rock"	Nuclear	0.421	22.8	0.579	30.1		
"Wet hard rock"	Nuclear	0.467	25.0	0.626	32.1		
"Dry rock"	TNT	0.240	13.5	0.508	26.9	0.513	27.1
Dry clay	TNT			0.560	29.2	0.641	32.6
Dry soil or soft rock	Nuclear	0.435	23.5	0.633	32.3		
Dry soil	TNT	0.259	14.5	0.485	25.9	0.541	28.4
Dry-to moist sand	TNT	0.366	20.1				
Moist loess and moist silt	TNT	0.511	27.1	0.449	24.2	0.552	28.9
Wet soil or soft rock	Nuclear	0.373	20.5	0.529	27.9		
Wet sand	TNT	0.347	19.1	0.482	25.8	0.649	33.0
Shale and tuff	TNT		—	0.468	25.1	0.500	26.6
Saturated clay shale	TNT	0.294	16.4	0.466	25.0	0.488	26.0
Sandy overburden	Slurry	—		0.480	25.6		

* Equivalent sideslope = $\tan^{-1}$ (depth/radius).

Table 8. Proportions of true craters.

Material	Explosive	Charge depth: Zero — Crater depth / Crater radius	Zero — Equivalent sideslope* (°)	For maximum crater radius — Crater depth / Crater radius	For maximum crater radius — Equivalent sideslope* (°)
Sandstone	TNT	0.483	25.8	0.723	35.9
Rock	Nuclear	0.419	22.8	0.937	43.1
Desert alluvium	Nuclear	0.371	20.4	1.081	47.2
Sandstone*	Dynamite	0.333	18.4	0.257	14.4
Chalk*	Dynamite	0.267	14.9	0.842	40.1
Marlstone*	Dynamite	0.100	5.7	0.754	37.0
Granite*	Dynamite	0.286	15.9	0.233	13.1

* May not be representative results (small-scale tests).

(representing small-scale tests) show shallower slopes. When the charge is deep enough to produce maximum radius, the equivalent sideslope of the true crater is steep in most cases—36° to 47°. Two entries in Table 8 (small-scale tests in sandstone and granite) give very shallow angles for deep charges, but these results are suspect.

Although the cube root scaling of linear crater dimensions is not accepted universally, there is general agreement that *crater volume* can be scaled with respect to the charge weight, or the energy yield. This is equivalent to assuming constant specific energy for the cratering process, irrespective of the size of the event. In fact, the reciprocal of volume per unit weight is a specific energy if multiplied by the energy per unit weight of the explosive. The scaled volume itself is the reciprocal of the traditional "powder factor" used in blasting practice.

As the charge depth increases from zero, crater volume increases up to some maximum value, after which it falls again, reaching zero at the criti-

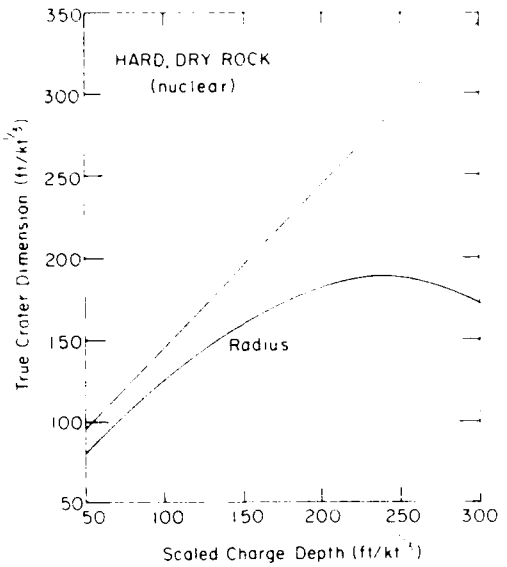

Figure 39. Scaled dimensions of true craters formed in hard rock by nuclear explosions. (After Hughes 1968.)

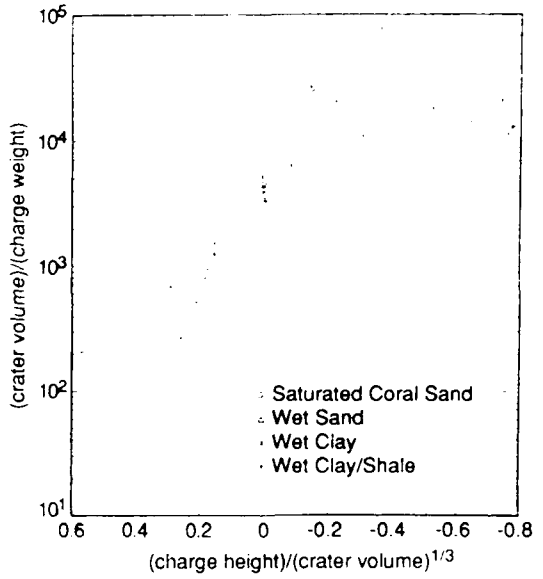

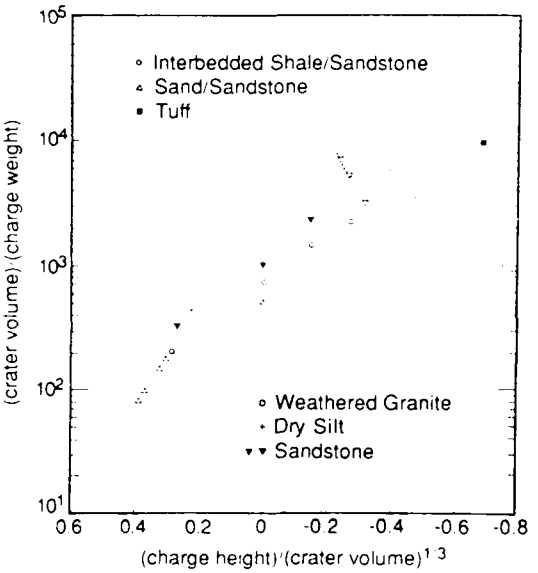

Figure 40. "Cratering efficiency" for high explosives in various rocks and soils. (Cooper 1976.)

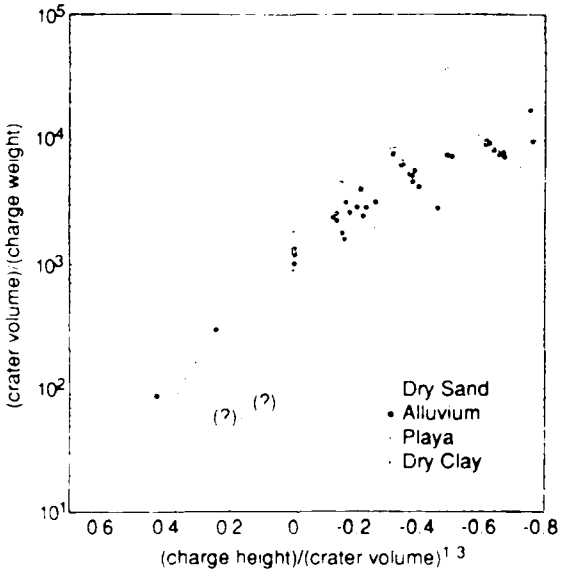

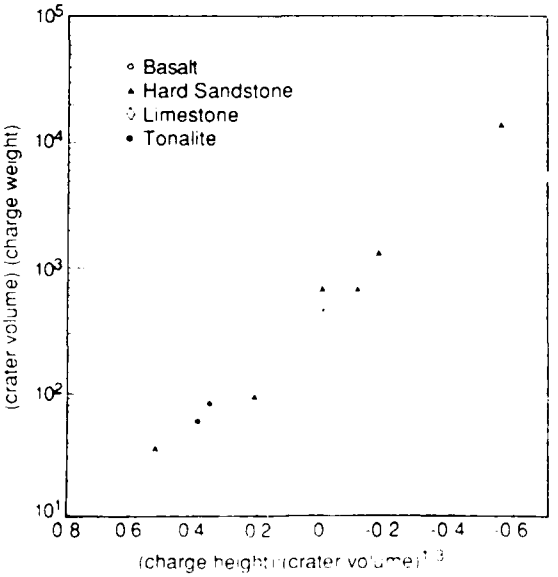

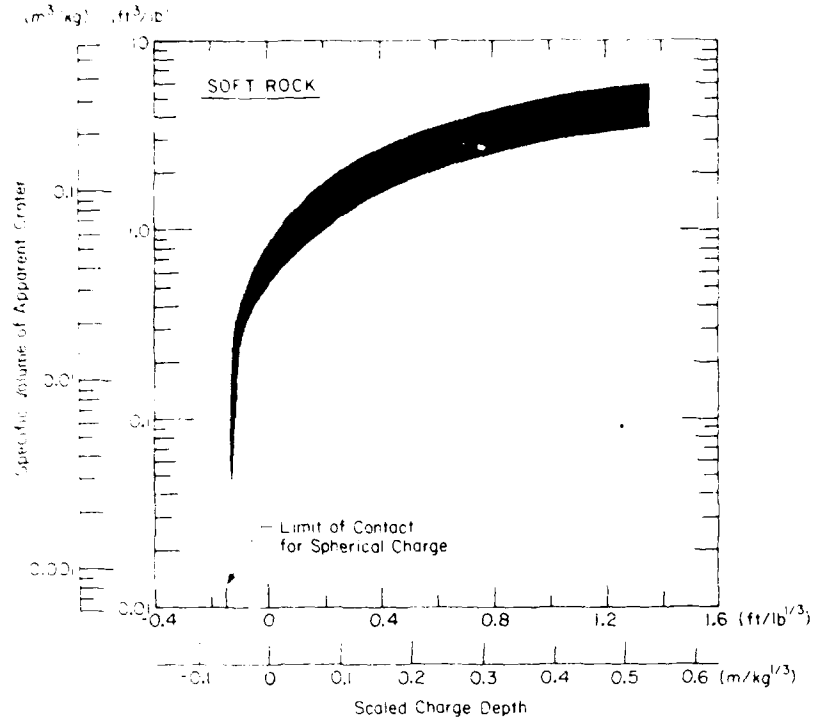

Figure 41. Specific volume of the apparent crater as a function of scaled charge depth in soft rock. (Reinterpretation of data from Fig. 40.)

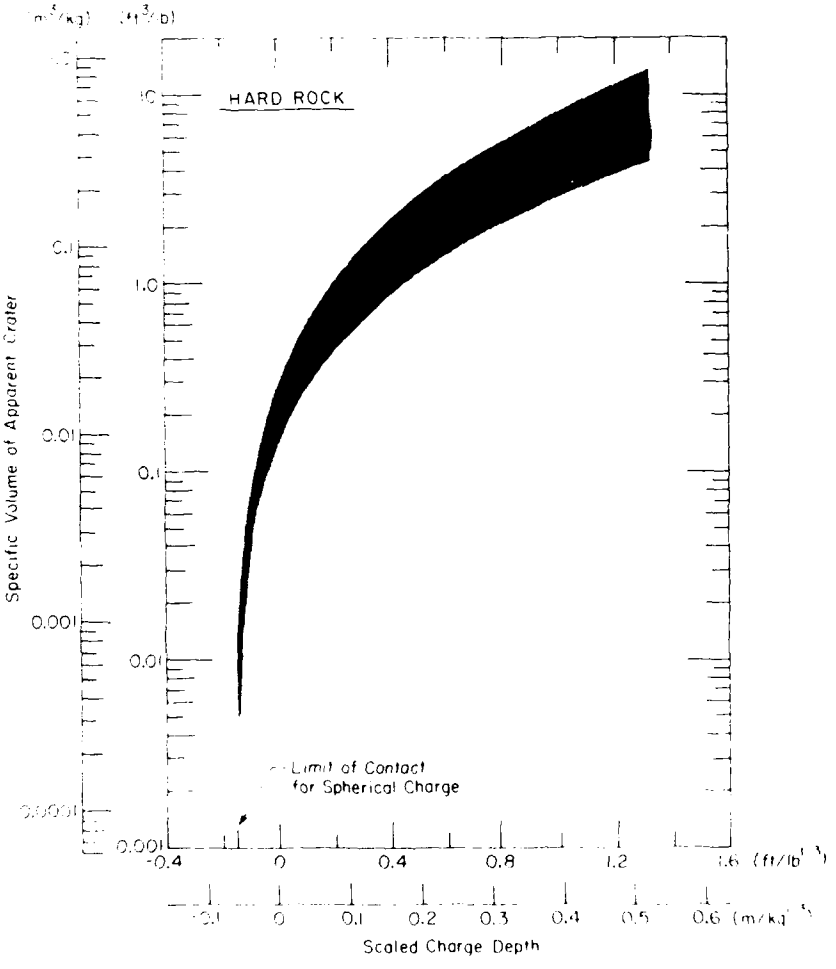

Figure 42. Specific volume of the apparent crater as a function of scaled charge depth in hard rock. (Reinterpretation of data from Fig. 40.)

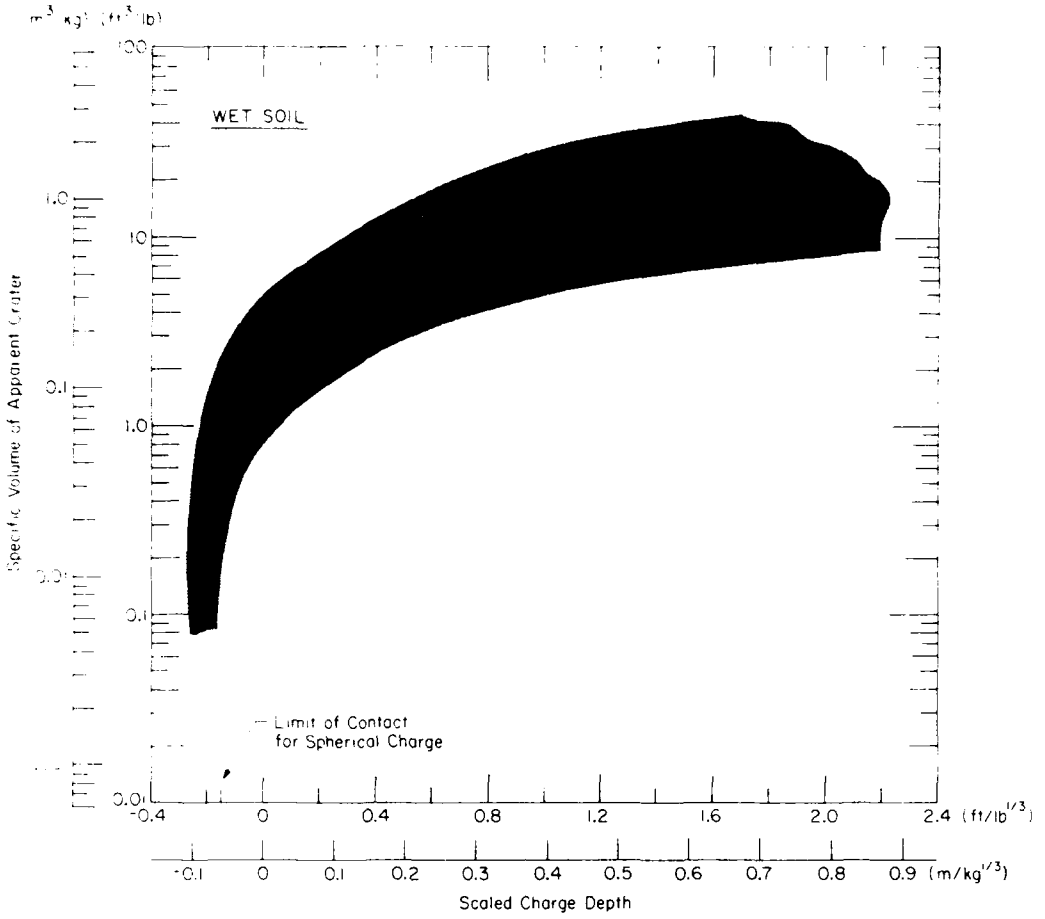

Figure 43. Specific volume of the apparent crater as a function of scaled charge depth in wet soils. (Reinterpretation of data from Fig. 40.)

cal charge depth. Figures 27–29 give examples of the trend for apparent crater volume; Figures 30–34 show the trend for true crater volume.

For consideration of weapons effects, the blaster's terms "powder factor" (lb/yd³) or "specific charge" (kg/m³) have been replaced by the inappropriate term "cratering efficiency," typically expressed in units of ft³/ton for HE craters (which is really specific volume). Since crater volume is of secondary concern in the context of weapons effects, test data are less readily available than are data for the linear dimensions of craters.

High explosive test data for a variety of ground materials have been summarized in some of the literature by plotting the "cratering effiency" against a dimensionless charge depth (Fig. 40). This dimensionless charge depth is the actual charge depth normalized with respect to the cube root of the apparent crater volume for that charge depth. Such plots are not directly useful for prediction and design, so Figures 41–44 give the same information converted to conventional cube root scaling. The range of the data is insufficient to show the decrease in specific volume as charge depth approaches critical depth, but the results for negative charge depth (air bursts) illustrate how crater volume becomes insignificant once the charge ceases to be in contact with the ground surface. A spherical charge of typical high explosive ceases to contact the surface when its center is at a scaled height of more than 0.15 ft/lb$^{1/3}$ (0.06 m/kg$^{1/3}$).

When cratering data for high explosives are summarized, the standard reference explosive is TNT. The *cratering performance for a different explosive* can be accounted for by multiplying the actual weight of that explosive by a conversion factor in order to obtain an approximately equivalent weight of TNT (Table 9). These factors, especially the one for nuclear explosions, should be applied with caution.

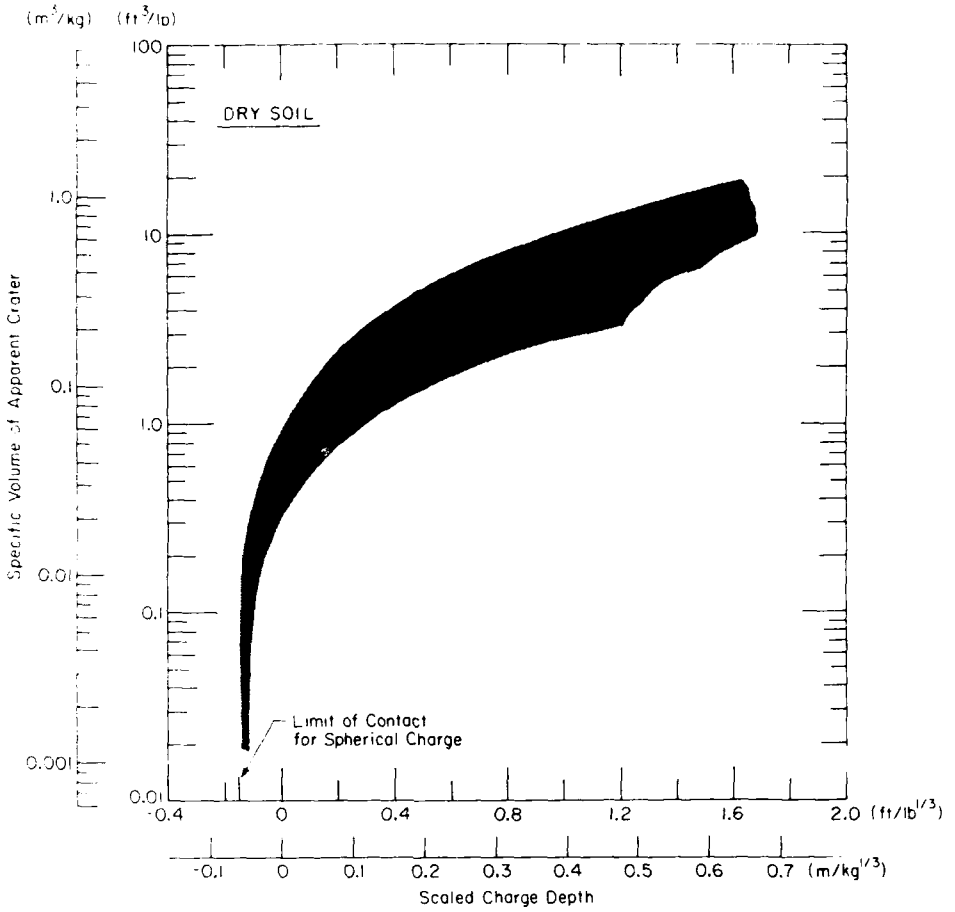

Figure 44. Specific volume of the apparent crater as a function of scaled charge depth in dry soil. (Reinterpretation of data from Fig. 40.)

Table 9. Adjustment factors for cratering efficiency. (Non-nuclear data from Rooke et al. 1974.)
Multiply weight of explosive by *F* to obtain equivalent TNT weight.

Explosive	F, *Cratering factor*
TNT*	1.00
Dynamite (40%)	0.68
Ammonium nitrate	1.00
Nitromethane	1.10
C-3, C-4	1.34
Pentolite (PETN/TNT)	1.23
Amatol (AN/TNT)	0.94
Nuclear†	0.5

* Heat of detonation taken as 10^9 cal/ton or 10^{12} cal/kiloton.

† Nominal kiloton or megaton "weight" to be multiplied by *F*.

CRATERS IN FROZEN GROUND, ICE AND SNOW

Apparent craters in frozen materials

Test data for apparent craters in frozen soils, massive ice, and dense snow have been compiled and plotted in appropriate combinations (Mellor 1985). Representative data bands for these plots are shown in Figures 45–48, permitting easy comparison with corresponding data for common rocks and soils. Characteristic crater dimensions are summarized in Table 10.

Figure 45a represents the combined data for variation of crater *radius* with charge depth in *frozen silt*. The general trend is fairly clear, with radius reaching its maximum value of 1.8 to 2.7 ft/lb$^{1/3}$ (0.7 to 1.1 m/kg$^{1/3}$) at a scaled charge depth around 1.7 to 2.1 ft/lb$^{1/3}$ (0.7 to 0.8 m/kg$^{1/3}$). Critical charge depth, at which crater radius becomes zero, appears to be around 2.7 to 3.3 ft/lb$^{1/3}$ (0.8 to

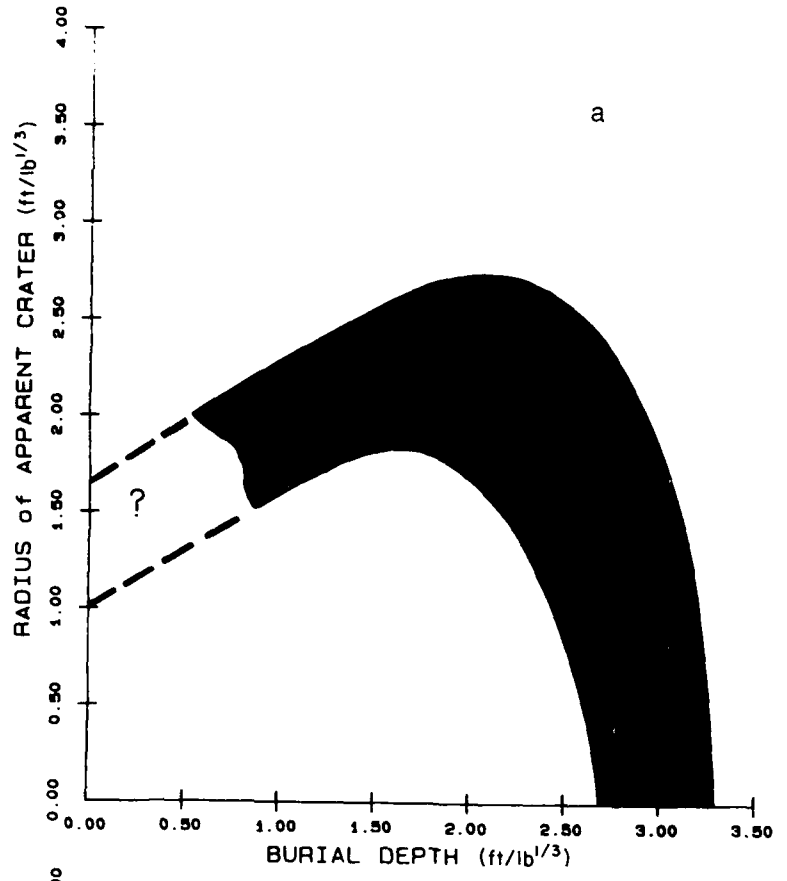

Figure 45. Scaled dimensions of apparent craters in frozen silt. (Data from McCoy 1965, Mellor 1971, Riddoch 1979, Smith 1980.)

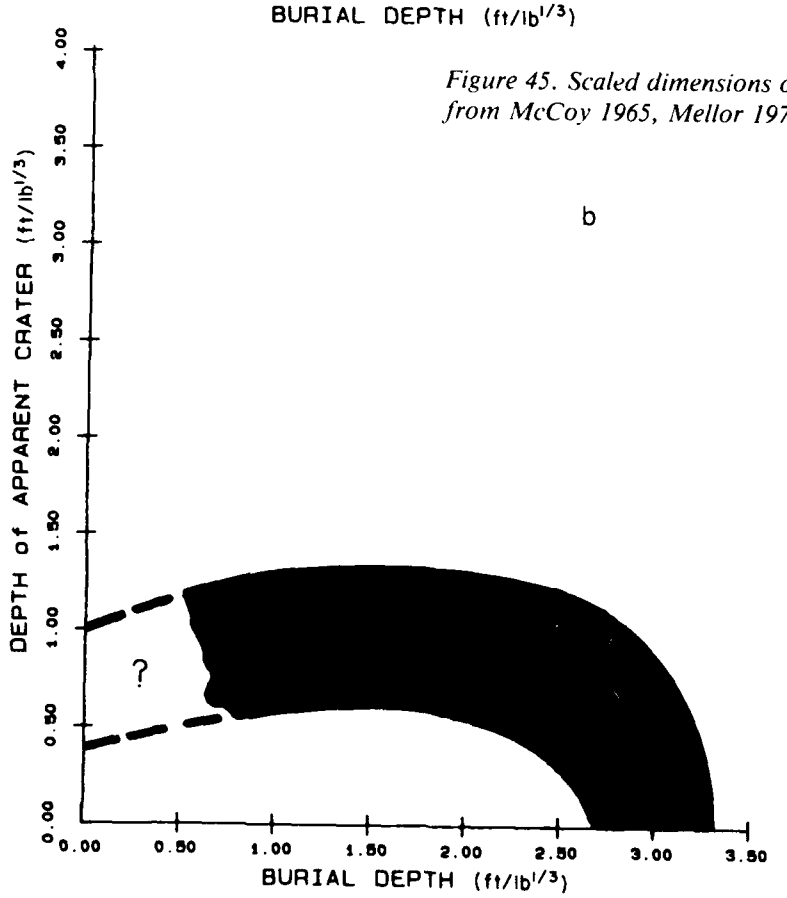

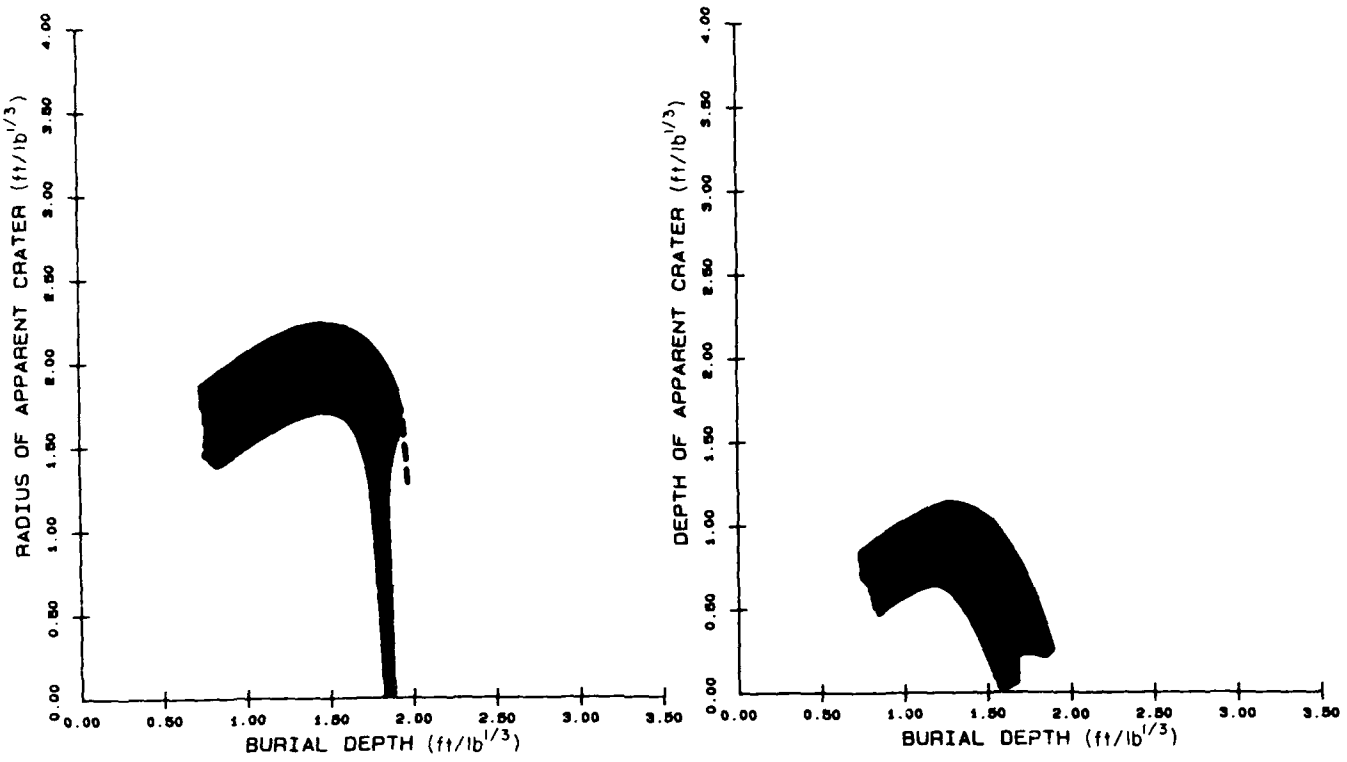

Figure 46. Scaled dimensions of apparent craters in frozen till. (Data from Livingston and Murphy 1959, Mellor and Sellmann 1970, Bauer et al. 1974, Smith and Mellor 1975, Smith 1980, Simpson 1981.)

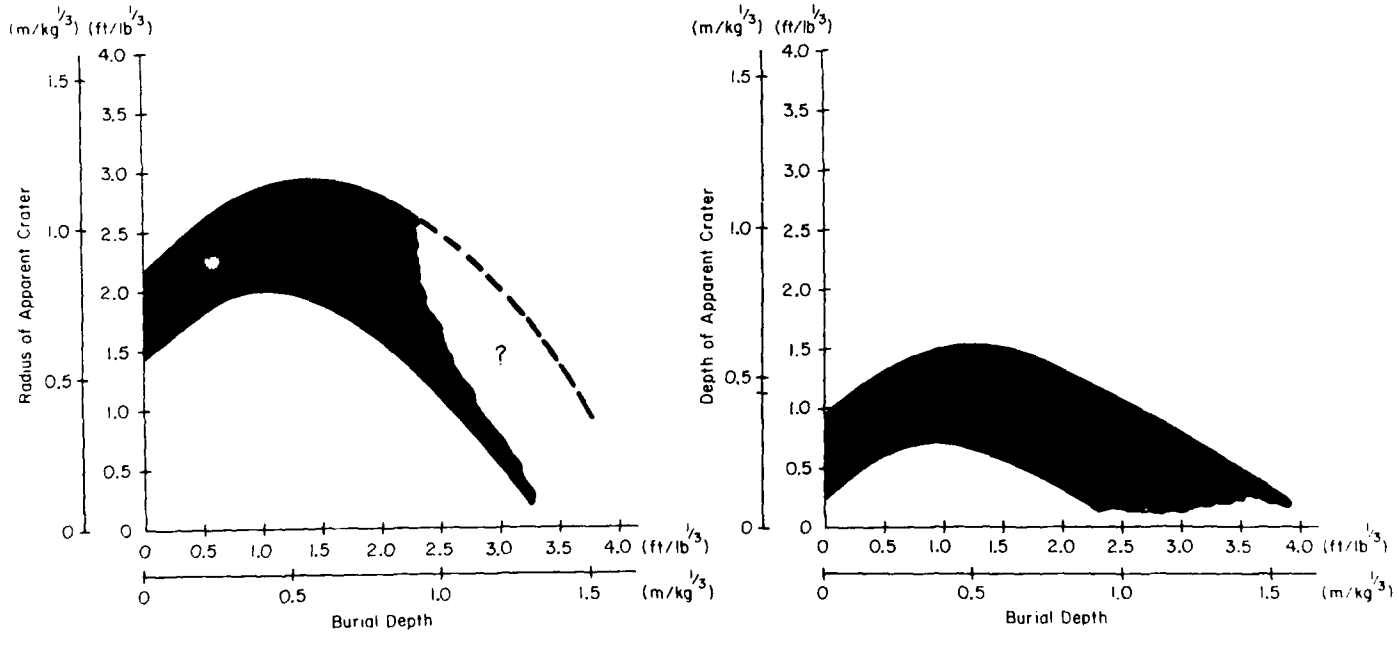

Figure 47. Scaled dimensions of apparent craters in massive ice. (Data from Livingston 1960.)

Table 10. Dimensions of apparent craters in frozen ground, ice and snow.

Material	Crater radius, ft/lb$^{1/3}$ (m/kg$^{1/3}$)		Crater depth, ft/lb$^{1/3}$ (m/kg$^{1/3}$)		Critical charge depth, ft/lb$^{1/3}$ (m$^{1/3}$/kg) for	
	Maximum crater radius	Optimum charge depth	Maximum crater depth	Optimum charge depth	Zero crater radius	Zero crater depth
Frozen silt	1.8-2.7 (0.7-1.1)	1.7-2.1 (0.7-0.8)	0.6-1.3 (0.2-0.5)	≈ 1 (≈ 0.4)	2.7-3.3 (0.8-1.3)	2.7-3.3 (0.8-1.3)
Frozen till	1.7-2.2 (0.7-0.9)	1.3-1.5 (0.5-0.6)	0.7-1.1 (0.3-0.4)	1.3-1.4 (0.5-0.6)	1.8-? (0.7-?)	1.6-2.0 (0.6-0.8)
Massive ice	2.0-2.8 (0.8-1.1)	1.1-1.4 (0.4-0.6)	0.8-1.4 (0.3-0.6)	0.7-1.5 (0.3-0.6)	(3.4-4.2) (1.3-1.7)	(2.5-4.0) (1.0-1.6)
Dense snow	2.4-4.3 (1.0-1.7)	2.5-3.5 (1.0-1.4)	0.4-1.5 (0.2-0.6)	1.0-2.0 (0.4-0.8)	— —	— —

1.3 m/kg$^{1/3}$). These values are consistent with the corresponding values for the true crater (see next section), but the maximum radius of the true crater is roughly 40% greater than the maximum radius of the apparent crater. The data do not provide values for the radius of the apparent crater that is produced by a contact burst (charge depth zero).

Figure 45b represents the combined data for the *depth* of the apparent crater in *frozen silt*. Over the range of the data, there is not much systematic variation until the critical charge depth is reached. From the general downward trend of the data band, the apparent crater seems deepest at the relatively shallow charge depth of 1 ft/lb$^{1/3}$ (0.4 m/kg$^{1/3}$).

Figure 46 represents the combined data for *frozen till*. The range of values for scaled charge depth is too limited for definition of a clear trend. As in many blasting tests, the investigators were interested in optimum blast design, to the exclusion of data extremes. Both crater radius and crater depth seem to reach maximum values at charge depths around 1.3 to 1.5 ft/lb$^{1/3}$ (0.5 to 0.6 m/kg$^{1/3}$). This differs from the optimum range for the true crater (see below), which is about 1.8 to 2.1 ft/lb$^{1/3}$ (0.71 to 0.83 m/kg$^{1/3}$). The maximum radius of the true crater is appreciably bigger than that of the apparent crater—by 25% to 65%. Critical depth for the apparent crater seems to be about 1.6 to 2.0 ft/lb$^{1/3}$ (0.6 to 0.8 m/kg$^{1/3}$), which is shallower than the critical depth for the true crater.

The original radius data for apparent craters in *massive ice* show very wide scatter as charge depth approaches the critical value. Taking the data bands for crater radius and crater depth together (Fig. 47), it looks as if the apparent crater reaches maximum size when charge depth is in the range 1.0 to 1.5 ft/lb$^{1/3}$ (0.4 to 0.6 m/kg$^{1/3}$). By contrast, the true crater (Fig. 51) reaches maximum size when the charge depth is in the range 3 to 4 ft/lb$^{1/3}$ (1.2 to 1.6 m/kg$^{1/3}$). For the apparent crater, critical charge depth seems to be close to 3 to 4 ft/lb$^{1/3}$ (1.2 to 1.6 m/kg$^{1/3}$).

The data for other frozen materials are insufficient to establish trends. For practical purposes, the results for frozen clay shale, and for ice-rich till covered by peat, are not significantly different from the results for frozen silt.

The limited amount of data for unfrozen (thawed) soil provides some indication of the effect of freezing on crater size. The results for unfrozen silt show both crater radius and crater depth somewhat greater than corresponding values for the frozen state. The same is true when the data for unfrozen gravel are compared with results for frozen till. The actual data can be found elsewhere; a summary is given by Mellor (1985).

Data for apparent craters in *deep, dense snow* are shown in Figure 48. Crater radius has maximum values in the range 2.4 to 4.3 ft/lb$^{1/3}$ (1.0 to 1.7 m/kg$^{1/3}$), and these values are obtained when the charge depth is in the range 2.5 to 3.5 ft/lb$^{1/3}$ (1.0 to 1.4 m/kg$^{1/3}$). There is not much systematic variation of crater depth with charge depth for charge depths less than 3 ft/lb$^{1/3}$ (1.2 m/kg$^{1/3}$). The maximum depth of the apparent crater is in the range 0.4 to 1.5 ft/lb$^{1/3}$ (0.2 to 0.6 m/kg$^{1/3}$) and these maximum values occur when charge depth is in the range 1 to 2 ft/lb$^{1/3}$ (0.4 to 0.8 m/kg$^{1/3}$). Existing data for snow do not provide a clear indication of critical charge depth.

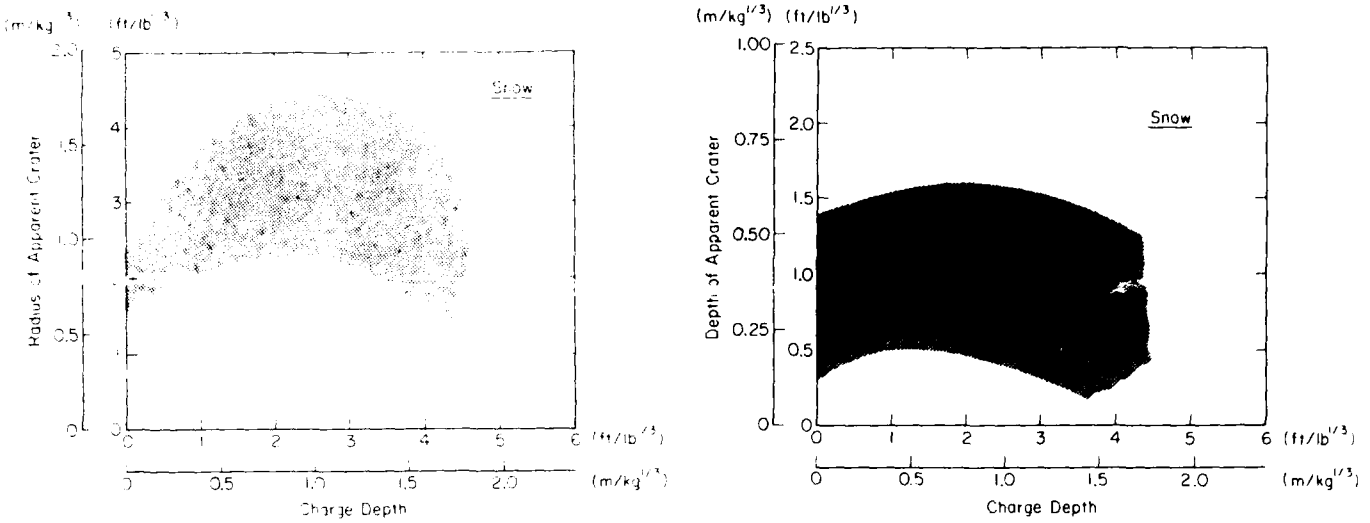

Figure 48. Scaled dimensions of apparent craters in dense snow. (Data from Fuchs 1957, Livingston 1968.)

True craters in frozen materials

Measurements on true craters are more difficult to make than are corresponding measurements on apparent craters. Nevertheless, a considerable body of data exists for frozen silt, frozen gravel, massive ice, and dense snow (Fuchs 1957, Livingston and Murphy 1979, Livingston 1960, 1968, McCoy 1965, Mellor and Sellmann 1970, Mellor 1971). These results have been compiled and plotted elsewhere (Mellor 1972, 1973). For present purposes the detailed data plots are replaced by representative data bands, as shown in Figures 49–52. Characteristic crater dimensions are summarized in Table 11.

Figure 49a gives an impression of the variation of crater *radius* with charge depth for true craters in *frozen silt*. Radius reaches maximum values when charge depth is in the range 2.1 to 2.7 ft/lb$^{1/3}$ (0.8 to 1.1 m/kg$^{1/3}$). With charge depth in this range, the crater radius is between 2.4 and 4.0 ft/lb$^{1/3}$ (1.0 to 1.6 m/kg$^{1/3}$).

Figure 49b shows how the *depth* of the true crater varies with charge depth in *frozen silt*. Until optimum charge depth is reached, the bottom of the crater ranges from charge depth to about 0.8 ft/lb$^{1/3}$ (0.3 m/kg$^{1/3}$) below the charge depth.

The *specific volume* of the true crater in *frozen silt* (Fig. 49c) indicates a well defined value for optimum charge depth—about 2.2 ft/lb$^{1/3}$ (0.9 m/kg$^{1/3}$). However, at this optimum charge depth the range of specific volume is wide—from 18 to 54 ft^3/lb (1.1 to 3.4 m^3/kg).

Table 11. Dimensions of true craters in frozen ground, ice and snow.

Material	Crater radius, ft/lb$^{1/3}$ (m/kg$^{1/3}$)		Crater depth, ft/lb$^{1/3}$ (m/kg$^{1/3}$)		Critical charge depth, ft/lb$^{1/3}$ (m/kg$^{1/3}$) for		Crater volume,		Critical charge depth, zero specific volume, ft/lb$^{1/3}$ (m/kg$^{1/3}$)
	Maximum crater radius	Optimum charge depth	Maximum crater depth	Optimum charge depth	Zero crater radius	Zero crater depth	Maximum crater vol. ft^3/lb (m^3/kg)	Optimum charge depth ft/lb$^{1/3}$ (m/kg$^{1/3}$)	
							volume	depth	
Frozen silt	2.4–4.0	2.1–2.7	2.0–3.2	2.3–3.0	2.9–?	2.8–3.2	18–54	≈ 2.2	2.8–?
	(1.0–1.6)	(0.8–1.1)	(0.8–1.3)	(0.9–1.2)	(1.2–?)	(1.1–1.3)	(1.1–3.4)	(≈ 0.9)	(1.1–?)
Frozen till	2.1–4.2	1.9–2.7	1.6–3.4	2.0–2.8	2.2–3.2	2.2–3.1	13–35	2.1–2.3	2.2–2.9
	(0.8–1.7)	(0.8–1.1)	(0.6–1.3)	(0.8–1.1)	(0.9–1.3)	(0.9–1.2)	(0.8–2.2)	(0.8–0.9)	(0.9–1.2)
Massive ice	3.1–4.9	3.5–4.0	—	—	4.2–5.7	—	38–118	3.3–4.2	4.0–5.8
	(1.2–1.9)	(1.4–1.6)	—	—	(1.7–2.3)	—	(2.4–7.4)	(1.3–1.7)	(1.6–2.3)
Dense snow	2.8–4.4	2.0–2.6	—	—	5.0–7.6	—	45–120	3.3–4.3	—
	(1.1–1.7)	(0.8–1.0)	—	—	(2.0–3.0)	—	(2.8–7.5)	(1.3–1.7)	—

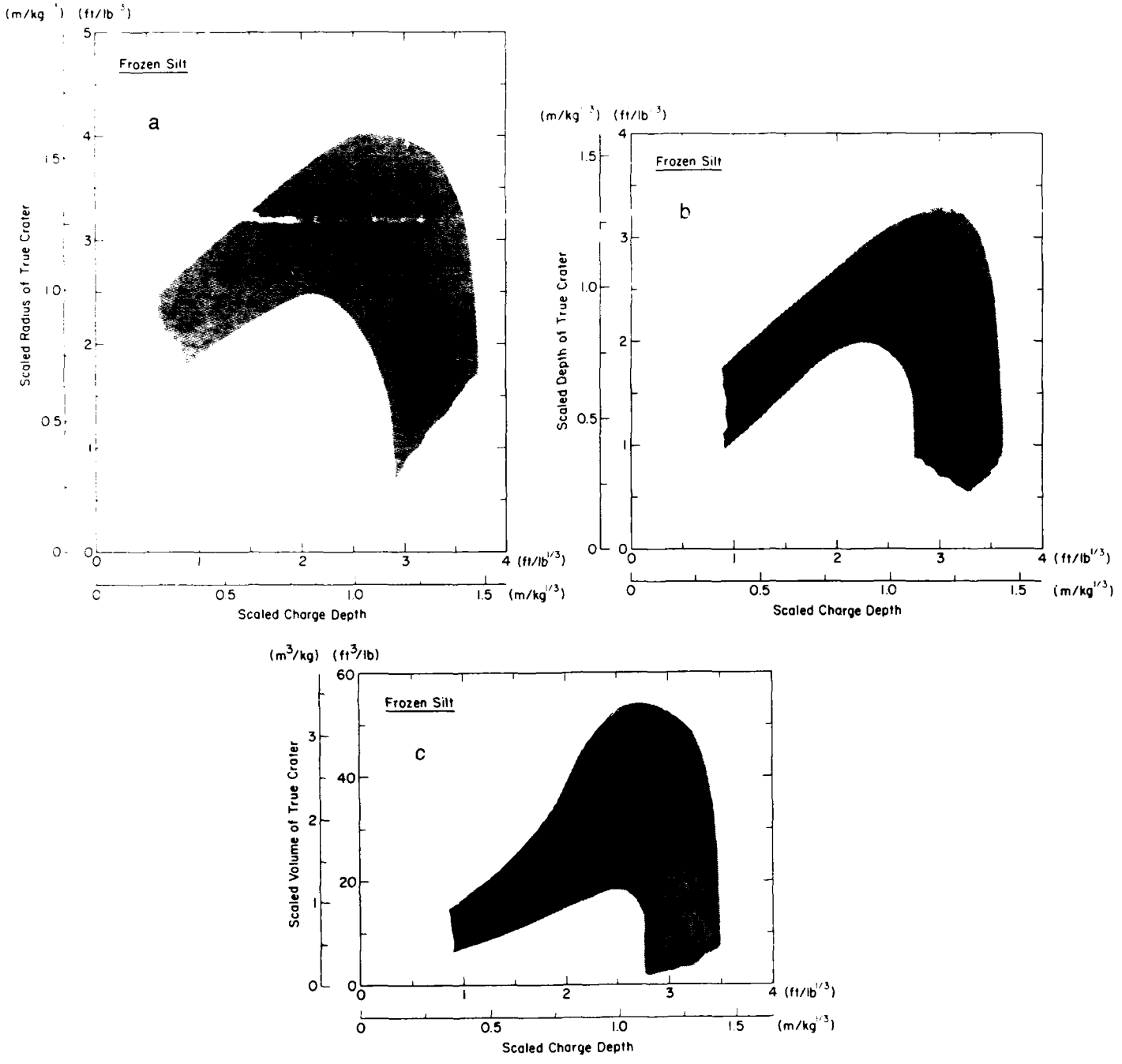

Figure 49. Scaled dimensions of true craters in frozen silt. (Data from McCoy 1965, Mellor and Sellmann 1970, Mellor 1971.)

Figure 50a gives the general magnitude of true crater *radius* in *frozen till.* The data used for this plot were obtained in frozen tills which contained both gravel and fine-grained soil, and also in clean ice-bonded gravels. The upper limit of crater radius in frozen till is not much different from the upper limit in frozen silt, and optimum charge depths are similar for the two materials. However, because some tills are stronger and denser than typical silts, the lower limit of crater radius is lower for tills than for silt, and critical charge depth can be smaller in tills than in silt. Crater radius has maximum values in the range 2.1 to 4.2 ft/lb$^{1/3}$ (0.8 to 1.7 m/kg$^{1/3}$), and these maximum values are ob-

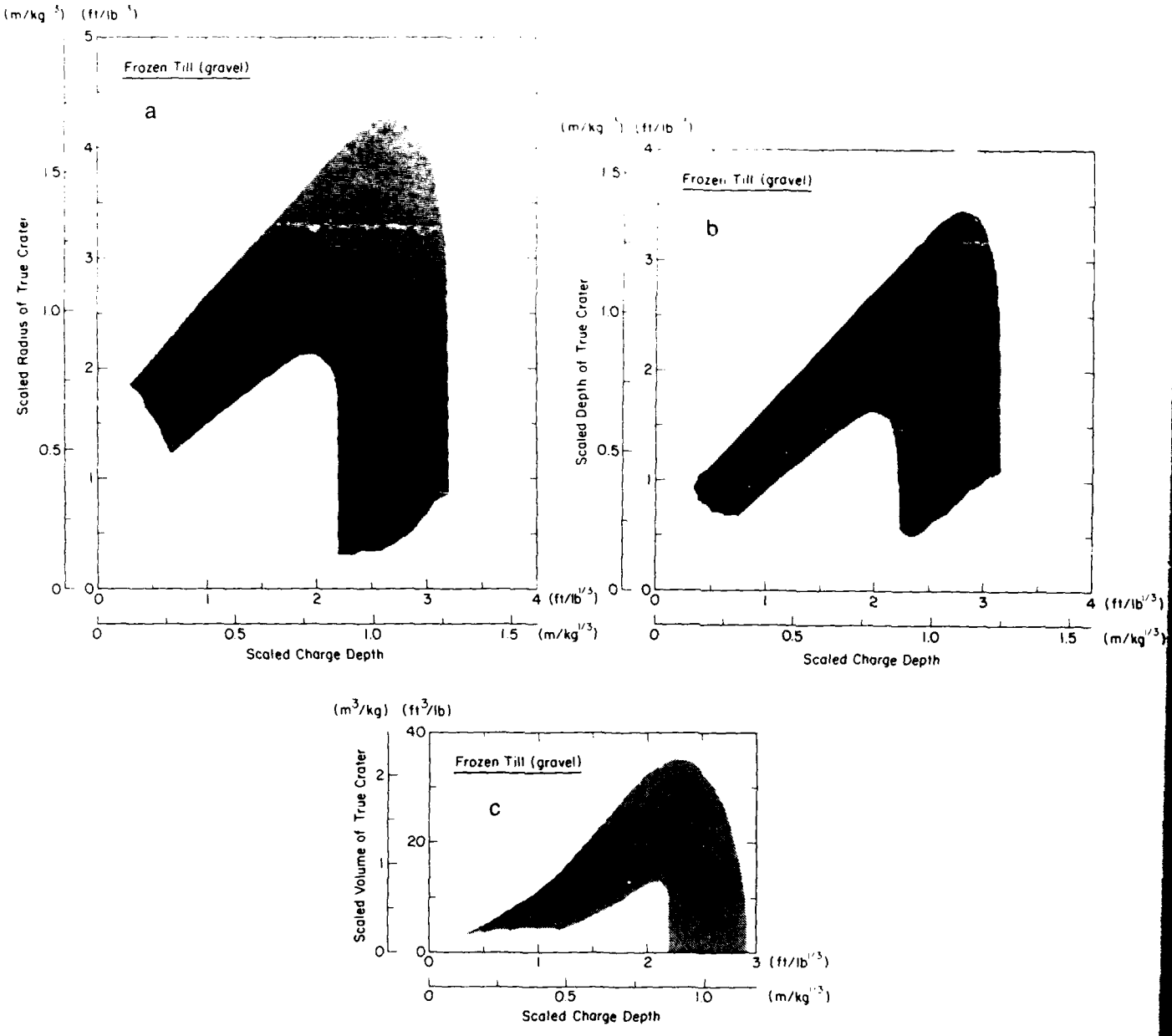

Figure 50. Scaled dimensions of true craters in frozen till or frozen gravel. (Data from Livingston and Murphy 1959, Mellor and Sellmann 1970, Smith and Mellor 1975.)

tained when charge depth is in the range 1.9 to 2.7 ft/lb$^{1/3}$ (0.8 to 1.1 m/kg$^{1/3}$).

Figure 50b represents the variation of crater *depth* with charge depth in *frozen till*. The trend is broadly similar to that for frozen silt, but crater depth is smaller over most of the range of charge depths, and critical depths are somewhat shallower in frozen till.

Figure 50c shows how *specific volume* varies with charge depth for true craters in *frozen till*. Maximum specific volume is in the range 13 to 35 ft^3/lb (0.8 to 2.2 m^3/kg) when charge depth is close to optimum, i.e. 2.1 to 2.3 ft/lb$^{1/3}$ (0.8 to 0.9 m/kg$^{1/3}$).

True craters in massive *ice* are appreciably bigger than those in frozen ground. Figure 51a gives crater *radius* as a function of charge depth in *ice*. Maximum values of radius are in the range 3.1 to 4.9 ft/lb$^{1/3}$ (1.2 to 1.9 m/kg$^{1/3}$) when charge depth is in the range 3.5 to 4 ftlb$^{1/3}$ (1.4 to 1.6 m/kg$^{1/3}$).

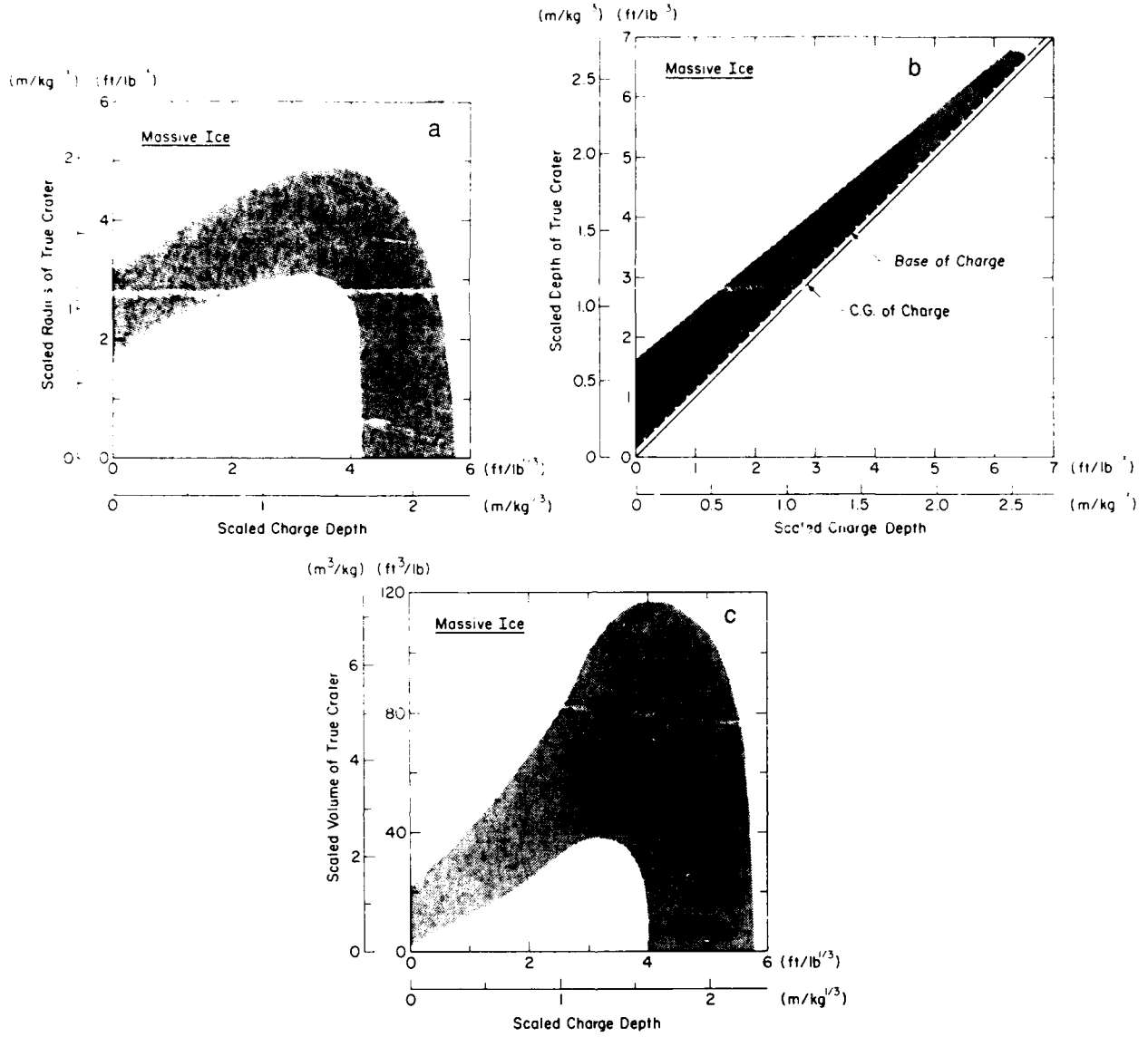

Figure 51. Scaled dimensions of true craters in massive ice. (Data from Livingston 1960.)

Figure 51b shows true crater *depth* in *ice*. The form of presentation differs from that used for frozen ground, in that the base of the broken ice is plotted for charge depths that exceed critical depth (the camouflet range). The depth of the true crater ranges from the base of the charge to a level that is 1.5 to 0.5 ft/lb$^{1/3}$ (0.6 to 0.2 m/kg$^{1/3}$) below the base of the charge.

The *specific volume* for true craters in ice (Fig. 51c) has maximum values in the range 38 to 118 ft^3/lb (2.4 to 7.4 m^3/kg) when charge depth is in the range 3.3 to 4.2 ft/lb$^{1/3}$ (1.3 to 1.7 m/kg$^{1/3}$).

Dense snow, such as is found in the surface layers of polar ice caps and in well-settled seasonal snow packs, is much weaker than ice, and less dense by a factor of 2 to 3. Nevertheless, the dimensions of the true crater in snow are not very much different from those in ice.

Figure 52a shows crater *radius* as a function of charge depth for *dense snow*. Compared with corresponding plots for ice and frozen ground, the transition from optimum depth to critical depth is less abrupt. Maximum values of radius are in the range 2.8 to 4.4 ft/lb$^{1/3}$ (1.1 to 1.7 m/kg$^{1/3}$) when charge depth is in the range 2.0 to 2.6 ft/lb$^{1/3}$ (0.8 to 1.0 m/kg$^{1/3}$).

The *depth* of the true crater in *snow* is consistently below the base of the charge—in the range 0.35 to 1.4 ft/lb$^{1/3}$ (0.14 to 0.57 m/kg$^{1/3}$) below the charge base.

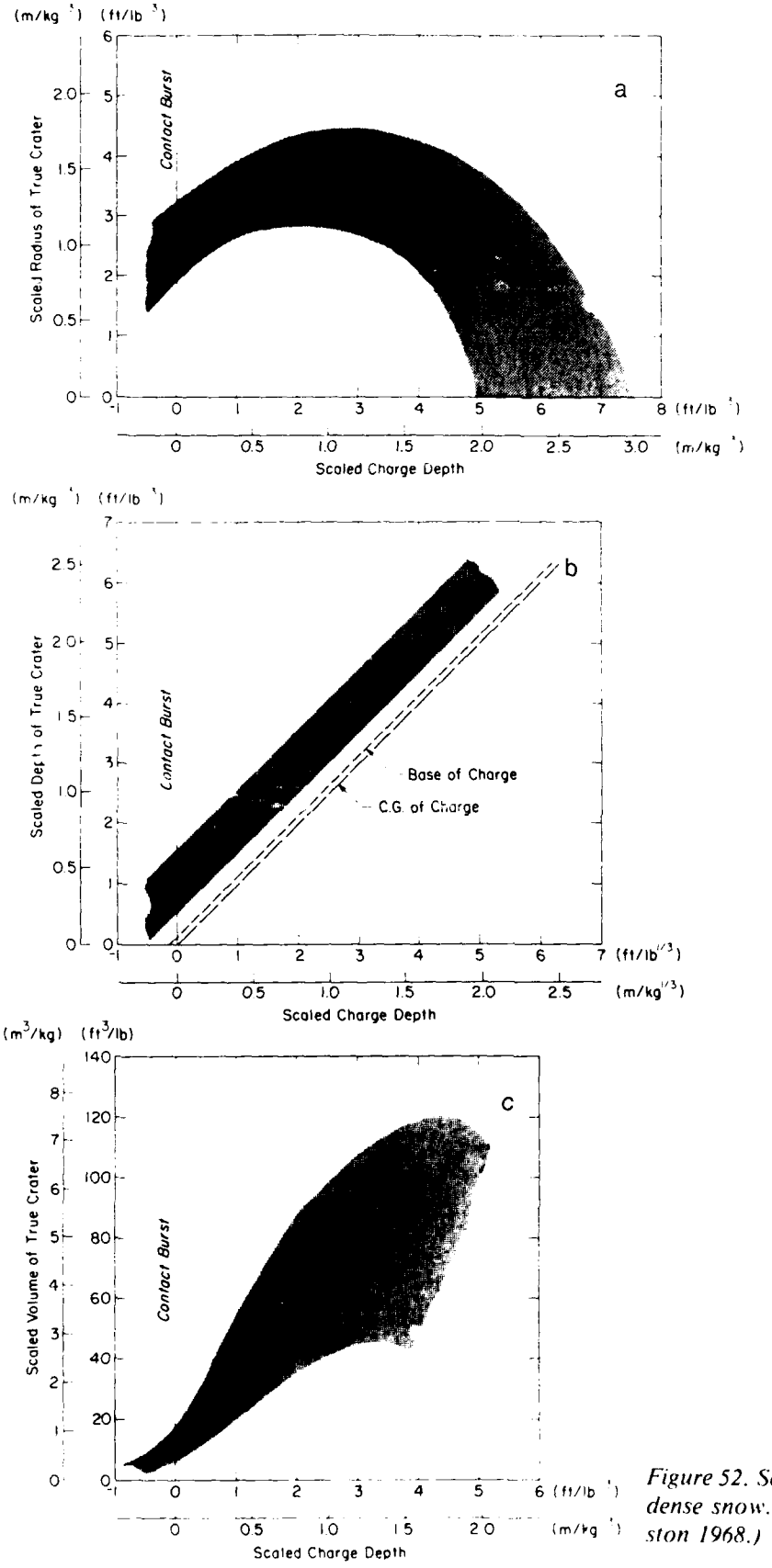

Figure 52. Scaled dimensions of true craters in dense snow. (Data from Fuchs 1957, Livingston 1968.)

The *specific volume* in *snow* has maximum values in the range 45 to 120 ft^3/lb (2.8 to 7.5 m^3/kg). These values are obtained when charge depth is in the range 3.3 to 4.3 $ft/lb^{1/3}$ (1.3 to 1.7 $m/kg^{1/3}$).

ROW CRATERS, DITCHES AND SINKING CUTS

In military engineering, a line of overlapping craters may be required in order to form an obstacle. The composite crater is usually termed a *row crater*. In construction, explosives may be used either to form a ditch directly, or to fracture the ground so that a ditch can be excavated mechanically. The operation is usually referred to as *trench blasting*, or *ditch blasting*.

The simplest way to make a row crater or ditch is to place a line of closely spaced cratering charges at optimum depth. If the charges are widely spaced, each produces its own independent crater of radius R_1, following the relations that were given previously. When the center-to-center spacing of the charges (s) is such that $s \geq 2R_1$, there is no overlap and the craters are independent, except for possible interference of the crater lips and some exchanges of debris. However, values of s up to $3R_1$ to $4R_1$ may be adequate for creating a vehicle barrier in military operations, since the crater lips form mounds. Much closer spacing is needed to develop a continuous row crater, or ditch, but when s is sufficiently small, say $s < 1.4R_1$, the width of the resulting ditch can exceed $2R_1$ and the depth of the ditch can exceed the depth of a single crater.

The width and depth of a row crater are often discussed in terms of an "enhancement factor." If R_1 is the radius of the apparent crater for a single charge, and D_1 is the corresponding depth, the apparent width of the row crater B_r and the apparent depth of the row crater D_r are such that $B_r/2R_1 > 1$ and $D_r/D_1 > 1$ when $s/2R_1 < 0.7$ (i.e. $s < 1.4R_1$). The general trend given by test data is shown in Figure 53; the enhancement factor can reach about 1.6 when s/R_1 is decreased to about 0.55. To obtain optimum enhancement in this way, the charge depth should be increased as s/R_1 decreases. For a given charge spacing s/R_1, the optimum charge depth d_c is obtained from Figure 53 as $d_c = (B_r/2R_1)d_{c_1} = (D_r/D_1)d_{c_1}$, where d_{c_1} is the charge depth optimized for a single apparent crater.

When trenches are to be blasted for construction work, various methods can be used. If individual explosive charges are intended to break the ground material and to excavate it in a single operation, the procedure is identical to that described above for row craters; the linear apparent crater is accepted as the finished trench. If the ditch is for land drainage, water flow can sometimes flush out blast debris that is loose and fine-grained. By contrast, if the operation is to be more conservative, with limits on explosive consumption, flyrock (ejecta), ground motion, airblast, and overbreak, then the emphasis is on production of overlapping *true* craters, with optimized breakage. The design parameters for the true crater are obtained for a single crater that has its charge depth just less than critical depth, and the degree of overlap is decided by adjustment of both charge spacing and charge depth. The broad aim is to break up the rock within the planned limits of the excavation, while avoiding overbreak and ejection of missiles. Fragmented material is dug out with a backhoe or something similar.

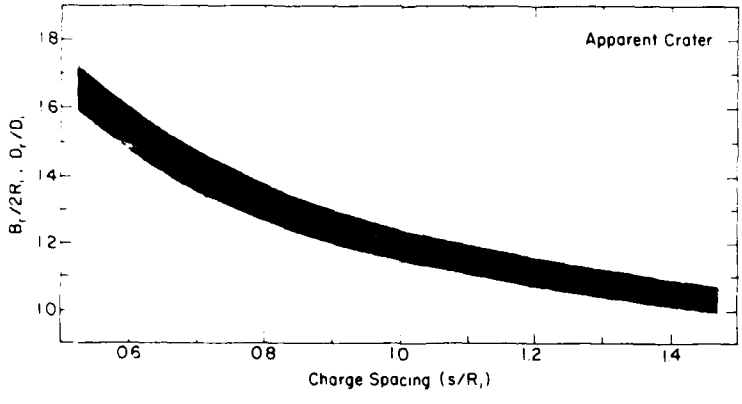

Figure 53. Enhancement of dimensions for the apparent crater when closely spaced charges are fired in a row. (After Rooke et al. 1974, U.S. Army 1984.)

A single row of cratering charges is less than ideal for excavation of a steep-sided trench in rock, but the alternative of using multiple rows of smaller charges is sometimes prohibitive in terms of drilling and loading effort. One possibility is to use a single row of vertically delayed deck charges (Mellor and Sellmann 1970).

For pipeline trenching in rock, the end of the trench may be advanced by a technique similar to bench blasting.

Special explosives and delay detonators have been developed for trenching; both the cartridges and the caps resist premature detonation by propagation.

Another way to make a large trench, or an antitank ditch, is to lay a linear charge (sausage charge, or pipe charge) in a narrow excavated cut, with some backfill (stemming). In this case, the charge is emplaced like an underground cable or small diameter pipe, using slot-cutting equipment instead of shothole drills. Rough estimates of the required charge per unit length can be made from row crater data; if W is the required weight of each charge in a row with charge spacing s, the equivalent charge per unit length is W/s. Such an estimate is only a first approximation, since shock propagation and attenuation are two-dimensional rather than three-dimensional, but it permits the use of available data from single-crater tests. An alternative approach is to regard the buried linear charge as a column charge of the type that would be used in bench blasting. With burial depth B and charge diameter D, the effective range of B/D in hard material might be 20 to 40.

Ditches in soft ground can be blasted by using small cartridges of ditching dynamite or a modern AN water gel equivalent. The necessary shotholes can be drilled easily with a simple auger or a driving bar (punch). When cartridges of approximately 1.25 in. (32 mm) diameter are used, each hole has a collar distance of 6 to 12 in. (150 to 300 mm), preferably fully stemmed. Tables 12 and 13 give guidelines for soft ground ditching with either a single row of charges or multiple rows. One of the traditional methods for ditching in *wet* soils relies on propagation (sympathetic detonation) between the individual charges. Cartridges of sensitive explosive, usually ditching dynamite (i.e. 50% straight dynamite), are tamped into saturated soil at fairly close spacing, without any kind of connection between the individual charges. The first charge in the row is fired by a single cap, and the blast then propagates from charge to charge by shock transmission. In wet ground, with temperatures above freezing, reliable propagation can be achieved over scaled distances of approximately 2

Table 12. Ditching in soft ground with single row of charges. (After C.I.L. 1984.)

Cartridges per hole (1¼ × 8 in.)	*Depth to top of charge (in.)*	*Distance between holes (in.)*	*Probable depth of ditch (ft)*	*Probable top width of ditch (ft)*	*Explosive consumption (lb/100 ft)*
½	6-8	12	1.5	4	25
1	6-12	15	2.5	6	40
2	6-12	18	3	8	65
3	6-12	21	4	10	85
4	6-12	24	5	13	100
5	6-12	24	6	16	125

Table 13. Ditching in soft ground with multiple rows of charges. (After C.I.L. 1984b.)

Cartridges per hole (1¼ in. × 8 in.)	*Hole spacing (in.)*	*Row spacing (in.)*	*Depth of ditch (ft)*	*Number of rows*									
				3		*5*		*7*		*9*		*11*	
				(ft)	*(lb/100 ft)*	*(ft)*	*(lb/100 ft)*	*(ft)*	*(lb/100 ft)*	*(ft)*	*(lb/100 ft)*	*(ft)*	*(lb/100 ft)*
1	15	30	2.5-3	11	80	—	—	—	—	—	—	—	—
2	18	36	3-3.5	11	133	14	200	—	—	—	—	—	—
3	21	42	4-4.5	13	172	17	257	20	343	—	—	—	—
4	24	48	5-5.5	17	200	21	300	25	400	29	500	—	—
5	24	48	6-6.5	20	250	24	315	28	500	32	625	36	750

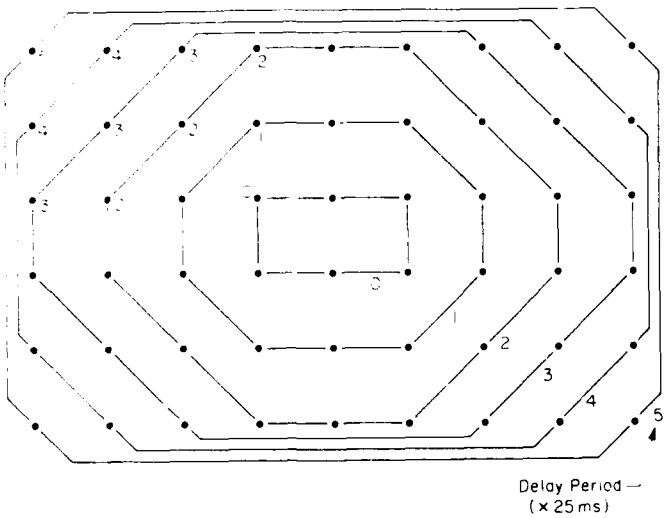

Figure 54. Example of the layout, connections and delays for charges used to make a sinking cut.

ft/lb$^{1/3}$ (0.8 m/kg$^{1/3}$). The loads and spacings given in Tables 12 and 13 should provide reliable propagation with ditching dynamite in wet soil.

A *sinking cut* is a multi-charge blast that produces a pit in a surface which is close to horizontal. In essence, a sinking cut is an array of many cratering charges set deep enough to avoid much throw or flyrock. Ideally, the broken rock forms a mound of fragments that can be excavated easily by mechanical equipment.

The simplest form of sinking cut would be an array of compact cratering charges set just shallower than critical depth and fired simultaneously to give overlapping craters. However, in typical practice extended column charges in small-diameter boreholes are likely to be used, and delays are employed, both to improve the breakage and to reduce ground vibrations. This makes the sinking cut more like a tunnel-blasting round. Figure 54 shows the general arrangement for a sinking cut when the pit is to be roughly equidimensional in plan. If the pit is to be long and narrow, more like a ditch, then the delay pattern can be arranged to displace material towards the centerline.

The powder factor for sinking cuts is typically about 0.75 to 1.5 lb/yd^3 (0.44 to 0.89 kg/m^3). In terms of specific volume, these values translate to a typical range of 18 to 36 ft^3/lb (1.1 to 2.2 m^3/kg), with a lower limit around 11 ft^3/lb (0.7 m^3/kg). Such values are not much different from specific volumes for the true crater when a single charge is fired at optimum depth in common rocks (see Fig. 30–35).

Sinking cuts are typically up to 15 to 20 ft (4.6 to 6.1 m) deep, but can be as much as 40 ft (12 m). Shotholes are usually drilled below the required finished grade to allow for the uneven surface that results from cratering blasting.

Repetitive crater blasts produce some enlargement of a crater. The idea is to first fire a charge at

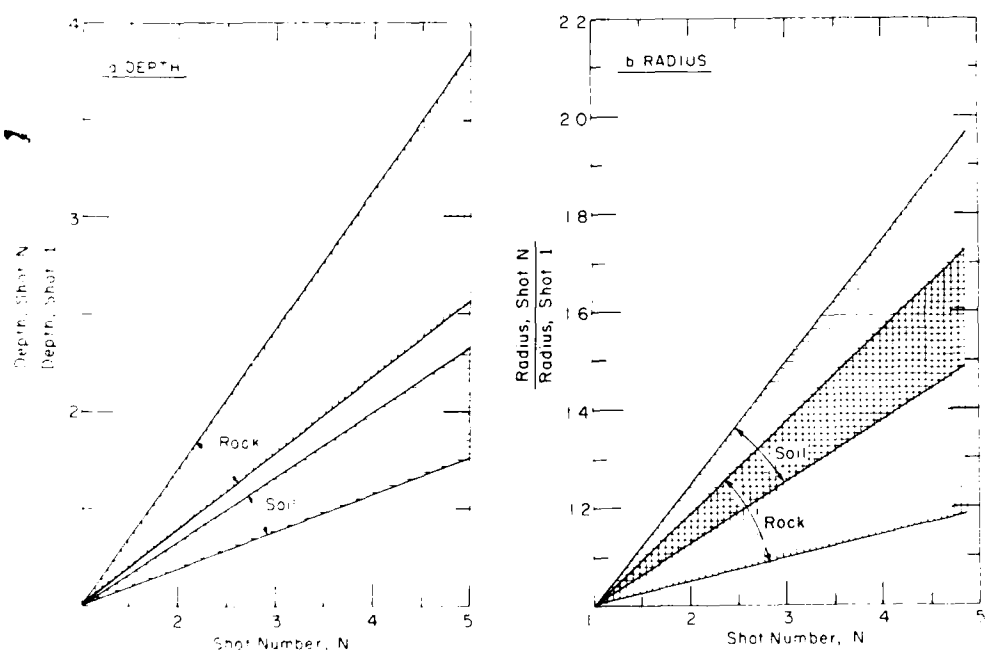

Figure 55. Effect of repeated explosions on the dimensions of apparent craters in rock and soil. After Rooke et al. 1974, U.S. Army 1984.)

or near the surface, then to fire a second charge of equal size at the bottom of the crater, and so on. This procedure, which is referred to as *nail driving*, gives significant increase of crater depth while producing relatively little increase of the crater radius at ground level. Figure 55 indicates the magnitude of the effect for the radius and depth of true craters in rock and soil.

UNDERWATER CRATERS AND TRENCHES

In considering the process of cratering underwater, it is helpful to draw a parallel with standard crater blasting on dry land. In one case the soil or rock is overlain with air, in the other case with water, which is a thousand times more dense. Systematic study of underwater cratering has not gone very far, so it is necessary to speculate on how the various processes might be affected.

For comparison of cratering on dry land and underwater, we assume that the water depth is sufficient to prevent direct blowout through the water/air surface. We also recognize that the strength S of soil or rock has two components, an inherent cohesion c and an "internal friction" that increases with the applied compressive stress p, such that $S = c + p\tan\phi$, where ϕ is an effective angle of internal friction. We also note that some soils and rocks are impermeable, while others are permeable, allowing pore water pressure to equilibrate with the surface fluid pressure.

With these things in mind, the following effects seem likely:

1. For impermeable underwater materials, the "internal friction" component of strength will increase with increasing water depth, since p increases, but the effect is small.

2. For permeable granular soils which have low cohesion ($c \rightarrow 0$), submersion will reduce the strength below the "dry land" value, since the effective unit weight of the soil grains is decreased by buoyancy (p is lower for a given depth in the soil).

3. When a crater is formed, fragmented material will settle to angles of repose smaller than corresponding angles in air, and loose material is likely to wash back into the crater by water motion.

4. When a charge detonates at the interface between the water and the bed material, the overlying water confines the explosion more than air would do for a surface charge on dry land. In effect, the charge is mud-capped by the water, and energy transfer to the underlying solid is likely to be more efficient than it would be in air.

5. The breakout and heave of material from a buried explosion will be subdued by the inertial resistance of overlying water.

6. Ejected fragments meet much higher resistance in water than in air, since the fluid density is about a thousand times higher.

Taking into account all of these potential effects, certain net results can be expected. For strong materials and relatively shallow water, a charge set directly on the bed could break more of the bottom material than an equivalent surface charge in air would do, but ejected fragments will not travel very far or very fast. A charge buried in strong material is likely to be less effective than an

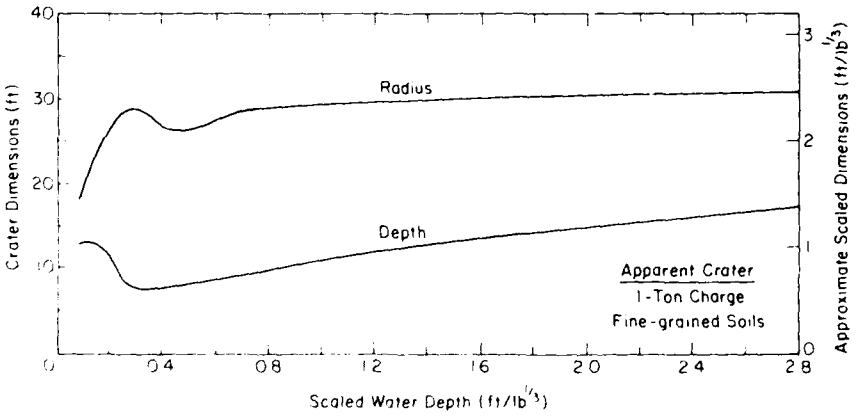

Figure 56. Dimensions of underwater apparent craters in fine-grained soils as a function of scaled water depth. One-ton charge fired in direct contact with the bed of the water body. (Rooke et al. 1974.)

equivalent cratering charge on dry land, as bubble expansion effects are subdued by overlying water. In weak bed sediments at relatively shallow depths, a charge set directly on the bed is likely to displace more material than an equivalent charge in air, but the final dimensions of the crater will be affected by "washback" and by the shallower angles of repose that are common underwater. Buried charges in weak underwater sediments could displace more material than equivalent charges on land, since the effective strength of the soil is lower underwater. However, the throw of the material is likely to be suppressed, leaving a relatively small apparent crater.

Actual data are sparse. Figure 56 shows the radius and depth of the apparent crater for a 1-ton charge set directly on fine-grained underwater material, with scaled water depth as a variable. At very shallow water depth, the explosion vents directly to air and the crater dimensions are affected strongly by washback (unless the water depth is less than the minimum height of the crater lip). When the scaled water depth exceeds 0.8 ft/lb$^{1/3}$, the crater dimensions are more than twice the dimensions that would be expected for fine-grained dry soils on land (radius 0.9 to 1.3 ft/lb$^{1/3}$, depth 0.3 to 0.5 ft/lb$^{1/3}$). There does not appear to be any published information on point-charge craters in rock, or on true craters (except for situations where the scaled water depth is very small, in which case there is not much difference from blasting in saturated soil or rock on land).

Guidelines for underwater trenching in coral have been given by Hallanger (1976), although the information provided is incomplete. Diagrams indicate the trench cross sections produced by various types and amounts of explosive (Fig. 57), and it is assumed here that these cross sections are for the apparent linear crater. Water depth is not specified, but lack of geometric similarity as charge weight increases suggests that the water is shallow enough for venting and washback to be significant and variable with charge size. The charge per unit length is known for Bangalore torpedoes (Fig. 57a); it is approximately 2 lb/ft for a single tube (9 lb of main charge plus a booster for each 5-ft length). Figure 57b refers to packs, each containing 20 lb of explosive, but the spacing is not given explicitly (spacing of 3-4 ft is mentioned, perhaps for each heap of explosive packages, or perhaps only for single 20-lb packages). Figure 57b refers to a non-standard hose charge designated "M8 demolition charge"; the results are not consistent with those for Bangalore torpedoes, possibly because the hose charges covered more horizontal width.

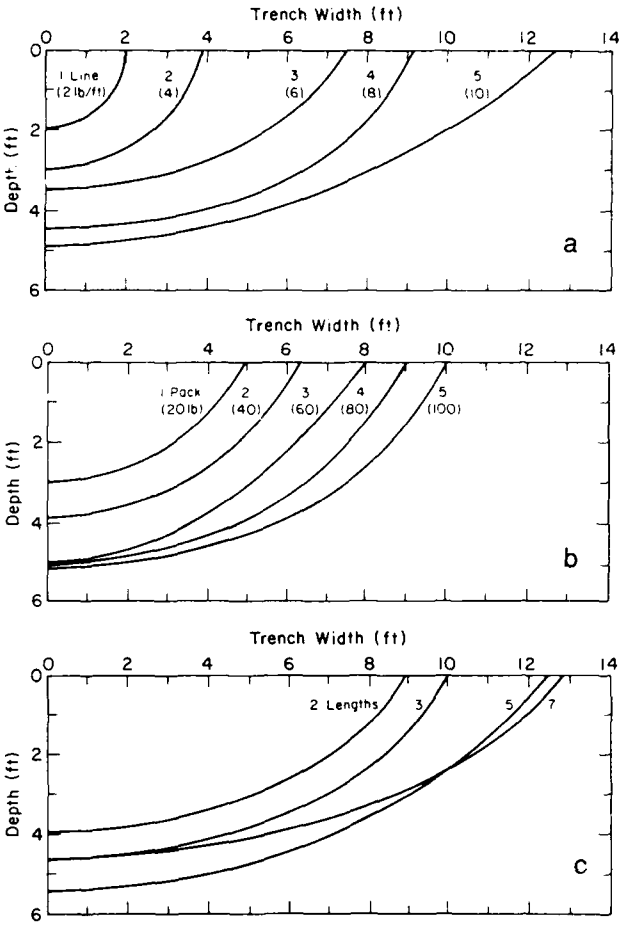

Figure 57. Dimensions of underwater trenches in coral when linear charges are fired directly on the bed: a) Bangalore torpedoes (2 lb/ft), b) packs of explosive (20 lb each) at unspecified intervals (perhaps 3-4 ft), c) hose charges (unit weight not specified). (Hallanger 1976.)

When multiple charges are used under water, propagation is possible. This can be an advantage in providing a simple way to initiate multiple charges of sensitive explosive. It can also be a disadvantage if there is a requirement for delays between charges. To avoid propagation, it may be necessary to use insensitive explosives and caps.

BOMB AND SHELL CRATERS

Representative dimensions for craters formed in soils by old-style bombs and shells are provided by measurements made during World War II. Table

Table 14. Representative dimensions of bomb craters. (After U.S. Army 1965.)

Bomb (kg)	Depth of burial (ft)	Crater diameter (ft)	Crater depth (ft)	Soil	Remarks
50	1.0	16.5	4.7	Clay	
	7.1	19.3	5.2	Clay	
	11.4	6.0	2.5	Chalk	
	?	8.5	2.0	Railway embankment	
	16.0	9.5	1.7	Clay	Deep camouflet
	?	10.0	1.0	Sand and gravel	
100	7.5	18.5	5.2	Clay	
250	8.0	33.8	9.0	Clay	
	?	12.0	4.0	Clay	
	12.5	36.3	9.7	Clay	
	16.0	24.0	6.8	Clay	
	22.0	27.0	6.2	Clay	Camouflet
500	16.0	42.0	9.0	Clay	
1000	20.0	57.0	14.0	Clay	

Table 15. Probable size of shell craters in compact soil. (After U.S. Army 1965.)

	Small penetration depth		Moderate penetration depth	
Shell	Diameter (ft)	Depth (ft)	Diameter (ft)	Depth (ft)
75 mm	4.0	1.5	5.0	3.0
105 mm	6.5	2.5	7.5	3.75
155 mm	10.0	4.0	12.0	5.0
8 in.	11.5	4.0	13.5	5.0
240 mm	14.0	4.0	15.5	5.5

Table 16. Measured crater sizes for shells with delay fuses penetrating sandy clay. (After U.S. Army 1965.)

	Average			Maximum recorded		
Shell	Length (ft)	Width (ft)	Depth (ft)	Length (ft)	Width (ft)	Depth (ft)
75 mm	6	5	4	10	6	5
105 mm	7	7	4	8	8	4
155 mm	12	11	6	14	12	8
240 mm	19	19	7	—	—	—

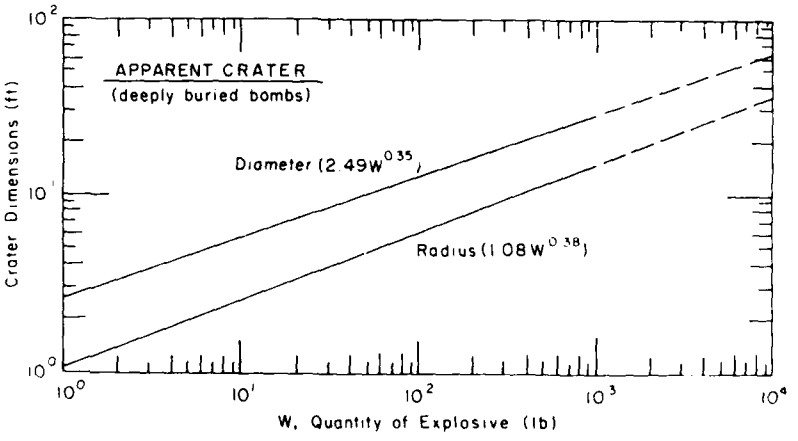

Figure 58. Dimensions of apparent craters produced by deeply buried bombs. (Rooke et al. 1974.)

14 gives some values for bombs of various sizes and for various penetration depths. Tables 15 and 16 give crater dimensions for shells of various sizes with varying depths of penetration prior to detonation. Trends of more recent data were given by Rooke et al. (1974), as shown in Figure 58. Craters from deeply buried bombs are deeper and narrower than those from equivalent cratering charges, perhaps because the ballistic penetration prepares a preferential venting path. Near-surface detonation of shells apparently forms craters somewhat larger than those of equivalent stationary charges, probably because the kinetic energy at impact contributes to crater formation (inert projectiles form impact craters that are quite similar to explosion craters).

EJECTED FRAGMENTS
(Flyrock, ejecta, missiles)

In planning blasting operations or assessing explosion effects, it is useful to know something about the range, size and quantity of flyrock. It may also be useful to have information on impact angles, maximum heights reached by projectiles, and the thickness of debris blanketing the area around the crater.

The characteristics of flyrock depend on the charge weight, the charge depth, and the properties of the ground material. The range and altitude of flyrock increase as charge size increases; the total amount of flyrock and the thickness of the debris layer also increase with charge size. Loose material, such as sand, obviously dislodges more easily than cohesive material like rock, but big chunks of cohesive material can be thrown much further than small grains. A charge lying directly on the ground surface (zero charge depth) acts something like a punch, or an impacting projectile, kicking flyrock up from an annular zone around the charge at fairly steep ejection angles (Fig. 59). When the charge is buried, flyrock ejection angles tend to increase as charge depth increases, while the horizontal range of projectiles decreases. Eventually, just before charge depth reaches the critical depth for camouflet, most of the fragments rise vertically and flop back down into the crater.

Quantitative information on flyrock is sparse and some of the published relations are puzzling. In some discussions of fragment ejection, the basic question of how far flyrock travels is completely ignored.

Simple tables of safe distance from "charges placed on or in the ground" have been based on a criterion of 300 ft/lb$^{1/3}$ (119 m/kg$^{1/3}$) for military operations, with an increase of the safe distance to 350 ft/lb$^{1/3}$ for quarrying operations (U.S. Army 1967). For heavy *surface charges* (0.5–500 ton), Johnson (1971) quotes relations developed by Vortman (1967):

$$R_{max} = A\,W^{0.4} \tag{23}$$

where R_{max} is the maximum range of ejected fragments, W is charge weight, and A is a constant for a particular charge shape. When R_{max} is in feet and W is in tons (TNT equivalent), A has the value 1470 for a spherical charge and 630 for a hemispherical charge (round side up). The exponent 0.4 is not explained; Rooke et al. (1974) suggest that the range of missiles from surface explosions scales as $W^{0.3}$ (which is inconsistent with their scaling for buried explosions). For buried charges, the maximum flyrock travel is a function of both charge weight and charge depth. The only published relations (Fig. 60–61; see Vortman 1967, Johnson 1971, Rooke et al. 1974) employ a curious scaling. Charge depth is scaled in the usual

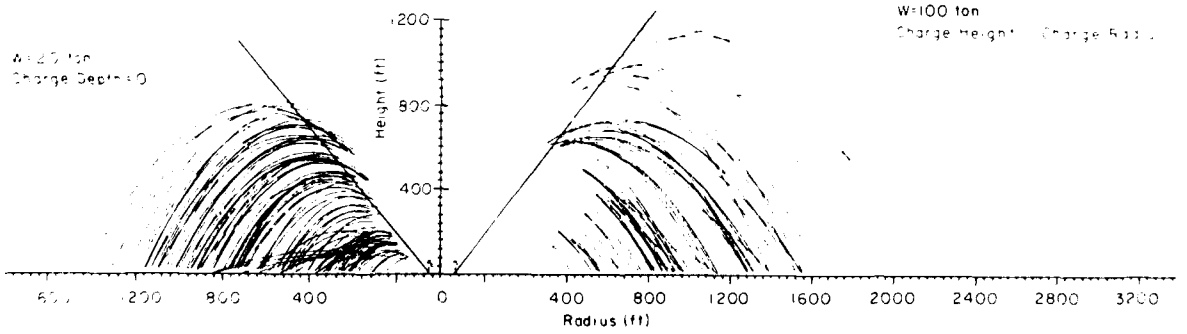

Figure 59. Trajectories of flyrock for 20-ton and 100-ton charges in direct contect with the ground surface.

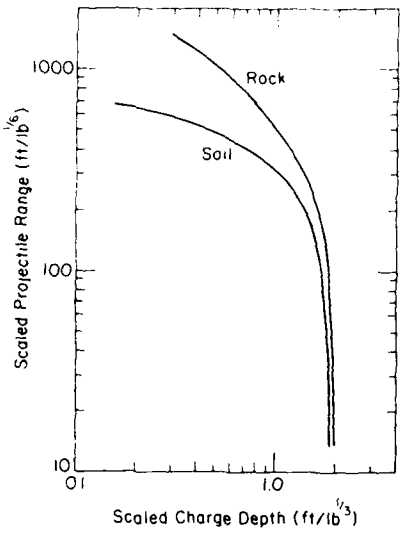

Figure 60. Scaled flyrock range as a function of scaled depth for charges buried in soil and rock. See text for queries concerning sixth root scaling. (After Rooke et al. 1974.)

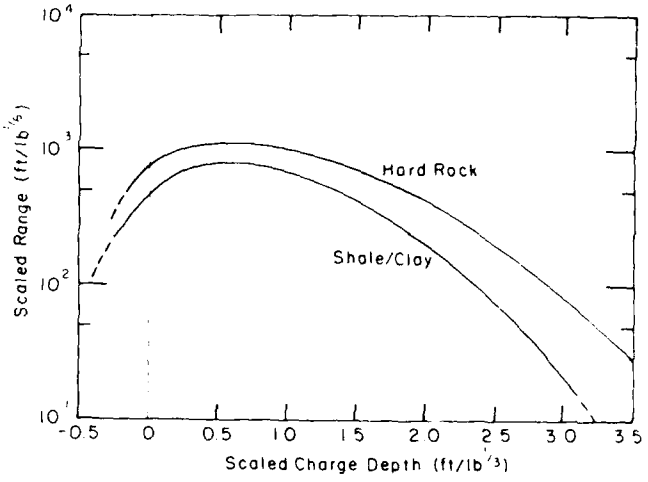

Figure 61. Scaled flyrock range for charges in, and above, hard rock and clay shale. See text for queries concerning sixth rooth scaling. (After Rooke et al. 1974.)

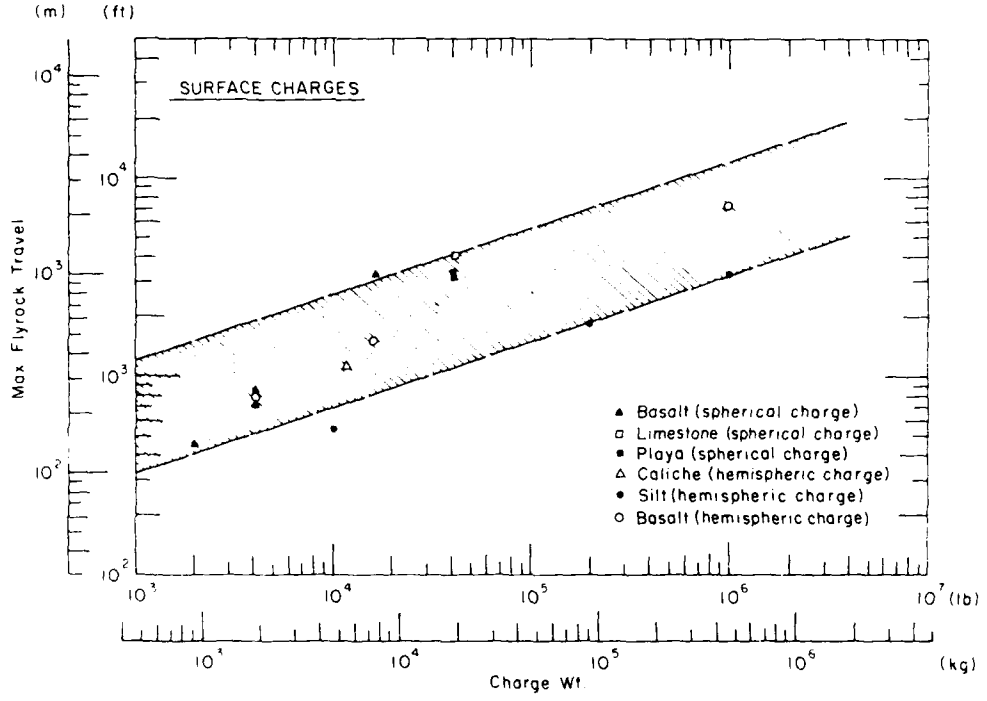

Figure 62. Maximum flyrock range plotted against charge weight for surface charges set on various ground materials. The shaded band indicates a cube root trend.

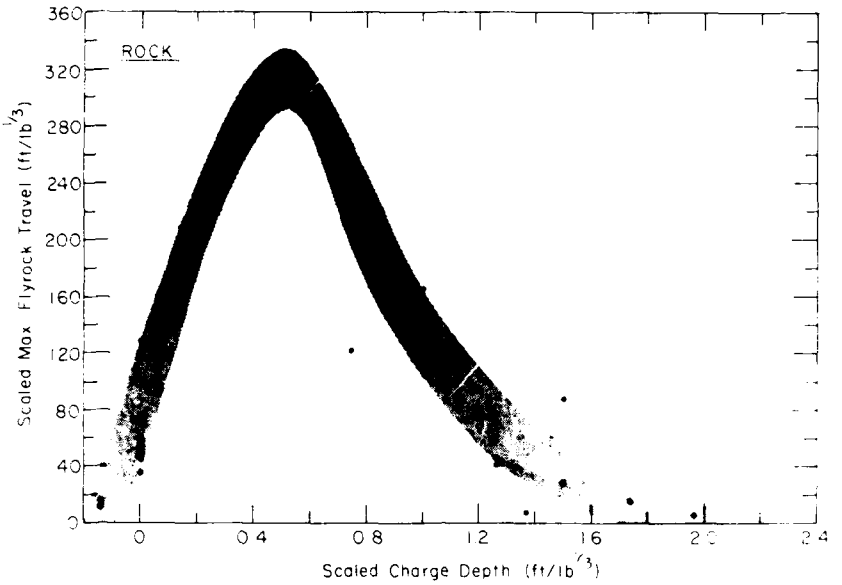

Figure 63. Maximum flyrock range plotted against charge depth in rock, employing cube root scaling for both range and depth.

way with respect to the cube root of charge weight, but flyrock range is scaled with $W^{1/6}$. This implies a very weak dependence on charge size. It also conflicts with the finding that time and velocity scale as $W^{1/6}$ (Cooper and Sauer 1977, Wisotski 1977), as required by dimensional analysis when the gravitational acceleration is invariant. Since large fragments follow almost ballistic trajectories, elementary ballistics gives range proportional to the square of velocity, time, or the product of velocity and time, i.e. ballistic range for large fragments should be proportional to $W^{2/6}$, or $W^{1/3}$.

After examining the data used by Vortman (1967) and later writers, it is hard to accept the empirical scaling of flyrock range by a one-sixth power of charge weight. Only the data for zero charge depth (Fig. 62) can be used to test the hypothesis directly, and these results certainly do not justify rejection of cube root scaling. For points representing the same material and charge type, the exponent is about 0.4 (as in eq 23). Cube root scaling of all the data for rock (Fig. 63) suggests a plausible relation between maximum flyrock range and charge depth, with scatter similar to that found in typical data for crater dimensions. The scaled data for soils (Fig. 64) show no significant correlation between flyrock range and charge depth, perhaps because these materials are highly pulverized by the explosions, leaving few blocky projectiles that can be thrown to extreme range.

Kinney and Graham (1985), in a discussion that

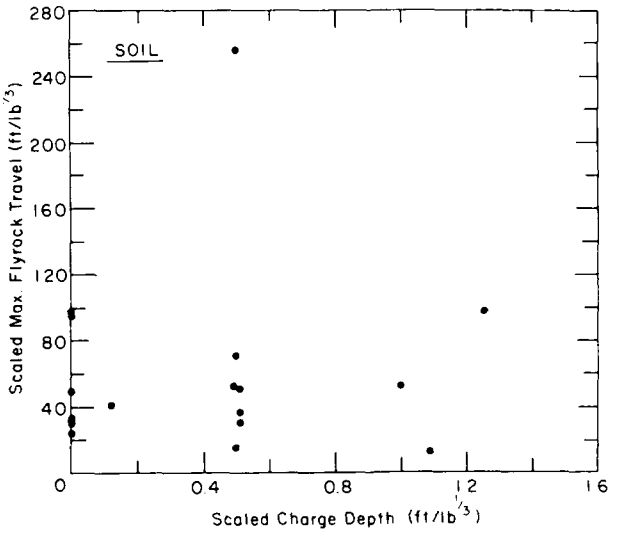

Figure 64. Scaled flyrock range plotted against scaled charge depth in soil. There is no significant correlation for this set of data (see text.)

seems to refer mainly to casing fragments from surface explosions, accept cube root scaling without question. They give maximum missile range R_{max} as

$$R_{max} = 45\, W^{1/3}\ \text{m} \qquad (24)$$

when W is in kg of TNT equivalent. For safety distances in bomb disposal work, they quote $R/W^{1/3}$

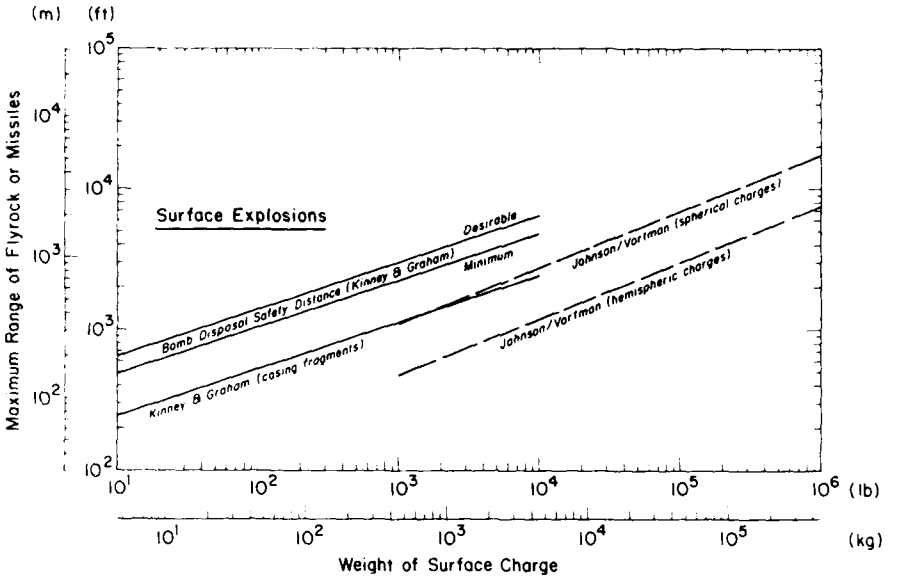

Figure 65. Safety recommendations for bomb disposal on the ground surface (cube root scaling), together with flyrock range predictions for surface explosions (scaling exponent 0.4).

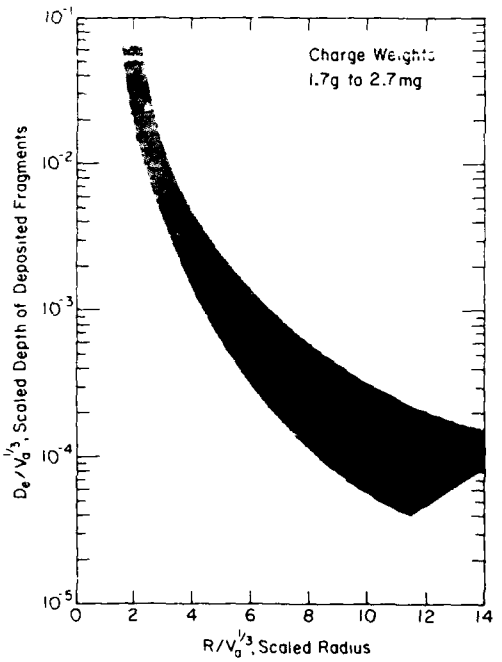

Figure 66. Variation of the depth of deposited fragments with distance from the explosion. The scaling factor is the cube root of the volume of the apparent crater (something not likely to be known before the event). (After Andrews 1977.)

= 120 m/kg$^{1/3}$ as the desired distance and $R/W^{1/3}$ = 90 m/kg$^{1/3}$ as the minimum distance (Fig. 65).

In a study of flyrock from bench blasts, Roth (1979) gave some consideration to flyrock from crater blasts, but did not reach firm conclusions.

Some military texts give more attention to the depth of ejected material on the ground surrounding the crater than to the flyrock range. Data are given in scaled form, using the cube root of apparent crater volume as the normalizing factor. Figure 66 gives a relation between debris depth and ground radius that is based on actual data points. Figure 67 gives a relation extended to greater radii. The uncertainty in debris depth is apparently very great at the largest radii plotted—more than three orders of magnitude.

Most of the ejected material falls close to the lip of the crater. Figure 68 shows the distribution of total flyrock volume with radial range from ground zero. The range is scaled with respect to the radius of the apparent crater, and it can be seen that for buried explosions about 80% of the material is deposited within about 5 crater radii from ground zero. For near-surface explosions, 80% of the flyrock is deposited within about 7 crater radii from ground zero. Glasstone et al. (1977) state that the deposit of ejected material from a nuclear explosion is continuous out to a radius of approximately 2 to 3 crater radii, and suggest that 80% to 90% of the total amount of eject-

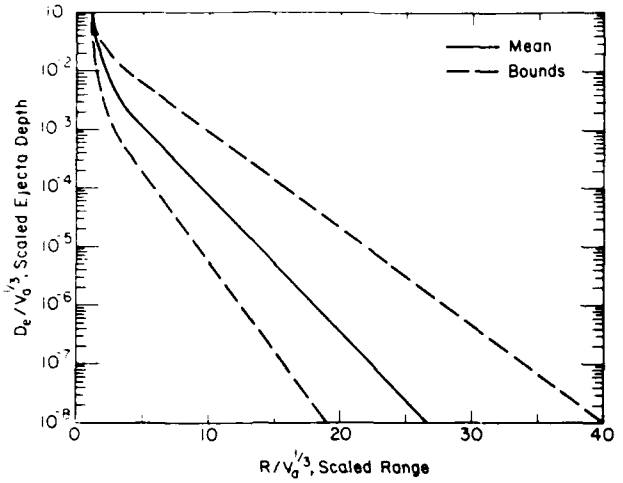

Figure 67. Variation of the depth of deposited fragments with distance from the explosion. Note the very great uncertainty at the upper limits of range. (U.S. Army 1984.)

ed debris falls within this zone. The charge depth is not specified.

The material that travels farthest as flyrock is likely to originate in a near-surface zone around ground zero. Conversely, the material that originates close to the boundary of the true crater is likely to finish up as fallback. Figure 69 gives an indication of the likely travel distance for material from the crater of a 20-ton explosion at a scaled depth of approximately 0.8 ft/lb$^{1/3}$ (0.3 m/kg$^{1/3}$). Figure 70 gives corresponding information for a 100-ton explosion at a scaled depth of about 0.2 ft/lb$^{1/3}$ (0.07 m/kg$^{1/3}$).

For protection against bombardment by flyrock, it is useful to have some information on probable angles of impact. In nuclear weapon analyses, impact angles for ejecta are computed, making assumptions about ejection angles and drag coefficients, and using calculated impact vel-

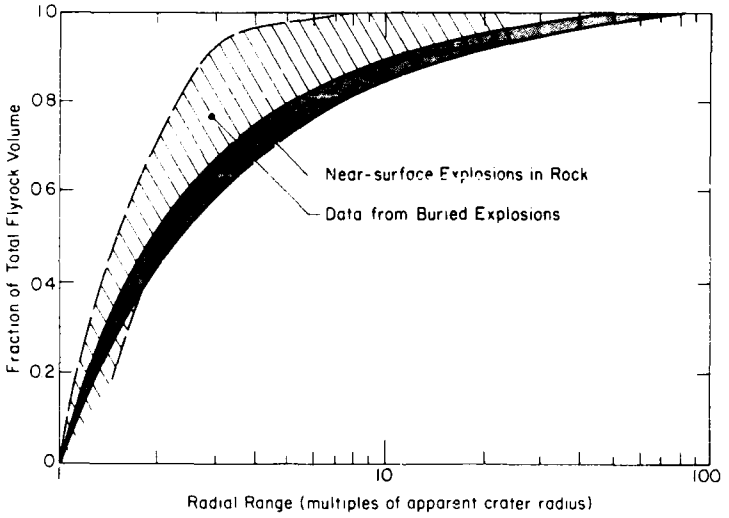

Figure 68. Distribution of debris volume with distance from the explosion. (Rooke et al. 1974.)

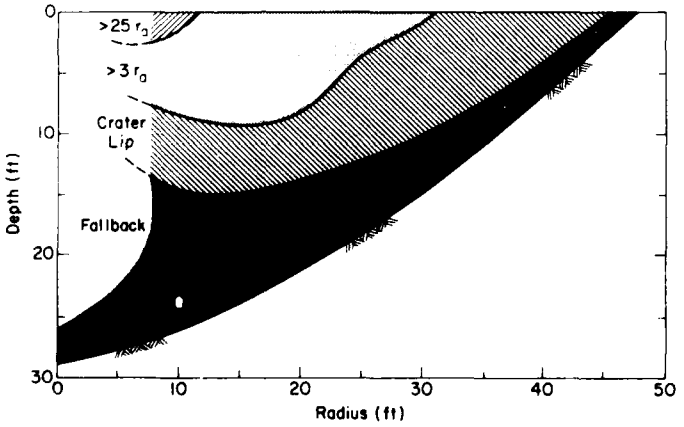

Figure 69. Travel distance of materials originating in various parts of the crater formed by a 20-ton explosion. Material near the top of the shot hole can be blown more than 25 crater radii from ground zero. Material that originates near the boundary of the true crater is likely to finish up as fallback. (Rooke et al. 1974.)

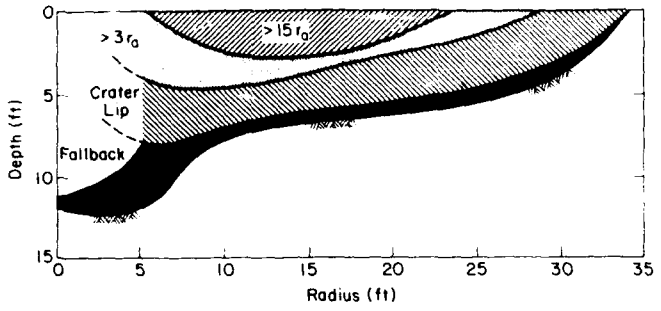

Figure 70. Travel distance of material originating in various parts of the crater formed by a 100-ton explosion at very shallow scaled depth. (Rooke et al. 1974.)

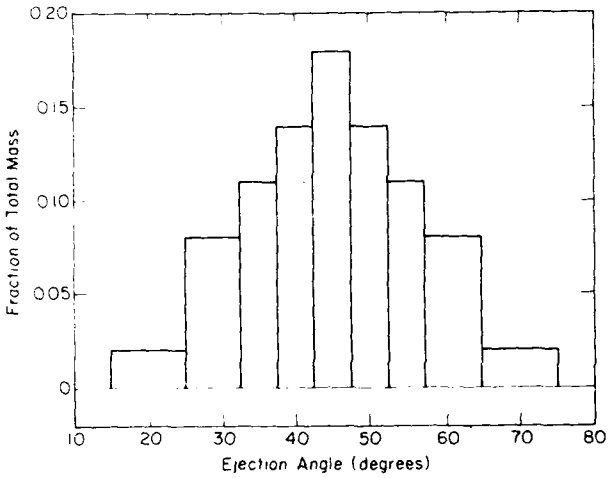

Figure 71. Ejection angles for large fragments thrown out by large surface explosions. (U.S. Army 1984.)

ocities (U.S. Army 1984). Ejection angles are assumed to range from 15° to 75°, with the peak of the distribution near 45° (Fig. 71). These computations are for large surface explosions. The observed trajectories for large fragments shown in Figure 59 suggest that the impact angles near maximum range are about 50° to 60° from the horizontal. There are no available data for buried explosions.

Impact velocities have been measured for fragments from surface explosions, and it has been concluded that velocity scales with respect to the one-sixth power of charge weight (Seebaugh 1977, Wisotski 1977). Velocity varies with fragment size, but the maximum fragment velocities V_{max} given by Seebaugh (1977) can be expressed as

$$V_{max} = 56.6\,W^{1/6} \quad \text{m/s}$$
$$= 17.25\,W^{1/6} \quad \text{ft/s} \qquad (25)$$

with W in tons. If this relation is valid, and if the particles it describes follow approximately ballistic trajectories, then flyrock range should scale with $W^{1/6}$, not $W^{1/4}$ as shown in Figures 60 and 61 or, less seriously, with $W^{1/2.5}$ as indicated by eq 23.

GROUND VIBRATIONS

Elastic waves near the ground surface

An earlier discussion of deep underground explosions dealt with the propagation and attenuation of elastic waves. In that discussion, the main concern was with waves spreading spherically inside solid ground, and with stress, strain, displacement and velocity in the ground material. However, when blasting operations or weapons effects are being considered, the main concern is with disturbance near the surface of the ground, since that is where most structures and human activities are located. In this section we are concerned with near-surface regions that are far enough from the explosion for waves to have attenuated down to elastic waves. In other words, the "seismic region" that is beyond the crater or explosion cavity, and also beyond the zone where there is permanent deformation of the ground.

The behavior of waves near the ground surface is very complicated, even for idealized conditions. An underground explosion first propagates *body waves* in a spherical pattern. These body waves include: 1) the *compression wave* (also called P-wave, dilatational wave, longitudinal wave, or irrotational wave), and 2) the *shear wave* (also

called S-wave, transverse wave, or rotational wave). As the compression wave passes through an element of ground material, it produces transient compression and rarefaction, with particle motion in the radial direction of propagation. The shear wave is the transverse, or distortional, component of the disturbance, with particle motion and strain that is normal to the radial propagation direction. The shear wave is slower than the compression wave, roughly by a factor of 2. Displacements in a horizontally propagating S-wave are resolved into horizontal and vertical components labeled SH and SV waves respectively.

On reaching a horizontal ground surface, the body waves reflect and they also transform part of the energy into *surface waves*, which travel along the surface, creating significant disturbance to a depth of about one wavelength. The P-wave and the vertical component of the S-wave couple and create a surface wave called the *Rayleigh wave*, in which particle motion follows an elliptic path in a vertical plane that is parallel to the radial propagation direction. The Rayleigh wave is a bit slower than the shear wave, and its amplitude attenuates exponentially with depth below the surface. The other type of surface wave is a *Love wave*, in which particle motion is transverse in the horizontal plane, i.e. an SH wave. Love waves depend on the existence of one or more layers parallel to the surface. Rayleigh waves are non-dispersive in a uniform medium (i.e. propagation velocity is independent of frequency) but both Rayleigh waves and Love waves are dispersive in a layered system (i.e. propagation velocity varies with frequency).

In real situations the ground surface is often irregular instead of being perfectly flat, and the subsurface geology can give varying rock properties, with multiple layers and interfaces that are not necessarily parallel to the surface. Wave propagation then becomes much more complicated than it is in a uniform medium or in a simple layered system. Furthermore, the explosion itself is not always a fully contained underground explosion; it can vent and create air blast, so that some ground disturbance is excited by air blast. In commercial blasting where delays are used, multiple explosions occur in close sequence, sending out a succession of waves from different source locations. Detailed analysis of the various waves and their components is important in some areas of research, but because of all the complications, damage predictions have to be based on a simplified description of net ground motion.

In the consideration of weapons effects, the problem of ground motion tends to be more general. In military texts, the body-wave and shear-wave type of disturbance that was just discussed is called *direct-induced ground shock*, since it results from direct coupling of energy to the ground. Another disturbance, lagging well behind the direct shock, can be produced by the eruption effects during crater formation. This is referred to as *crater-induced ground shock*. When explosions are near the ground surface, or above it, there is another disturbance called *airblast-induced ground shock*. This disturbance is a complicated one, since the airblast shock front travels over the surface, giving a distributed source of varying intensity, with varying times of origin. The following notes cover only direct ground shock, with emphasis on the radial distances at which ground motion is near the limit for causing structural damage.

Ground motion is usually measured by some type of seismograph set on the ground surface, or attached to the surface. Ideally, it should measure three orthogonal components of acceleration (preferably horizontal radial, horizontal transverse, and vertical), and it should record the disturbance as a function of time. Some simple devices measure only peak values of disturbance. The ground motion can be described in terms of acceleration, velocity, and displacement, either for a single directional component or for the resultant of the three components (vector sum). When assessing the effects of commercial blasting, ground vibration is now usually expressed in terms of particle velocity. For prediction of weapons effects, both acceleration and velocity are used. Frequency is a significant variable, but it is not always feasible to include it in predictive schemes. Measuring devides for monitoring commercial blasting should have a frequency range of approximately 2 to 200 Hz.

Attenuation of surface vibrations

When an explosion is buried and the point of observation is well below the surface, wave propagation is essentially spherical and it is reasonable to scale distance with respect to the cube root of charge weight (or energy yield), as discussed earlier. By contrast, when a concentrated explosion is underground but the point of observation is at the ground surface, part of the energy propagates spherically into the earth but part spreads two-dimensionally in the surface layers. Under these conditions, neither cube root scaling (spherical spreading) nor square root scaling (cylindrical spreading) is wholly appropriate. As a first guess,

one might expect cube root scaling to be the best approximation at small scaled radii from ground zero for a deep blast, with square root scaling giving the best approximation at large scaled radii from a shallow blast, where the propagation path is not far from horizontal and most of the disturbance is caused by surface waves, which propagate in two dimensions.

Prediction equations for ground motion from large buried explosions were given by Hughes (1968), Johnson (1971) and Mattes (1971). The attenuation equations for peak particle acceleration a and peak particle velocity v were given in the form

$$a = k_a W^{0.7} r^{-2} \tag{26}$$

$$v = k_v W^{0.73} r^{-1.87} \tag{27}$$

where W is charge weight, r is radial range, and the constants k_a and k_v depend on the ground material at the detonation point and at the observation point. Rewriting these in terms of scaled radius:

$$a = k_a (r/W^{0.35})^{-2} \tag{28}$$

$$v = k_v (r/W^{0.39})^{-1.87}. \tag{29}$$

Thus the scaling is intermediate between cube root ($W^{0.33}$) and square root ($W^{0.5}$), but closer to cube root. The relations are considered valid for charge weights from 1 to 1000 tons (TNT equivalent). From graphical displays of the equations (Johnson 1971) it appears that the range of applicability might be approximately $7 < \bar{r} < 300$ ft/lb$^{1/3}$, using cube root scaling for convenience. Values of k_a and k_v for fully contained explosions are shown in Table 17.

Table 17. Ground motion constants for large underground explosions. (From Johnson 1971.)

Ground material at detonation point	*Ground material at point of observation*	k_a*	k_v*
High strength rock	Rock	4.5×10^4	$20 \times 10^$
High strength rock	Soil	9.7×10^4	$67 \times 10^$
Weak rock	Rock	1.8×10^4	8.3×10^4
Weak rock	Soil	4.2×10^4	28×10^4
Soil	Rock	0.8×10^4	3.3×10^4
Soil	Soil	1.6×10^4	11×10^4

* Units of k_a and k_v are such that a and v are given in multiples of g and in in./s respectively when r is in feet and W is in tons.

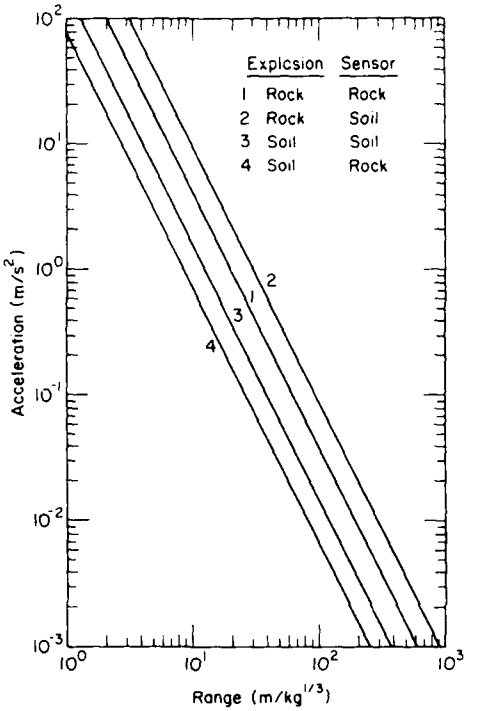

Figure 72. Attenuation of peak particle acceleration with scaled distance for various combinations of ground conditions. See text for notes on applicability. (Adapted and scaled from graphs given by Mattes 1971.)

Figures 72 and 73 give graphical approximations of eq 28 and 29, using cube root scaling for radial distance. These approximations should be acceptable for charge weights in the range 0.1 to 10 tons, and for fairly short distances from the explosion.

Ground vibrations from commercial blasting operations are usually described and regulated in terms of peak particle velocity, and the main concern is often vibration at considerable distance from the blast. The U.S. Bureau of Mines accepts square root scaling of distance as the best approximation under these circumstances (Wiss and Linehan 1979, Siskind et al. 1980, Dick et al. 1983), as do other agencies (e.g. Konya and Walter 1985). The attenuation relation for peak particle velocity v then takes the form

$$v = k(r/W^{1/2})^{-n} \tag{30}$$

where W is the charge weight for each separate explosion (charge weight per delay). In studies for the Bureau of Mines, scattered data from a variety of sources were used to derive many different values of k and n, and separate values were obtained

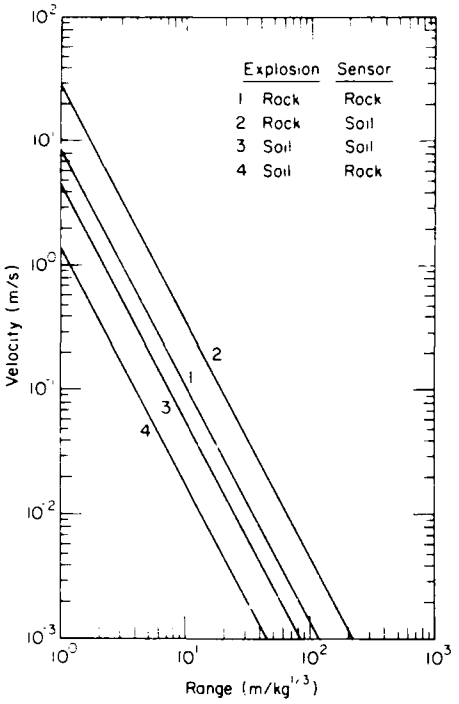

Figure 73. Attenuation of peak particle velocity with scaled distance for various combinations of ground conditions. See text for notes on applicability. (Adapted and scaled from graphs given by Mattes 1971.)

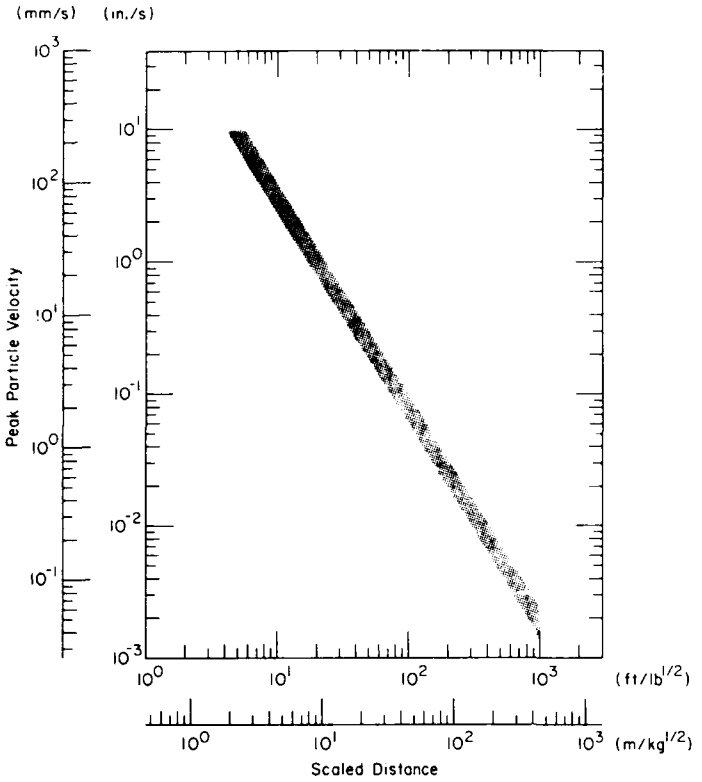

Figure 74. Representative attenuation for particle velocity in typical ground material, as determined from vibration studies relating to commercial blasting. (See, for example, Siskind et al. 1980.)

for radial, vertical and transverse components of particle motion. No firm recommendations for overall representative values of k and n were offered, but n was mostly in the range 1.2 to 1.8. The range of data for v was approximately 0.006 to 7 in./s (0.15 to 180 mm/s), with $(r/W^{1/2})$ in the range 3.5 to 800 ft/lb$^{1/2}$. DuPont (1980) accepts the values $n = 1.6$ and $k = 160$ when v is in in./s, r is in ft, and W is in lb (per delay period of 8 ms or more). Konya and Walter (1985) accept $n = 1.6$ and $k = 100$ for the radial component when the same units are used. The attenuation will obviously vary with the type of ground material, but Figure 74 shows representative behavior for unspecified ground conditions.

LITERATURE CITED

Andrews, R.J. (1977) Characteristics of debris from small-scale cratering experiments. In *Impact and Explosion Cratering*. New York: Pergamon Press, p. 1089-1100.

Anonymous (1970) Water as a stemming material: Its use in Western European countries. *Colliery Guardian*, May.

Atchison, T.C. and W.E. Tournay (1959) Comparative studies of explosives in granite. U.S. Bureau of Mines, Report of Investigations 5509.

Atchison, T.C. and J. Roth (1961) Comparative studies of explosives in marble. U.S. Bureau of Mines, Report of Investigations 5797.

Atchison, T.C. and J.M. Pugliese (1964a) Comparative studies of explosives in granite. U.S. Bureau of Mines, Report of Investigations 6434.

Atchison, T.C. and J.M. Pugliese (1964b) Comparative studies of explosives in limestone. U.S. Bureau of Mines, Report of Investigations 6395.

Atchison, T.C., W.I. Duvall and J.M. Pugliese (1964) Effect of decoupling on explosion-generated strain pulses in rock. U.S. Bureau of Mines, Report of Investigations 6333.

Bauer, A. (1975) Progress report on hole springing tests in unfrozen and frozen overburden. Defence Research Establishment Suffield, Ralston, Alberta, Canada, Suffield Memorandum 6/75.

Bauer, A., P.N. Calder, R.R. Maclachlan and M.N. Robson (1972) Ditching and cratering with explosives. In *Proceedings of Symposium on Military Applications of Commercial Explosives, 28-29 August, Defence Research Establishment, Valcartier, Quebec.* Sponsored by the Technical Cooperation Program Working Panel 0-2 (Explosives), p. 248-275.

Bauer, A., P.N. Calder, W.A. Crosby and R.D. Heater (1974) Cratering and ditching with explosives in frozen soils, Part 2. Contract Report No. 01GR 7020351 for Defence Research Establishment, Suffield, Alberta, Canada.

Beaudet, P.R., C.R. Cassity, A.H. Davis and P.P. de Caprariis (1969) Models for calculating close-in motions from underground nuclear explosions. U.S. Atomic Energy Commission, Nevada Operations Office, NVO-1163-165.

Benert, R. (1961) Excavations in frozen ground—Critical depth shots (100 and 500 lb) in Fort Churchill till. USA Cold Regions Research and Engineering Laboratory, Technical Report 79. AD 652 715.

Bourque, R.F. (1970) Project Trencher evaluation of aluminized blasting agents for cratering and hole springing. USA Engineer Nuclear Cratering Group, Livermore, California, Technical Report 28.

Cattermole, J.M. and W.R. Hansen (1962) Geologic effects of the high-explosive tests in the USGS tunnel area, Nevada Test Site. U.S. Geological Survey Professional Paper 382-B. U.S. Government Printing Office.

C.I.L. Inc. (1984) *Blaster's Handbook*. North York, Ontario: Technical Marketing Services—Explosives, Canadian Industries, 6th edition.

Conway, J.A. and J.W. Meyer (1970) Cratering in Greenland Icecap snow. USA Engineer Waterways Experiment Station, Vicksburg, Mississippi, Miscellaneous Paper N-70-6.

Cooper, H.F. (1976) Estimates of crater dimensions for near-surface explosions of nuclear and high explosive sources. R&D Associates for Lawrence Livermore Laboratory, Report RDA-TR-2604-001.

Cooper, H.F. (1977) A summary of explosion cratering phenomena relevant to meteor impact events. In *Impact and Explosion Cratering* (D.J. Roddy et al., Ed.). New York: Pergamon Press, p. 11-14.

Cooper, H.F. and F.M. Sauer (1977) Crater-related ground motions and implications for crater scaling. In *Impact and Explosion Cratering* (D.J. Roddy et al., Ed.). New York: Pergamon Press, p. 1133-1164.

D'Andrea, D.V., R.L. Fischer and A.D. Hendrickson (1970) Crater scaling in granite for small charges. U.S. Bureau of Mines, Report of Investigations 7409.

Dick, R.A., L.R. Fletcher and D.V. D'Andrea (1983) Explosives and blasting procedures manual. U.S. Department of the Interior, Bureau of Mines Information Circular IC 8925.

du Pont (1980) *Blasters' Handbook*. Wilmington, Delaware: E.I. du Pont de Nemours and Company, Incorporated (1980 printing of 1977 edition).

Duvall, W.I. and T.C. Atchison (1957) Rock breakage by explosives. U.S. Bureau of Mines, Report of Investigations 5456.

Duvall, W.I. and B. Petkof (1959) Spherical propagation of explosion-generated strain pulses in rock. U.S. Bureau of Mines, Report of Investigations 5483.

Fogelson, D.E., W.I. Duvall and T.C. Atchison (1959) Strain energy in explosion-generated strain pulses. U.S. Bureau of Mines, Report of Investigations 5514.

Fourney, W.L., C. Young and R.D. Dick (1985) Problem areas in modified in-situ fragmentation blasting. In *Fragmentation by Blasting*. Society for Experimental Mechanics, p. 129-146.

Fuchs, A. (1957) Effects of explosives on snow. USA Snow, Ice and Permafrost Research Establishment (SIPRE), Special Report 23. AD 203 809.

Gaffney, E.S. (1984a) Effect of strain rate-dependent yield strength on crater scaling relations. *Geophysical Research Letters,* **11**(2): 121-123.

Gaffney, E.S. (1984b) Hugoniot of water ice. In *Proceedings of the NATO Advanced Study Workshop on Ices in the Solar System, Nice.*

Gillespie, R.H. (1972) Hole springing. USA Engineer Waterways Experiment Station, Explosive Excavation Research Laboratory, Technical Report E-72-24.

Glasstone, S. and P.J. Dolan, Ed. (1977) *The Effects of Nuclear Weapons*. U.S. Department of Defense and U.S. Energy Research and Development Administration, 3rd edition (revision of Glasstone 1962). (Available from Superintendent of Documents, U.S. Government Printing Office, Washington, D.C. 20402.)

Hallanger, L.W. (1976) Interim field guide to

nearshore underwater explosive excavation. U.S. Navy Civil Engineering Laboratory, Port Hueneme, Technical Report R843.

Henrych, J. (1979) *The Dynamics of Explosion and Its Use*. Amsterdam: Elsevier Scientific Publishing Co.

Holsapple, K.A. and R.M. Schmidt (1980) On the scaling of crater dimensions. 1: Explosive processes. *Journal of Geophysical Research*, **85**(B12): 7247-7256.

Holzer, F. (1965) Measurements and calculations of peak shock wave parameters from underground nuclear detonations. *Journal of Geophysical Research*, **70**(4): 893-905.

Hughes, B.C. (1968) Nuclear construction engineering technology. USA Engineer Nuclear Cratering Group, Livermore, California, Technical Report 2.

Ingram, L.F. and J.N. Strange (1958) Blast-pressure measurements in snow. USA Engineer Waterways Experiment Station, Miscellaneous Paper 2-274.

Ingram, L.F. and S.H. Halper (1960) Measurements of explosion-induced shock waves in ice and snow, Greenland, 1957 and 1948. USA Engineer Waterways Experiment Station, Miscellaneous Paper 2-399.

Joachim, C.E. (1964) Structures in an arctic environment. Report 3: Airblast and subsurface shock of high explosive tests. USA Engineer Waterways Experiment Station, Technical Report 1-649.

Joachim, C.E. (1967) Shock transmission through ice and snow. USA Engineer Waterways Experiment Station, Technical Report 1-794.

Johnson, S.M. (1971) Explosive excavation technology. USA Engineer Nuclear Cratering Group, Livermore, California, Technical Report 21.

Khristoforov, B.D. and A.N. Romashov (1967) Determination of compression wave parameters in rock. *Fizika Goreniya i Vzryva*, **3**(1): 137-142.

Kinney, C.F. and K.J. Graham (1985) Explosive shocks in air. Springer-Verlag, 2nd edition.

Knudson, H.L., J.W. Meyer, S.B. Price and A.D. Rooke (1972) Effects of stemming on high-explosive cratering. USA Engineer Waterways Experiment Station, Miscellaneous Paper N-72-6.

Konya, C.J. and E.J. Walter (1985) Rock blasting. U.S. Department of Transportation, Federal Highway Administration. (Available from Superintendent of Documents, U.S. Government Printing Office, Washington, D.C. 20402.)

Kutter, H.K. and C. Fairhurst (1971) On the fracture process in blasting. *International Journal of Rock Mechanics and Mining Sciences*, **8**(3): 181-202.

Livingston, C.W. (1960) Explosions in ice. USA Snow, Ice and Permafrost Research Establishment, Technical Report 75. AD 276 605.

Livingston, C.W. (1968) Explosions in snow. USA Cold Regions Research and Engineering Laboratory, Technical Report 86. AD 672 056.

Livingston, C.W. and G. Murphy (1959) Excavations in frozen ground. Part II: Explosion tests in frozen glacial till, Ft. Churchill. USA Snow, Ice and Permafrost Research Establishment, Technical Report 30. AD 233 474.

Mattes, R.W. (1971) Study of explosives for lunar applications. USA Engineer Nuclear Cratering Group, Livermore, California, Technical Report 25.

McCoy, J.E. (1965) Excavations in frozen ground, Alaska, 1960-61. USA Cold Regions Research and Engineering Laboratory, Technical Report 120. AD 616 314.

Mellor, M. (1971) Blasting tests in frozen ground, 1971. USA Cold Regions Research and Engineering Laboratory, Technical Note (unpublished).

Mellor, M. (1972) Use of liquid explosives for excavation of frozen ground. In *Proceedings of Symposium on Military Applications of Commercial Explosives, 28-29 August, Defence Research Establishment, Valcartier, Quebec*. Sponsored by the Technical Cooperation Program Working Panel 0-2 (Explosives), p. 329-340. (Also USA Cold Regions Research and Engineering Laboratory, Miscellaneous Paper 600.)

Mellor, M. (1973) Controlled release of avalanches by explosives. In *Symposium on Advances in North American Avalanche Technology, Reno*. U.S. Department of Agriculture, Forest Service, Technical Report RM-3, p. 37-49.

Mellor, M. (1985) Apparent craters from explosions in frozen ground. USA Cold Regions Research and Engineering Laboratory, Technical Note (unpublished).

Mellor, M. and P.V. Sellmann (1970) Experimental blasting in frozen ground. USA Cold Regions Research and Engineering Laboratory, Special Report 153. AD 738 798.

Mellor, M. and P.V. Sellmann (1974) Blasting tests in seasonally frozen ground. USA Cold Regions Research and Engineering Laboratory, Technical Note (unpublished).

Nicholls, H.R. (1962) Coupling explosive energy to rock. *Geophysics*, **27**(3): 305-316.

Nicholls, H.R. and V.E. Hooker (1962a) Comparative studies of explosives in salt. U.S. Bureau of Mines, Report of Investigations 6041.

Nicholls, H.R. and V.E. Hooker (1962b) Shear and longitudinal waves from HE detonations in

granite. Advanced Research Projects Agency/Defense Atomic Support Agency, Report no. E48.1.

Nicholls, H.R. and V.E. Hooker (1965) Comparative study of explosives in granite. U.S. Bureau of Mines, Report of Investigations 6693.

Noren, C.H. (1968) Pressure-time measurements in rock. In *Proceedings of 9th Symposium on Rock Mechanics*. American Institute of Mining, Metallurgical and Petroleum Engneers, p. 285-296.

Olson, J.J., R.J. Willard, D.E. Fogelson and K.E. Hjelmstad (1973) Rock damage from small charge blasting in granite. U.S. Bureau of Mines, Report of Investigations RI 7751.

Piekutowski, A.J. (1974) Laboratory scale high explosive cratering and ejecta phenomenology studies. Air Force Weapons Laboratory, Kirtland AFB, New Mexico, Technical Report AFWL-TR-72-155.

Piekutowski, A.J. (1977) Cratering mechanisms observed in laboratory-scale high-explosive experiments. In *Impact and Explosion Cratering* (D.J. Roddy et al., Ed.). New York: Pergamon Press, p. 67-102.

Riddoch, R.G. (1979) Cratering and ditching in frozen soils. M.E. thesis, Department of Civil Engineering, Royal Military College of Canada, Kingston, Ontario.

Rooke, A.D., B.L. Carnes and L.K. Davis (1974) Cratering by explosives: A compendium and an analysis. USA Engineer Waterways Experiment Station, Weapons Effects Laboratory, Technical Report N-74-1.

Roth, J. (1979) A model for the determination of flyrock range as a function of shot conditions. U.S. Bureau of Mines, Open File Report OFR 77-81.

Seebaugh, W.R. (1977) A dynamic crater ejecta model. In *Impact and Explosion Cratering* (D.J. Roddy et al., Ed.). New York: Pergamon Press, p. 1043-1056.

Simpson, J.K. (1981) Explosive cratering in frozen media. M.E. thesis, Department of Civil Engineering, Royal Military College of Canada, Kingston, Ontario.

Simpson, J.K. and P.J. Jarrett (1983) Explosive excavation of frozen soils. In *Permafrost: Proceedings of 4th International Conference, 17-22 July, Fairbanks, Alaska*. Washington, D.C.: National Academy Press, p. 1160-1165.

Siskind, D.E. and R.R. Fumanti (1974) Blast-produced fractures in Lithonia granite. U.S. Bureau of Mines, Report of Investigations 7901.

Siskind, D.E., R.E. Steckley and J.J. Olson (1973) Fracturing in the zone around a blasthole, White Pine, Michigan. U.S. Bureau of Mines, Report of Investigations 7753.

Siskind, D.E., V.J. Stachura, M.S. Stagg and J.W. Kopp (1980a) Structure response and damage produced by airblast from surface mining. U.S. Bureau of Mines, Report of Investigations 8485.

Siskind, D.E., M.S. Stagg, J.W. Kopp and C.H. Dowding (1980b) Structure response and damage produced by ground vibration from surface mine blasting. U.S. Bureau of Mines, Report of Investigations 8507.

Smith, J.L. (1966) Shock pressure measurements from explosions in various media. USA Cold Regions Research and Engineering Laboratory, Technical Note (unpublished).

Smith, N. (1980) High-explosive cratering in frozen and unfrozen soils in Alaska. USA Cold Regions Research and Engineering Laboratory, CRREL Report 80-9. ADA 084 702.

Smith, N. and M. Mellor (1975) High-explosive cratering in seasonally frozen gravel. USA Cold Regions Research and Engineering Laboratory, Technical Note (unpublished).

U.S. Army (1965) Fundamentals of protective design (non-nuclear). Technical Manual 5-855-1, Washington, D.C.

U.S. Army (1967, 1971, 1986) Explosives and demolitions. Field Manual 5-25 (1986 edition subject to distribution restriction).

U.S. Army (1984) Designing facilities to resist nuclear weapon effects. Technical Manual 5-858-2.

Vortman, L.J. (1967) Maximum missile ranges from surface and buried explosions. Sandia Laboratory, Albuquerque, New Mexico, Report SC-RR-67-616.

White, J.W. (1973) An empirically derived cratering formula. *Journal of Geophysical Research*, **78** (35): 8623-8633.

Wisotski, J. (1977) Dynamic ejecta parameters from high explosive detonations. In *Impact and Explosion Cratering* (D.J. Roddy et al., Ed.). New York: Pergamon Press, p. 1101-1122.

Wiss, J.F. and P.W. Linehan (1979) Control of vibration and blast noise from surface coal mining (4 vol.). U.S. Bureau of Mines Open File Reports OFR-103(1)-79, OFR-103(2)-79, OFR-103(3)-79, and OFR-103(4)-79.

* U. S. GOVERNMENT PRINTING OFFICE: 1989 -600-057/ 2012